THESIS ON MECHANICAL ENGINEERING E82

Experimental Acoustic Characterization of Automotive Inlet and Exhaust System

HEIKI TIIKOJA

TUT PRESS

TALLINN UNIVERSITY OF TECHNOLOGY
Faculty of Mechanical Engineering
Department of Machinery

This dissertation was accepted for the defence of the degree of Doctor of Philosophy in Engineering on February 07, 2014.

Supervisor: Prof. Jüri Lavrentjev, Department of Machinery, Tallinn University of Technology

Opponents: Prof. Ragnar Glav, Department of Aeronautical and Vehicle Engineering, MWL, KTH Royal Institute of Technology, Sweden
Head of Acoustics, Truck Chassis Development, Scania CV AB, Södertälje, Sweden

Assoc. Prof. Villu Mikita, Institute of Technology, Estonian University of Life Sciences, Estonia

Defence of the thesis: March 14, 2014

Declaration:
Hereby I declare that this doctoral thesis, my original investigation and achievement, submitted for the doctoral degree at Tallinn University of Technology has not been submitted for any academic degree.

/Heiki Tiikoja/

European Union
Regional Development Fund

Investing in your future

ISSN 1406-4758
ISBN 978-9949-23-591-9 (publication)
ISBN 978-9949-23-592-6 (PDF)

MEHHANOTEHNIKA E82

Autode sisse- ja väljalaskesüsteemi akustilised katsetusuuringud

HEIKI TIIKOJA

TTÜ
KIRJASTUS

CONTENTS

LIST OF PUBLICATIONS

This thesis is based on the following publications which are presented at the end of this thesis and referred in the text by their Roman numerals I-IV:

Paper I
Tiikoja, H., Rämmal, H., Åbom, M., Bodén, H., Sound Transmission in Automotive Turbochargers, *SAE Technical Paper Series*, Paper 2011-01-1525, 1-12, 2011.

Paper II
Tiikoja, H., Rämmal, H., Åbom, M., Bodén, H., Investigations of Automotive Turbocharger Acoustics. *SAE International Journal of Engines*, 4(2), 2531-2542, 2011.

Paper III
Lavrentjev, J., Rämmal, H., Tiikoja, H., The Passive Acoustic Effect of Automotive Catalytic Converter, *SAE Technical Paper Series*, Paper 2011-24-0219, 1-8, 2011.

Paper IV
Tiikoja, H., Lavrentjev, J., Rämmal, H., Åbom, M., Experimental Investigations of Sound Reflection from Hot and Subsonic Flow Duct Termination. *Journal of Sound and Vibration*, 333(3), 788-800, 2014.

Approbations

16th AIAA/CEAS Aeroacoustics Conference (31st AIAA Aeroacoustics Conference), Stockholm, Sweden, 07-09 June, 2010.

Noise and Vibration Conference and Exhibition (SAE NVH 2011), Grand Rapids, Michigan, USA, 16-19 May, 2011.

Author´s contribution to the publications

The methodology to carry out the acoustic characterization of turbochargers, catalytic converters and duct termination was proposed by J. Lavrenjev, M. Åbom and H. Bodén. The measurements and data analysis was carried out by H. Tiikoja. The development of the test-rigs, including the automated measurement process and data acquisition system was performed by H. Tiikoja. The test-rigs improvements to increase the quality of the measured data were suggested by H. Tiikoja, J. Lavrentjev, M. Åbom and H. Bodén and developed and tested by H. Tiikoja. H. Tiikoja had a major role in writing *Papers I*, *II* and *IV* under the supervision of J. Lavrentjev, H. Rämmal, M. Åbom and H. Bodén, and participated in writing the *Paper III*.

INTRODUCTION

Traffic noise is one of the major noise sources in modern society. Although the noise radiation from a vehicle has been decreased continuously, noise pollution is still a problem due to the increasing intensity of the road transport.

The noise radiation from a vehicle originates from different sources and mainly depends on the engine load and speed of the vehicle. In order to successfully decrease emitted noise from the vehicle, the sources of the noise have to be localized and acoustic properties thoroughly understood. In the search for quieter engines there is a need for a better understanding of the acoustic properties of engine intake and exhaust system components. Besides silencers, successfully used over a century with the purpose of reducing acoustic pressure pulses originating from the internal combustion engine, a modern car intake and exhaust system consist of a number of elements, e.g. catalytic converter, particulate filter, turbocharger etc., which acoustical performance still needs to be better understood.

Recent trend in acoustic product design is so-called virtual prototyping, where computational models are used to optimize design. Although there are several commercial software programs available for acoustics, current simulation methodologies are still too generic to give accurate solutions e.g., for objects with complex geometries. In order to develop new computational models and improve existing ones, accurate experimental data is essential. This in turn creates a need for development of experimental methods.

Problem settings

The aim of the current study is to explore existing experimental methodologies for induct acoustic characterization and to improve these methods. To obtain accurate results, accuracy of the sensors, effective data acquisition systems, improvement of methodology etc., have to be considered. Development of measurement methods also highly depends on the application. The ambition here is to test methods applicability in harsh environment by using three different automotive inlet and exhaust system elements (turbocharger, catalytic converter, exhaust tailpipe) in conditions they are used in practice.

For the study of automotive turbochargers, accurate and efficient measurement methods to characterize compressor and turbine, have to be developed. This allows measuring acoustic data in the range where turbocharger is typically used in practice and could lead to generalized results, where conclusions about the turbocharger passive acoustical behavior can be drawn. In addition to the sound scattering in the turbochargers, it is also a high frequency aero-acoustic source. To investigate sound generation at different operating points and identify source mechanisms, reliable methods need to be developed.

With acoustic two-port method, sound scattering below the cut-on frequency of the first higher order propagating duct mode can be determined. Often measurement objects consist of a cascade of different objects with complex geometry. In order to focus on the acoustic effect of the smaller elements, decomposition of the complex system can be performed, where elements are studied separately by using two-port method. An example here would be catalytic converter, where relatively good models exist to predict acoustic effect of the casing, whereas predicting an acoustic performance caused by the viscous-thermal losses in the narrow tubes of honeycomb element can be a difficult task.

Acoustic reflection from an open end flow duct is a well studied problem in acoustics. There are different numerical models available to predict acoustic reflection in high temperature and flow conditions. To evaluate existing models, accurate methods for measuring the reflection of plane acoustic waves from a duct termination in hot gas flow have to be developed. Representing the acoustical conditions at the exhaust tailpipe, the data obtained is also important for e.g., effective modeling of exhaust systems.

The objectives of the present thesis are as follows:

1. To modify the acoustic one-port and two-port methods in order to reduce measurement error and measurement time in harsh measurement conditions.
2. To test the applicability of modified acoustic one-port and two-port methods by characterizing the flow duct elements in high flow, temperature and static pressure conditions.
3. By using the two-port method, experimentally investigate acoustic properties of automotive flow duct elements, such as turbocharger and catalytic converter.
4. By using the one-port method, experimentally investigate plane acoustic wave reflection from a hot jet flow duct termination. Also, compare obtained results with existing theory for hot flow duct termination, developed by Munt.

To reach the objectives the following tasks have to be completed:

1. Methodology for experimental investigation, together with related software and hardware, has to be developed in order to experimentally verify the proposed improvements in acoustic one- and two-port methods.
2. To investigate one-port method in high flow speed and high temperature conditions, an acoustic test-rig, to generate flow velocity up to $M = 0.3$ and temperature up to $T = 200$ °C, has to be developed.
3. To investigate modified two-port method applicability in harsh measurement conditions, experimental setup for acoustic characterization of turbochargers and catalytic converters has to be developed.
4. To increase the accuracy of measurement process, improved data acquisition system has to be developed for experimental investigation.
5. In order to implement modified one-port and two-port models, a powerful external source capable to create an acoustic field dominating over the flow noise, has to be developed.

LIST OF ABBREVIATIONS AND SYMBOLS

BOV	blow-off valve
BPF	blade passing frequency
CC	catalytic converter
CCGEx	Competence Centre for Gas Exchange
CPI	cells per inch
cRIO	compact reconfigurable input output module of National Instruments DAQ systems
DAQ	data acquisition
FPGA	field-programmable gate array
FWDM	full wave decomposition method
GUI	graphical user interface
ICE	internal combustion engine
IL	insertion loss
MMM	multi microphone method
MSS	multi step sine
NI	National Instruments
NR	noise reduction
OP	operating point
PID	proportional integral derivative
RPM	rotations per minute
SPL	sound pressure level
SS	stepped sine
SWR	standing wave ratio
TC	turbocharger
TCN	tip clearance noise
TL	transmission loss
TMM	two-microphone method
VTG	variable geometry turbine
WDM	wave decomposition method
WN	white noise

A	cross-sectional area of the duct
A	acoustic absorption coefficient
a	duct radius
c	speed of sound
d	diameter of the duct
f	frequency
f_u	upper frequency limit
G	pressure cross-spectrum
H	transfer function
He	Helmholtz number
i	imaginary unit
k	wave number
l	length between cross sections
$\dot{m}$	mass flow rate
M	Mach number
n	number of samples
p	acoustic pressure
q	acoustic volume velocity
R	acoustic reflection coefficient
s	microphone separation
S	scattering matrix
St	Strouhal number
T	acoustic transmission coefficient
T	temperature
T	two-port matrix
TL	transmission loss
U	cross-sectional averaged mean flow velocity
U_{cl}	centreline flow velocity
W	acoustic power
ρ	density
η	efficiency
λ	wave length
ω	angular velocity

1 EXPERIMENTAL TECHNIQUES

To experimentally describe the sound field in ducts and determine in-duct acoustic properties, two standard methods are used. Although the standing wave ratio (SWR) [1] method with traversing microphone can be used to get accurate results, it is time consuming and difficult to use in flow ducts [2]. Faster and more reliable measurements over a wide frequency range can be performed with two-microphone method (TMM) [3]. The method uses transfer functions between measurement microphones in order to completely describe sound field. This method is also applicable in a harsh measurement conditions e.g. in a presence of turbulent flow. To improve the accuracy of TMM, extra microphones are used, which leads to the multi microphone method (MMM), also often used. In the current chapter TMM will be described.

1.1 Wave decomposition method

In general, sound propagation in a duct with a presence of mean flow is a complex problem. However, in a straight cylindrical duct and below the first cut-on frequency, a sound field in frequency domain can be written as:

$$p(x,f) = p_+(f)\exp(-\mathrm{i}k_+x) + p_-(f)\exp(\mathrm{i}k_-x)\ , \tag{1}$$

$$u(x,f) = \frac{1}{\rho c}\left[p_+(f)\exp(-\mathrm{i}k_+x) + p_-(f)\exp(\mathrm{i}k_-x)\right]\ , \tag{2}$$

where p is the Fourier transform of the acoustic pressure, u is the Fourier transform of the particle velocity, x is the coordinate along the axis, + and – in subscript denote the wave propagation in negative and positive x-axis direction, f is the frequency, k is the wave number, ρ is the density, c is the speed of sound and i is the imaginary unit.

Because of the superposition of the sound waves propagating in negative and positive direction, no direct in-duct measurements could be performed to describe sound propagation. The theory underlying the decomposition of the sound wave into its two propagating wave amplitudes consists of two acoustic pressures, determined by the flush mounted microphones at two locations on the duct wall (see Figure 1). This method is known as the two-microphone method [3].

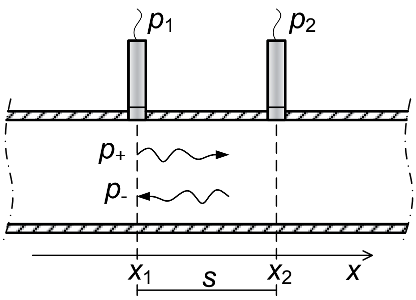

Figure 1. Schematic representation of a decomposition of sound waves

Acoustic pressures at microphones 1 and 2 (see Figure 1) can be presented as:

$$p_1(f) = p_{1+}(f) + p_{1-}(f) \ , \tag{3}$$

$$p_2(f) = p_{1+}(f)\exp(-\mathrm{i}k_+s) + p_{1-}(f)\exp(\mathrm{i}k_-s) \ , \tag{4}$$

where subscripts 1 and 2 denote the acoustic pressure wave at microphones 1 and 2 correspondingly and $s = x_2 - x_1$ is the microphone separation. By combining the equations (3) and (4), p_+ and p_- in the reference cross section x_1 can be expressed as:

$$p_{1+}(f) = \frac{p_1(f)\exp(\mathrm{i}k_-s) - p_2(f)}{\exp(\mathrm{i}k_-s) - \exp(-\mathrm{i}k_+s)} \ , \tag{5}$$

$$p_{1-}(f) = \frac{p_2(f) - p_1(f)\exp(-\mathrm{i}k_+s)}{\exp(\mathrm{i}k_-s) - \exp(-\mathrm{i}k_+s)} \ . \tag{6}$$

In equations (1)-(6), the wave number k can be determined [4] as $k_\pm = 2\pi f / (c(1 \pm M))$ where $M = U / c$ is the Mach number, c is the speed of sound and U is the flow velocity.

In equations (1)-(6), the sound attenuation has not been taken into account. There are several models available to describe sound attenuation in a duct; mainly associated with viscosity, heat conduction and interaction between sound and flow field. An overview of the developed models was given by Allam and Åbom [5]. To include the effects of visco-thermal damping the wave number can be obtained by using the model proposed by Dokumaci [6]:

$$k_\pm = \frac{2\pi f}{c} \frac{K_0}{(1 \pm K_0 M)} \ . \tag{7}$$

A model to describe dissipation of acoustic energy in a quiescent fluid is based on theory of Kirchoff [7], where the propagation coefficient K_0 is given by:

$$K_0 = 1 + \frac{(1-\mathrm{i})}{\sqrt{2}s}\left(1 + \frac{(\gamma-1)}{\xi}\right) - \frac{\mathrm{i}}{s^2}\left(1 + \frac{\gamma-1}{\xi} - \frac{\gamma}{2}\frac{\gamma-1}{\xi^2}\right), \tag{8}$$

where $\gamma = C_p / C_v$ is the ratio of specific heats, $\xi^2 = \mu C_p / \kappa_{th}$ is the Prandtl number, $s = a\sqrt{\rho_0 \omega / \mu}$ is the shear wave number, μ is the dynamic viscosity, C_p is the specific heat coefficient, κ_{th} is the thermal conductivity, a is the duct radius, ρ_0 is the ambient density and μ is the dynamic viscosity. At short propagating distances the sound wave attenuation is negligible.

The wave decomposition method (WDM) described by equations (5) and (6) is limited by the cut-on frequency of the duct, thus only the one dimensional plane wave mode will propagate in the duct. For a circular duct the cut-on frequency [8, 9] can be determined as:

$$f_c = \frac{1.841 \cdot c}{\pi \cdot d}(1 - M^2)^{1/2}, \tag{9}$$

where d is the diameter of the duct. Also, in the plane wave range, the TMM will be valid if the microphone pressure signals are linearly independent, i.e. if $ks / (1 - M^2) \neq \pi n$ where $n = 0,1,2...$. According to this, frequencies where microphone separation is multiple of half a wavelength should be avoided. The sensitivity for different type of errors was also studied by Åbom and Bodén [10] where the frequency range measured by the microphones separated by distance s, was restricted to the frequency range, described by:

$$0.1\pi\left(1 - M^2\right) < ks < 0.8\pi\left(1 - M^2\right). \tag{10}$$

To extend the frequency range in the plane wave range, an extra microphone with different separation s is used [10].

Measurement errors can be reduced by using multi-microphone method (MMM) [11, 12]. By using more measurement microphones, it is possible to suppress the bias errors by forming and solving an over-determined system [11] as:

$$\underbrace{\begin{pmatrix} e^{-\mathrm{i}k_+x_1} & e^{\mathrm{i}k_-x_1} \\ e^{-\mathrm{i}k_+x_2} & e^{\mathrm{i}k_-x_2} \\ \vdots & \vdots \\ e^{-\mathrm{i}k_+x_m} & e^{\mathrm{i}k_-x_m} \end{pmatrix}}_{\mathbf{E}} \underbrace{\begin{pmatrix} p_+ \\ p_- \end{pmatrix}}_{\mathbf{p}} = \underbrace{\begin{pmatrix} p_1 \\ p_2 \\ \vdots \\ p_m \end{pmatrix}}_{\mathbf{P}}, \tag{11}$$

where vector $\mathbf{p}$ consists of the positive and negative propagating pressure waves in the reference cross-section. Measured acoustic pressures will be in matrix $\mathbf{P}$ and the system can be solved by using a Moore-Penrose pseudo-inverse, if at least two rows in $\mathbf{E}$ are linearly independent.

Instead of the over-determination, the system of equations could be used to obtain an extra variable e.g. speed of sound or flow velocity [5]. By following the three-microphone method [13] the sound field at the microphones can be obtained by solving the nonlinear system of equations expressed as:

$$p_1(f) = p_{1+}(f) + p_{1-}(f) \ , \tag{12}$$

$$p_2(f) = p_{1+}(f)\exp(-\mathrm{i}k_+ s_2) + p_{1-}(f)\exp(\mathrm{i}k_- s_2) \ , \tag{13}$$

$$p_3(f) = p_{1+}(f)\exp(\mathrm{i}k_+ s_3) + p_{1-}(f)\exp(-\mathrm{i}k_- s_3) \ . \tag{14}$$

In order to have the same frequency range, the same microphone separation $s_1 = s_2$ must be used. The nonlinear system of equations in (12)-(14) can be solved by using e.g. Gauss-Newton iterative procedure and obtain three unknowns as p_+, p_- and c or U. The flow velocity and speed of sound obtained by the three-microphone method, compared to the results calculated with analytical model, can be seen in Figures 2-3.

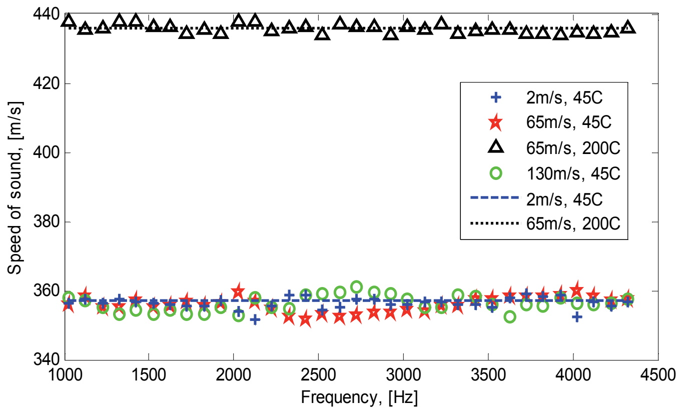

Figure 2. The flow velocity determined by using the three-microphone method (markers), compared to the theoretical (line)

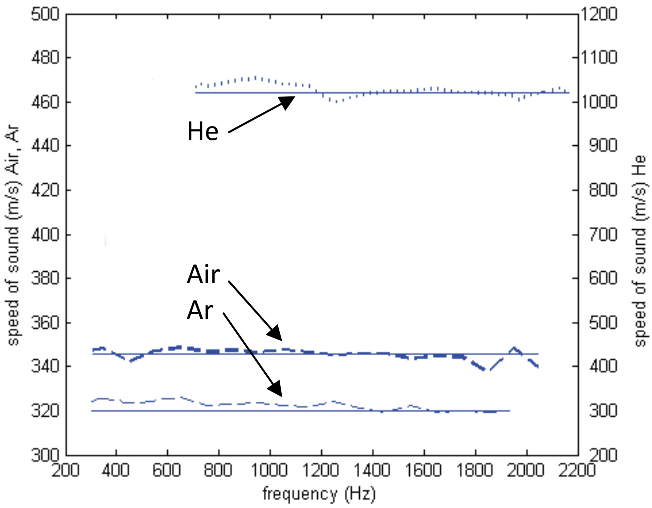

Figure 3. The speed of sound in air (dashed line in bold), argon (dashed line) and helium (dotted line) measured with three-microphone method [13], the speed of sound (solid lines) calculated

Note, that the fluctuations of experimentally determined speed of sound in Figures 2-3 present only the bias error due to numerical calculation method. Therefore it is essential to use the constant speed of sound over the frequency range.

Extra microphone positions were used by Allam and Åbom [5] for a full wave decomposition method (FWDM). In FWDM, in addition to the complex pressure amplitudes, complex wave numbers can be determined with at least four microphone positions. Another important aspect for the wave decomposition is the choice of the microphone positions. Instead of the uniform distribution suggested by Jang et al. [14], microphones were positioned in to two clusters, separated by long distance in order to determine damping of the propagating wave [15].

In order to use multiple microphones for the measurement, the microphones must be calibrated. The calibration procedure gives the relative response of the microphones to the identical sound pressure. This is usually performed by using a calibration duct in which all microphones are exposed to the same sound field. Calibration data is expressed as the transfer functions between the reference microphone and the microphone which is calibrated $H_{n1\,cal}$. Then the measured data $H_{n1\,meas}$ is used to calculate the resulting transfer function H_{n1} as:

$$H_{n1} = H_{n1\,meas} / H_{n1\,cal} \,, \tag{15}$$

where n in subscript refers to the microphone number and 1 to the reference microphone respectively.

Acoustic sound pressure values in the measurement duct can also be acquired by using a single microphone. The measurement error in case of using a single microphone will be smaller, since there is no need for the relative calibration of the microphone. However, this method is often not preferred due to the multiple measurements needed, leading to increased measurement time.

In *Paper IV*, it was found that in case the pressure transducers were used, the calibration curve was also considerably affected by the measurement conditions. Therefore, the transducer calibration must be performed for all measurement cases with different flow velocities and the open end calibration duct was inevitable. The discrepancy between the calibration curves apparent for the different flow cases can be seen in Figure 4.

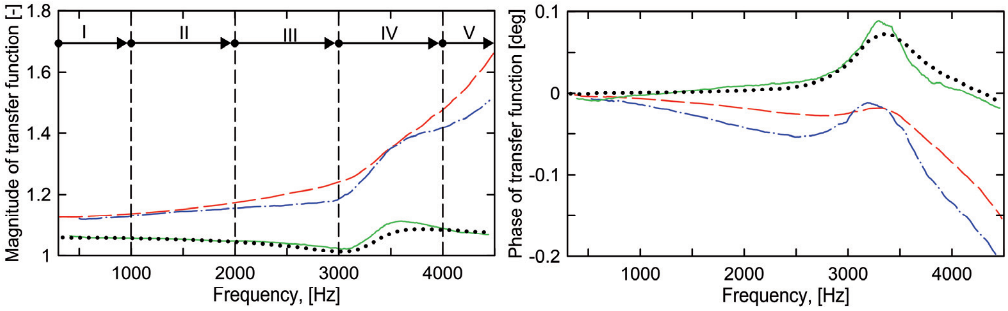

Figure 4. The magnitude and the phase recorded during the pressure-transducer calibration: ·····, H_{21} *measured at* $M = 0$; ——, H_{21} *measured at* $M = 0.15$; – – –, H_{31} *measured at* $M = 0$; –·–·–·, H_{31} *measured at* $M = 0.15$. *MSS technique with five frequency regions I - V, excitation direction indicated by the arrows*

1.2 Acoustic two-port model

Two-port method, originally developed with the theory of electric circuits, is an effective way to analyze sound propagation inside duct networks e.g. intake and exhaust system of an internal combustion engine.

There are different formulations of the two-port [4, 16, 17]. The key element of the model is the "black box" or two-port, where linear relation between two state vectors on each side exists. If the propagating pressure wave amplitudes p_+ and p_- (see equations (5) and (6)) are used as state variables, a scattering matrix form can be used to express the relationship between the two ports. Regardless of the form of the two-port calculated, all other forms can be obtained from linear transformation [18].

In Figure 5, a schematic representation of acoustic two-port is presented. Two ports (the inlet and outlet) of the element are referred to as side a and b, in respect to the direction of the mean flow. The acoustic pressures p are measured at the inlet and outlet side and the propagating pressure waves are determined by using the wave decomposition as described earlier in section 1.1. External sources (electro-dynamic drivers) A and B are used to excite the system from the up- or downstream side. The *x*-axis direction denotes the positive direction for the propagating pressure waves. It should be noted here, that the two-port model is valid for any kind of geometry of the acoustic test object, represented as a “black box” in Figure 5.

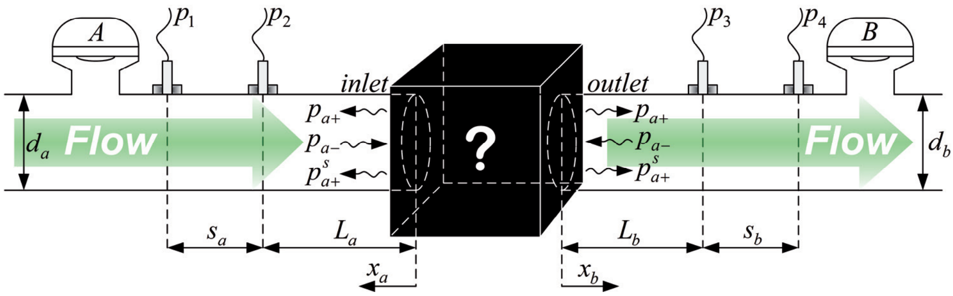

Figure 5. Schematic representation of an acoustic two-port

1.2.1 Passive two-port

Passive two-port has no noise sources between reference cross-sections *a* and *b*. Scattering matrix in passive acoustic two-port [19] contains 4 complex quantities at discrete frequencies, describing how incoming acoustic waves are reflected and transmitted through the acoustic element. To experimentally determine these unknowns, at least two microphones in the inlet and outlet side must be used to decompose acoustic pressure waves to p_+ propagating in positive and p_- propagating in negative direction, so the two-port can be represented as:

$$\underbrace{\begin{bmatrix} p_{a+} \\ p_{b+} \end{bmatrix}}_{\mathbf{p}_+} = \underbrace{\begin{bmatrix} S_{11} & S_{12} \\ S_{21} & S_{22} \end{bmatrix}}_{\mathbf{S}} \cdot \underbrace{\begin{bmatrix} p_{a-} \\ p_{b-} \end{bmatrix}}_{\mathbf{p}_-}, \tag{16}$$

where elements S_{11}, S_{22} describe the reflection and S_{12}, S_{21} describe the transmission of the incoming waves respectively.

To suppress the flow noise, the transfer functions H between the microphone signals and the reference signal can be used instead of sound pressures [20]. For the reference, electric signal driving the external sources can be used. The choice of the excitation signal was investigated by Allam in [21]. By using transfer functions, equation (16) can in matrix notation be expressed as:

$$\mathbf{H}_+ = \mathbf{S}\mathbf{H}_- . \tag{17}$$

To obtain the $\mathbf{S}$ matrix elements the acoustic state variables on the inlet and outlet side must be measured for two independent test cases. These test cases are created by using acoustic sources on the inlet and outlet side leading to the so-called two-source technique [18]. By performing the two different test cases, two states in equation (17) can be expressed in measurable quantities as:

$$\mathbf{H}_+ = \begin{bmatrix} H^I_{ea+} & H^{II}_{ea+} \\ H^I_{eb+} & H^{II}_{eb+} \end{bmatrix}, \ \mathbf{H}_- = \begin{bmatrix} H^I_{ea-} & H^{II}_{ea-} \\ H^I_{eb-} & H^{II}_{eb-} \end{bmatrix}, \tag{18}$$

so $\mathbf{S}$ matrix elements can be expressed as:

$$\begin{aligned} S_{11} &= (H^I_{ea+}H^{II}_{eb-} - H^{II}_{ea+}H^I_{eb-}) / \det(\mathbf{H_x}) \\ S_{12} &= (H^{II}_{ea+}H^I_{ea-} - H^I_{ea+}H^{II}_{ea-}) / \det(\mathbf{H_x}) , \\ S_{21} &= (H^I_{eb+}H^{II}_{eb-} - H^{II}_{eb+}H^I_{eb-}) / \det(\mathbf{H_x}) \\ S_{22} &= (H^{II}_{eb+}H^I_{ea-} - H^I_{eb+}H^{II}_{ea-}) / \det(\mathbf{H_x}) \end{aligned} \tag{19}$$

$$(\mathbf{H_x}) = (H^I_{ra-}H^{II}_{rb-} - H^{II}_{ra-}H^I_{rb-}) , \tag{20}$$

where e in the subscript refers to the transfer function between the microphone signal and reference signal e.g. loudspeaker voltage, I and II in the superscript indicate to the two independent test cases and $e = e_A$, $e = e_B$ are the electrical signals from the sources respectively. By applying the wave decomposition, the transfer functions in equation (18) can now be obtained from directly measurable quantities as:

$$\begin{aligned} H_{ea+} &= F_a[H_{ea1}\exp(\mathrm{i}k_{a-}s) - H_{ea2}] \\ H_{ea-} &= F_a[-H_{ea1}\exp(-\mathrm{i}k_{a+}s) + H_{ea2}] , \\ H_{eb+} &= F_b[H_{eb1}\exp(\mathrm{i}k_{b-}s) - H_{eb2}] \\ H_{eb-} &= F_b[-H_{eb1}\exp(-\mathrm{i}k_{b+}s) + H_{eb2}] \end{aligned} \tag{21}$$

where

$$F = [\exp(\mathrm{i}k_-s) - \exp(-\mathrm{i}k_+s)]^{-1} . \tag{22}$$

Matrix $\mathbf{S}$ can now be obtained by rewriting the equation (17) as:

$$\mathbf{S} = \mathbf{H}_+\mathbf{H}_-^{-1} . \tag{23}$$

Sampling of acoustic variables is typically performed at a distance from the test object and the phase shift of the scattering matrix elements can be compensated as [22]:

$$\mathbf{S}' = \mathbf{T}_+\mathbf{S}\mathbf{T}_-^{-1} , \tag{24}$$

where $\mathbf{S}'$ is the modified scattering matrix moved to the test object. In equation (24), $\mathbf{T}_{\pm}$ can be expressed as:

$$\mathbf{T}_{+} = \begin{bmatrix} \exp(-\mathrm{i}k_{a+}l_a) & 0 \\ 0 & \exp(-\mathrm{i}k_{b+}l_b) \end{bmatrix}, \ \mathbf{T}_{-} = \begin{bmatrix} \exp(\mathrm{i}k_{a-}l_a) & 0 \\ 0 & \exp(\mathrm{i}k_{b-}l_b) \end{bmatrix}, \tag{25}$$

where l_a and l_b are the distances from the reference cross section to the test object.

The performance of the in-duct acoustic element is typically described by using one or two of the following values: noise reduction, insertion loss or transmission loss coefficient. The measurement of level difference or noise reduction (NR) is widely used in experimental work due to the simplicity of the method. The method does not require anechoic termination or knowledge of the source impedance. Noise reduction is the difference between sound pressure levels (SPL) measured in upstream and downstream of the acoustic element, and can be expressed as:

$$NR = 10 \cdot \log\left(\frac{p^2_{RMS,before}}{p^2_{RMS,after}} \right). \tag{26}$$

Insertion loss (IL) is defined as the change in SPL at the duct outlet:

$$IL = 10 \cdot \log\left(\frac{W_{ref}}{W_{all}} \right), \tag{27}$$

where W_{ref} is the transmitted sound power for a reference system e.g. straight duct and W_{all} is the measure with test object.

Wave decomposition described earlier, leads to the determination of the complex acoustic pressures from which transmission loss (TL) as the reduction of acoustic power can be determined. Since the transmission loss depends only on the properties of the test object and is independent of the source and radiation impedance, it is widely used in engineering to characterize intake and exhaust system components. The transmission loss is directly related to the transmission part of the S-matrix elements and can be calculated as follows [18]:

$$TL = 10 \cdot \log\left(\frac{W_{in}}{W_{tr}} \right) = 10 \cdot \log \begin{cases} \dfrac{(1+M_b)^2 A_b \rho_a c_a}{(1+M_a)^2 A_a \rho_b c_b |S_{12}|^2}, & \text{upstream} \\ \dfrac{(1+M_a)^2 A_a \rho_b c_b}{(1+M_b)^2 A_b \rho_a c_a |S_{21}|^2}, & \text{downstream,} \end{cases} \tag{28}$$

where ρ is the air density, M is the Mach number, A is the cross-sectional area of the duct, c is the speed of sound and W_{in}, W_{tr} are the incident and transmitted acoustic powers respectively.

In order to characterize two-port in terms of energy propagation, power reflection, power transmission and power absorption coefficients can be obtained from the $\mathbf{S}$ matrix elements as:

$$|R|^2 = \frac{(1-M_a)^2}{(1+M_a)^2}|S_{11}|^2 \ , \tag{29}$$

$$|T|^2 = \frac{(1+M_b)^2}{(1+M_a)^2}|S_{21}|^2 \ , \tag{30}$$

$$|A|^2 = 1-|R|^2-|T|^2 \ , \tag{31}$$

where M is the Mach number and S_{11} and S_{21} are the scattering matrix elements describing the reflection and transmission respectively.

1.2.2 Active two-port

Besides the passive two-port described in previous section, there can also be a sound source inside the two-port. If so, the passive acoustic two-port presented earlier (see equation (16)) should be modified as:

$$\underbrace{\begin{bmatrix} p_{a+} \\ p_{b+} \end{bmatrix}}_{\mathbf{p}_+} = \overbrace{\underbrace{\begin{bmatrix} S_{11} & S_{12} \\ S_{21} & S_{22} \end{bmatrix}}_{\mathbf{S}}}^{\text{Passive part}} \cdot \underbrace{\begin{bmatrix} p_{a-} \\ p_{b-} \end{bmatrix}}_{\mathbf{p}_-} + \overbrace{\underbrace{\begin{bmatrix} p^s_{a+} \\ p^s_{b+} \end{bmatrix}}_{\mathbf{p}^s_+}}^{\text{Active part}} \ , \tag{32}$$

where p^s_+ is the source vector describing the sound generation in a plane-wave range inside the two-port. To obtain the source vector, one more measurement, this time without external sources, is required. By following the procedure described by Lavrentjev et al. [22] the source strength part of the two-port can be determined by using the cross spectra only. They also validated the theory by using loudspeakers as a reference source and applied the theory on experimental investigation of a fan. Source vector was obtained with the following expression:

$$\mathbf{p}^s = (\mathbf{E}-\mathbf{SR})(\mathbf{E}+\mathbf{R})^{-1}\mathbf{p} \ , \tag{33}$$

where $\mathbf{E}$ is the identity matrix, $\mathbf{p}$ the measured pressures and $\mathbf{R}$ is the reflection in up- and downstream of the object:

$$\mathbf{p} = \begin{bmatrix} p_a \\ p_b \end{bmatrix}, \ \mathbf{R} = \begin{bmatrix} R_a & 0 \\ 0 & R_b \end{bmatrix}. \tag{34}$$

Since the data was obtained at different cross sections, the transformation relation similar to equation (24) is needed. As shown by Lavrentjev et al. [22] this can be done by using equation (25) as:

$$\mathbf{p}^{\mathbf{s}\prime} = \mathbf{T}_+^{-1}\mathbf{p}^{\mathbf{s}} \ , \ \mathbf{R}' = \mathbf{T}_+^{-1}\mathbf{R}\mathbf{T}_- \ , \tag{35}$$

where $\mathbf{R}'$ and $\mathbf{p}^{\mathbf{s}\prime}$ are the transformed reflection matrix and source vector respectively. The method to determine source vector was also studied and improved by Holmberg [23] by introducing the over-determination.

Since the method presented above is only valid for plane wave frequency region up to first cut-on frequency, sources which generate noise predominantly at higher frequencies e.g. automotive turbocharger, cannot be characterized by using described approach. The sound generation of automotive turbocharger in the plane wave region is mainly of interest for conditions close to surge, where low frequency noise is generated [24]. Beyond the plane-wave range, assuming that the reflections at the duct terminations are small or can be suppressed by spatial averaging, the strength of acoustic modes G_{++} propagating in the duct away from the source can be estimated as:

$$G_{++} = \mathrm{Re}\left[\sum_{m \to n} G_{mn} / N\right], \tag{36}$$

where mn is the pressure cross-spectrums between a pair of pressure transducers and N is the number of spectra.

The passive two-port measurement technique presented in equation (16) does not assume anechoic terminations. The quality of the active part will be improved if the reflection free terminations are used [25]. In practice, it is challenging to build perfectly anechoic terminations. It requires horns that become quite large in dimensions for low frequencies [26]. In the current study (in *Paper I* and *Paper II*) a termination with some absorption was obtained by using a commercial dissipative car silencer. To direct the flow, rubber hose was used after the silencers that even further decreased reflections. The typical reflection coefficients for this type of terminations are presented in Figure 6.

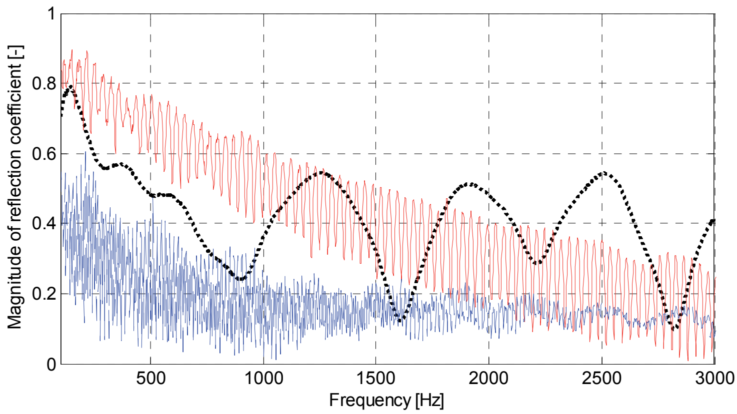

Figure 6. Anechoic termination measurement results: black dotted line is dissipative silencer, red and blue solid lines represent rubber hose with length of 4.7 m and 18.7 m respectively

As can be seen in Figure 6, a good result could be obtained from an 18.7 m rubber hose. The oscillations in the results correspond to the length of the hose. To measure the noise generated above the plane wave range, combination of rubber hose with the dissipative silencers could be used, giving the improved reflection for higher frequencies. It must be also noted here that during the measurement session there are also loudspeaker sections connected via side-branches to the inlet and outlet ducts. Giving extra reflection, these side branches should be designed as short as possible or be removed when the loudspeakers are not actively used.

Instead of direct (with an external source) method [27] described in the previous section, the two-port can be described also by multi-load methods (without an external source) [28]. Although the external source method provides better control of the sound spectrum, it is typically used in cases, where the acoustic field created by external loudspeakers is not suppressed by background noise [23].

At least two independent test cases with different load configurations [29] are necessary to obtain four unknown scattering-matrix complex values (see equation (37)). The over-determination of the measurement cases, initially suggested by Åbom [30] and experimentally tested by Allam et al. [31], can be used to improve measurement quality and can be expressed as:

$$\underbrace{\begin{pmatrix} p_{a+}^{I} & p_{a+}^{II} & \cdots & p_{a+}^{N} \\ p_{b+}^{I} & p_{b+}^{II} & \cdots & p_{b+}^{N} \end{pmatrix}}_{\mathbf{P}_{+}} = \underbrace{\begin{pmatrix} S_{11} & S_{12} \\ S_{21} & S_{22} \end{pmatrix}}_{\mathbf{S}} \underbrace{\begin{pmatrix} p_{a-}^{I} & p_{a-}^{II} & \cdots & p_{a-}^{N} \\ p_{b-}^{I} & p_{b-}^{II} & \cdots & p_{b-}^{N} \end{pmatrix}}_{\mathbf{P}_{-}}, \tag{37}$$

where $J = I, II \ldots N$ in superscript denote pressure amplitudes from different load cases. To obtain the scattering matrix from equation (37), the Moore-Penrose inversion algorithm can be used.

1.2.3 Enhanced external sources

In harsh measurement conditions, determination of the pressure signals can be a challenging task. To improve signal to noise ratio, similar to the study of Johnson and Fuller in [32], a number of external sound excitation sources can be applied simultaneously in order to maximize sound pressure level in the duct. In the current study, acoustic excitation was provided by powerful electro-dynamic driver (DAS ND-8) driven by a software-based signal generator trough the amplifier. The drivers were equipped with titanium diaphragm to avoid dome fracture due to mechanical fatigue and equipped with neodymium magnets for negligible magnetic strength loss at the highest operating temperatures.

The loudspeakers were modified to operate in high static pressure (up to 4 bar) and temperature (up to 200 °C) conditions. To avoid damage to the membrane due to sudden static pressure changes, the front and back of the driver was connected with a narrow tube to equalize the pressure. It was vital to remove all leakages trough the loudspeaker casing especially with high temperature conditions, where the flow through the casing can heat up the driver. Because of the heat transfer from the duct, the drivers were equipped with water-cooling units, mounted between duct and loudspeaker (see Figure 7). This solution gave the cooling capacity necessary to keep the temperature in a nominal range over a long period of time.

In *Paper I*, external source method was used to characterize the passive acoustic properties of an automotive turbocharger turbine, working at realistic operating conditions. To be capable to dominate over the high background noise levels, three excitation sources were used simultaneously to increase the SPL. To avoid pressure minimum occuring for all drivers at the same time, separation according to “golden cut ratio” was used. Electro-dynamic drivers were connected with the duct via side branches with minimal length in order to reduce reflections from the sudden area change. At the flow duct, perforated connecting area (>30% to be acoustically transparent) was used to retain the flow profile and reduce flow instabilities.

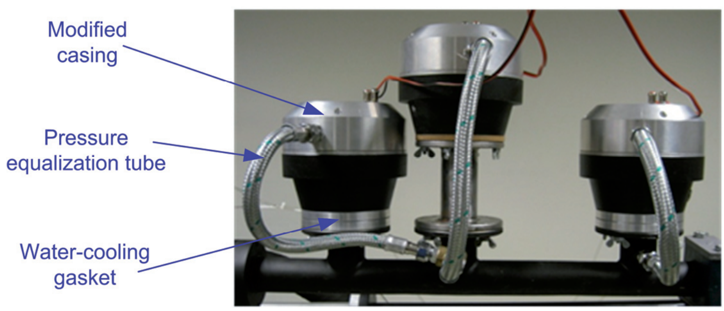

Figure 7. Picture showing the electro-dynamic drivers (with modifications) used as an acoustic external source

Because of the separation between the drivers, wave cancellation at certain frequencies would occur. To ensure resulting waves to interfere constructively, phase shift to the source signal driving the loudspeaker was applied. For all frequencies measured, one loudspeaker was considered as reference. Phase difference relative to the other two was measured by comparing the transfer functions from the loudspeaker input voltage to the microphone response (see Figure 8). This phase difference was applied during the actual measurement, to correct the signals fed to the loudspeakers.

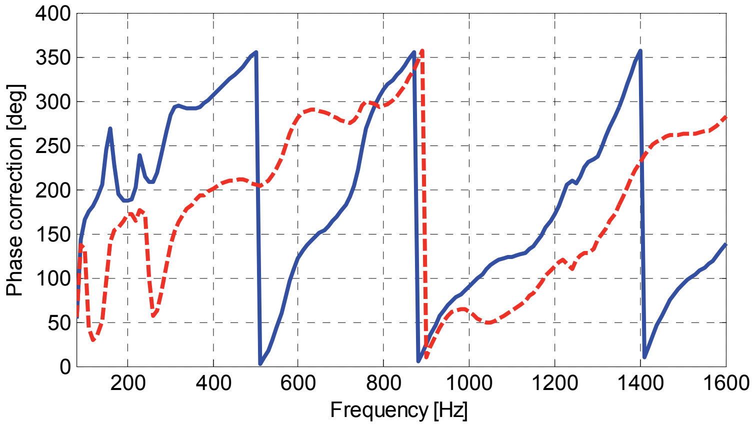

Figure 8. Phase shift measured between two loudspeakers relative to the first loudspeaker

The results before and after applying the phase compensation can be seen in Figure 9. By using all three loudspeakers and the phase shift technique, the sound wave amplitude propagating in the positive direction is maximized as expected.

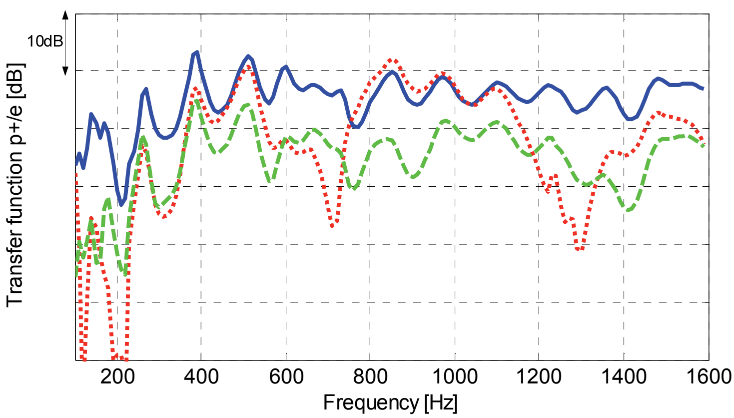

Figure 9. Pressure wave amplitude propagating in positive direction (p+) relative to loudspeaker voltage (e): one loudspeaker was playing (green dashed line), three loudspeakers without phase shift calibration (red dotted line) and three loudspeakers by applying phase shift (blue solid line)

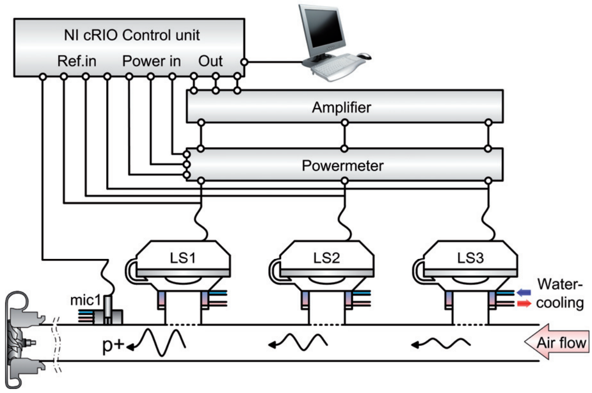

Figure 10. Test-rig to find maximum p+ value

In order to get the maximum sound pressure level (SPL) from the loudspeakers, it was important to run these drives close to maximum excitation level. Here this was defined as a certain maximum electric power fed to the loudspeakers, which will guarantee that they are not overloaded and damaged. To measure the power output fed to each speaker a custom made power meter was used (see Figure 10). Due to the variation in input impedance at the different loudspeaker positions the actual power fed to the speakers can vary significantly (see Figure 12). To keep a constant level for all excitation frequencies as close as possible to the maximum allowed, a proportional-integral-derivative (PID) feedback loop was set using the NI cRIO unit. As the name suggests, a PID algorithm consists of three basic parts - multiplication with a constant, integration and differentiation, where the constant and the time scales for integration and derivation are set to minimize the error (see Figure 11). The error, being the difference between the actual and the desired output of the system under control, was here the power fed to a loudspeaker. The PID output signal was then used to modify the voltage signal output from the NI cRIO unit which via the amplifier drives the loudspeakers (see Figure 10).

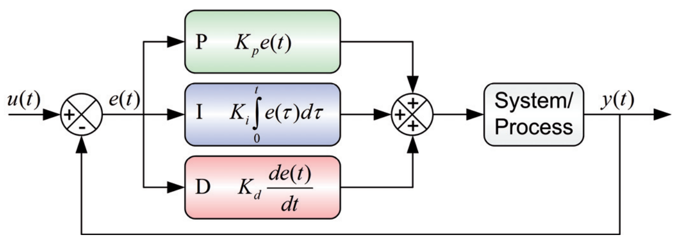

Figure 11. Block diagram of a basic PID control algorithm where $u(t)$ is the set point, $e(t)$ is the error and $y(t)$ is the process variable

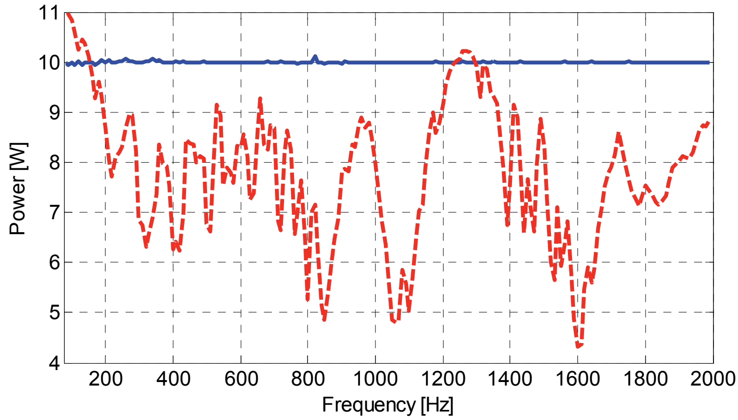

Figure 12. Loudspeaker power without controlling (red dashed line) and by using PID function (blue solid line). The prescribed power is set to 10 W

Figure 12 represents a typical example of how the PID control acts under measurements, keeping the power to the preset maximum (10 W). The two steps described in this section, i.e., the phase compensation and PID control are done for each frequency step just before the actual measurement starts. This phase calibration and amplitude (power) adjustment operation takes less than ten seconds before the measurement can start at a given frequency.

All the improvements described above made it possible to use the external source method in harsh conditions, to experimentally determine scattering matrix properties of the acoustic two-port.

Another improvement proposed and experimentally evaluated was external source method with simultaneous excitation. In harsh measurement conditions present in *Paper I* and *Paper II*, due to the unstable conditions (variation in temperature, pressure etc.), time to extract acoustic data was kept minimum to reduce measurement error.

With two-port model, to reduce the measurement time, both acoustic sources in the inlet and outlet side can be excited at the same time. To implement this technique a stepped sine excitation was used, where all the sound energy is concentrated into a single frequency, thus improving the signal-to-noise ratio. In *Paper I*, 20 was considered as an adequate number of averages to obtain the acoustic data. Both measurement cases to obtain the state variables for two-port model are performed simultaneously and the final result is combined from those two cases. The use of parallel excitation for two-port measurements has also been discussed by Pedrosa et al. [33] where uncorrelated white noise (WN) signals are used to excite the system. In the current study, white noise as an excitation signal was found to be unsuitable for measurements in harsh conditions, indicated also by the decreased coherence value in the experiments.

With external source method together with simultaneous excitation it was possible to reduce time for measurements and in the same way error in the result due to variations of the operating point (see Figure 22 and Figure 23). By using the simultaneous excitation method, it was possible to reduce the time for a measurement by a factor two or alternatively take twice as many averages.

In order to reduce measurement time a multi stepped sine (MSS) excitation technique was proposed and tested. The method was implemented in *Paper IV* in one-port model to determine acoustic pressure reflection from duct opening in a presence of high flow velocity. With this method a number of uncorrelated sine waves will be excited simultaneously and transfer functions will be calculated from the same data by using sine waves as different reference signals. The method was tested with five frequencies excited simultaneously (see Figure 4) where good compromise between the signal to noise ratio and the measurement time was achieved.

It should also be mentioned, that MSS method can be also implemented on two-port models, where together with simultaneous excitation technique presented earlier, considerable advantage over the conventional excitation technique can be achieved.

2 CHARACERIZATION OF INDUCT ACOUSTIC ELEMENTS

Besides the silencer, especially designed to reduce the noise level of the IC-engine, modern exhaust systems are equipped with many other components for various purposes. All these components, starting from the engine and ending with the tailpipe in the exhaust system, or the air intake on the inlet side, have an influence on the propagation of sound waves. To determine the sound radiation from an intake or exhaust system, knowledge about acoustic performance of all its components is essential.

2.1 Experimental setups

Acoustical methods presented in the previous chapter were used to experimentally characterize elements from automotive exhaust systems. Dedicated test-rigs were developed to determine properties of three induct elements: automotive turbochargers, catalytic converters and duct termination.

2.1.1 Test-rig for automotive turbocharger

Experimental investigation of acoustics of automotive turbochargers, presented in *Paper I* and *Paper II*, was performed at Royal Institute of Technology (KTH) Competence Centre of Gas Exchange (CCGEx) in Sweden. Within the laboratory of KTH CCGEx, acoustic test-rig was developed and used for complete acoustic characterization of automotive turbochargers. In particular, the passive and active acoustic effect of turbocharger compressor and turbine was investigated by implementing the acoustical two-port theory presented above.

A turbocharger is a force induced device to afford greater power output from an engine of given size. This increase in power output, compared to the naturally aspirated engines, is achieved because of the forced air (also proportionally more fuel efficiently burned) in the combustion chamber and can be expressed by the following equations [34]:

$$P = \frac{\eta_f \cdot \eta_v \cdot N \cdot V_d \cdot Q_{HV} \cdot \rho_{inl} \cdot F_{f/a}}{2} , \tag{38}$$

$$T = \frac{\eta_f \cdot \eta_v \cdot V_d \cdot Q_{HV} \cdot \rho_{inl} \cdot F_{f/a}}{4\pi} , \tag{39}$$

where P and T are the power and torque output of the engine, η_f and η_v the fuel conversion and volumetric efficiencies, Q_{HV} is the lower fuel heating value, ρ_a is the inlet air density and $F_{f/a}$ is the fuel/air ratio. As can be seen, turbocharging will increase the maximum power and torque by increasing ρ_a, whereas the other parameters remain constant.

In Figure 13, main parts of an exhaust driven turbocharger are shown. A centrifugal compressor is composed of a static inlet, an impeller with blades, a diffuser and a compressor housing (volute) to direct compressed air to the engine. The turbine wheel, used to convert exhaust energy into shaft power to drive the compressor, is surrounded by the turbine housing that collects exhaust gases and a nozzle with standing or moving blades, to direct them to the turbine wheel.

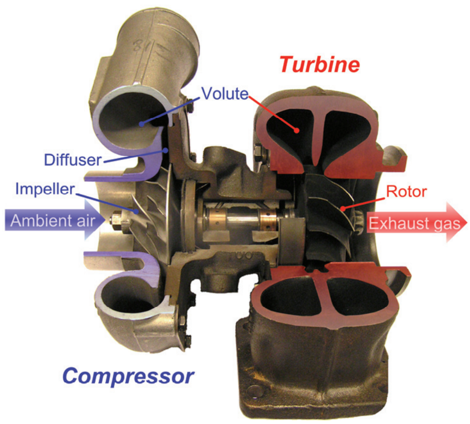

Figure 13. Cut-away view of a turbocharger with a centrifugal compressor (left) and a radial turbine (right)

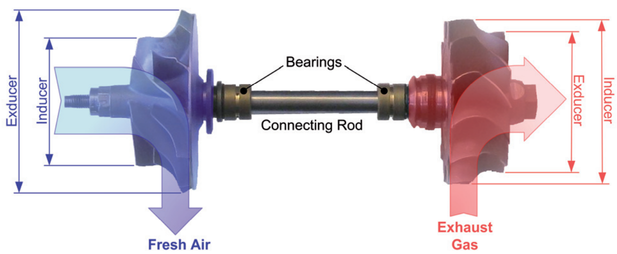

Figure 14. Turbocharger rotor assembly with the characteristic parameters

The main components of the rotor assembly are impeller, rotor and connecting rod (see Figure 14). The inducer diameter is defined as the diameter where the air enters the wheel and the exducer diameter where the air exits the wheel. Based on aerodynamics and air entry paths the inducer for a compressor wheel is the smaller diameter, whereas for a turbine wheel the inducer is the larger diameter. Trim is a common term used to express the relationship between the inducer and exducer. For both, turbine and compressor wheels, trim is calculated as:

$$Trim = (Inducer / Exducer)^2 \cdot 100 \ . \tag{40}$$

Another geometric characteristic used to describe turbocharger housing size is A/R (Area/Radius - see Figure 15) ratio, defined as the inlet (for compressors discharge) cross-sectional area divided by the radius from the turbocharger connecting rod centerline to the centroid (perpendicular of that area).

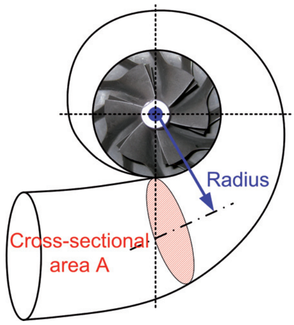

Figure 15. Illustration of housing showing A/R ratio

In order to describe the performance characteristics of a particular turbocharger, the compressor and turbine maps are introduced. In Figure 16 an example of typical compressor map with the main components is shown.

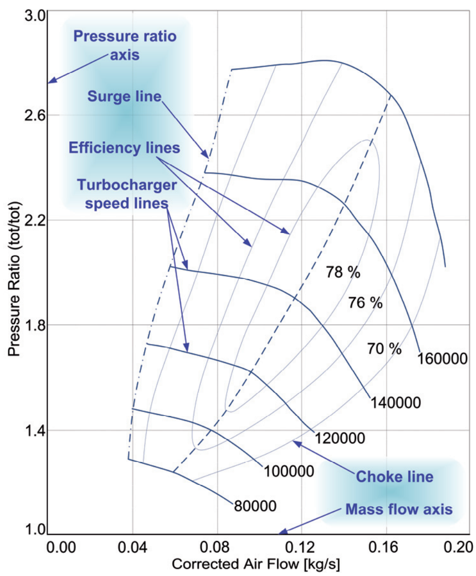

Figure 16. Example of the parts of the compressor data map

Corrected mass flow rate on the x-axis of the compressor map in Figure 16 represents the mass of air flowing through a compressor per second and can be calculated as:

$$W^* = W\sqrt{(T_{1c} + 273.15)/302.78}\,/\,(p_{1c}/96.17)\,, \tag{41}$$

where T_{1c} is the temperature and p_{1c} is the absolute pressure in compressor inlet respectively. Pressure ratio on the y-axis is defined as the absolute outlet pressure (compressor discharge pressure) divided by the absolute inlet pressure. Turbocharger speed lines are lines of constant speed and between these lines, speed can be estimated by interpolation. By increasing the turbocharger rotational speed, the pressure ratio- and/or mass flow rate increases. These three parameters have mainly been used in this thesis to describe the operational points of the turbocharger during the acoustic measurement.

The surge line is defined as the left hand boundary (see Figure 16) of the compressor map. The region on the left of this line represents flow instabilities and can lead to premature turbocharger failure due to heavy thrust loading. To keep the compressor out of surge bypass or blow-off valves are used. These valves allow the airflow, at critical conditions, to be re-circulated back to the compressor inlet or directed to the atmosphere.

The choke line is the right hand boundary of the compressor map (see Figure 16). Choke is typically defined by the line where the efficiency drops below a certain level but also related to the fact that choked flow conditions are reached. Beside the surge line on the left and choke line on the right, the compressor map is also limited by the maximum rotational speed line on the top.

Finally, efficiency lines are concentric regions on the maps where the line near the center represents peak efficiency and as the rings move out from center, the efficiency drops until the surge and choke limits are reached. The most efficient area is typically indicated by the line between the surge and choke line.

The acoustic test-rig for automotive turbocharger, developed at KTH CCGEx laboratory, was operated by supplying turbine with dried compressed air. Test-rig was connected with the compressors and tanks stored away from the laboratory through a duct system. In order to run the test-rig in stable conditions the installation was capable to maintain a stable mass-flow up to $\dot{m} = 0.5\ kg/s$ with pressure fluctuation less than 1%. In addition to the flow rate measurements in acoustic rig, the mass flow rate of the compressed air was also accurately measured by a hot film flow meter (ABB FMT500-IG) connected to the laboratory inlet line. In the laboratory, upstream the test-rig, the air passes an 18 kW electric heater connected to the duct-work. The temperature of the compressed air entering to the turbine was increased up to 100 °C to avoid the temperature from dropping below the dew point downstream the turbine. The temperature of the compressed air was automatically set and maintained by a custom-built PID controller module with temperature fluctuations less than 1%. The status of the acoustic test-rig, developed during the studies, is shown in Figure 17.

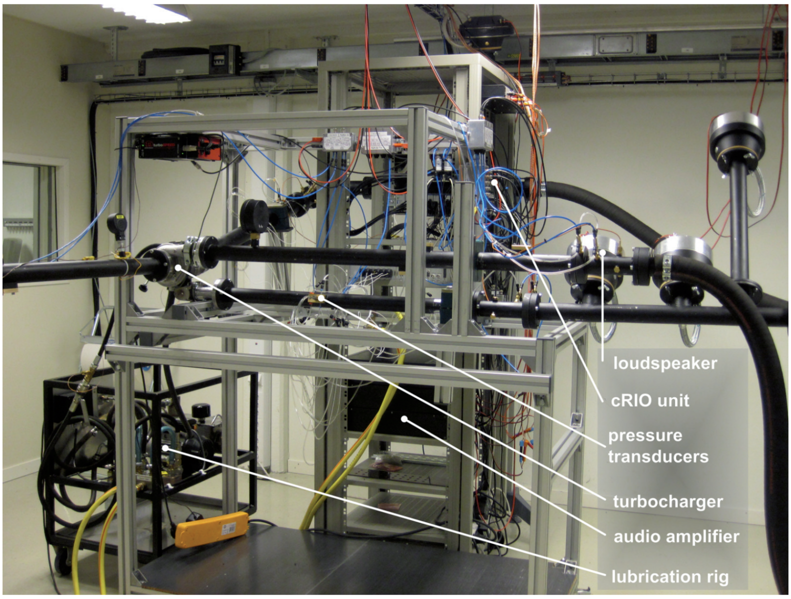

Figure 17. Photo of the test facility in KTH CCGEx laboratory implemented for investigations of automotive turbochargers

Experimental characterization of the acoustical properties of turbochargers is a challenging task, especially at the operating conditions where devices like turbochargers are designed to work. The test-rig was designed for complete acoustic characterization, including both the compressor and turbine of the turbocharger. To apply the acoustic two-port measurement technique a number of aspects had to be considered. Because of the harsh environment inside the duct, stronger acoustic excitation had to be developed in order to improve the signal-to-noise ratio, especially for turbine measurements. Other improvements were related to the quality of the measured data by implementing a two-source method with simultaneous excitation and better anechoic terminations. Measurement system was developed as a fully automated, where all test parameters (temperatures, pressures, RPM, flow speeds etc.) were saved automatically for later analysis.

2.1.2 Test-rig for measuring acoustic properties of CC elements

In *Paper III*, a dedicated test facility (see Figure 18) was designed in Tallinn University of Technology (TUT) research laboratory of Chair of Automotive Engineering, to determine the acoustic two-port data of the catalytic converter honeycomb elements (see Figure 29) in realistic operating conditions. The honeycomb was mounted into the test section by using the flanged steel ducts so that the duct diameter was constant (42 mm) for all the samples.

To measure the CC elements close to realistic operating conditions, air flow up to 60 m/s was generated by using the two-stage high pressure blower. Directly after the blower, electric heater unit was used to heat the flow up to 200 °C. Pitot-tube and K-type thermocouples were centrally mounted into the center line of the test duct for the flow and temperature measurements. Water-cooled piezo-resistive pressure transducers, conditioned and amplified by the dynamic signal analyzer, were used to perform the acoustic wave decomposition. Acoustic excitation was provided by using an electro-dynamic drivers and WN signal. Signal acquisition and the acoustic excitation were controlled by PC-based virtual instrument developed in LabVIEW.

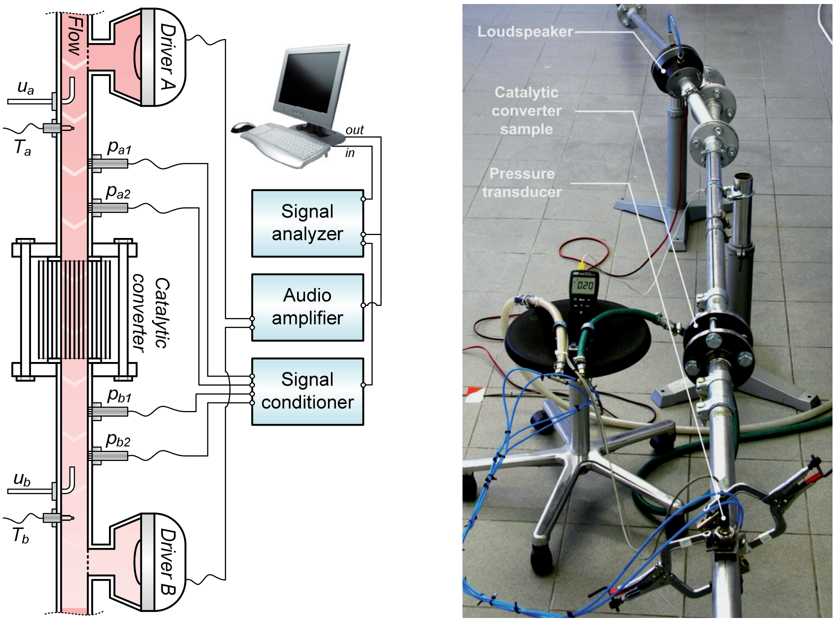

Figure 18. Drawing (left) and picture (right) of the experimental set-up test section, designed for acoustic characterization of catalytic converter samples in hot mean flow conditions

2.1.3 Test-rig for open duct termination

In *Paper IV*, a dedicated test-rig (see Figure 19 and Figure 20) was developed in TUT, research laboratory of Chair of Automotive Engineering, to investigate the acoustic wave reflection in air jets with temperatures ranging from room temperature up to 200 °C and flow speeds up to 130 m/s $(M = 0.3)$. Measurements were carried out in a 2.0 m long stainless steel circular test duct with an inner diameter of $d = 0.042$ m and 1.5 mm wall thickness. A jet exhausting out of the termination was generated by high pressure centrifugal blower (Kongskilde 300TRV) driven by a 22 kW electric motor. The outlet from the blower was equipped with a vibro-damper and a commercial ventilation silencer to suppress the flow fluctuations. To heat the airflow originating from the blower a 22.5 kW electric heater unit, installed to the stagnation chamber with a volume of $0.15\ m^3$, was used. The temperature of the exhausting jet was automatically set by a custom-built PID controller module.

Acoustic excitation was provided by an electro-dynamic driver (DAS ND-8) via the power amplifier (Velleman VPA2100MN). Electro-dynamic driver, mounted into a side branch of 0.2 m and diameter of 0.042 m, positioned 30 duct diameters away from the duct opening allowed to assume fully developed turbulent flow profile. The driver was controlled by custom built software based signal generator (LabVIEW).

To measure acoustic and static pressures, ¼ inch piezo-resistive pressure transducers (Kulite WCT-312M-25A) with signal conditioner (Dewetron) were used. The pressure transducers were flush mounted to the inner duct walls and evenly distributed around the duct cross-section. Due to the high temperature conditions during the tests (200 °C) all the sensors were water cooled. Signal acquisition was performed by a NI signal analyzer PCI-4474 and a purpose built PC based virtual instrument in LabVIEW.

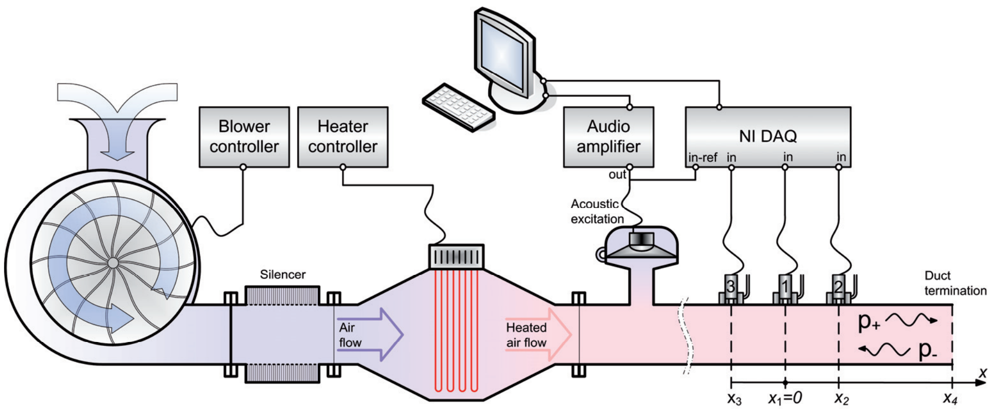

Figure 19. A sketch of the experimental set-up for the measurements in TUT

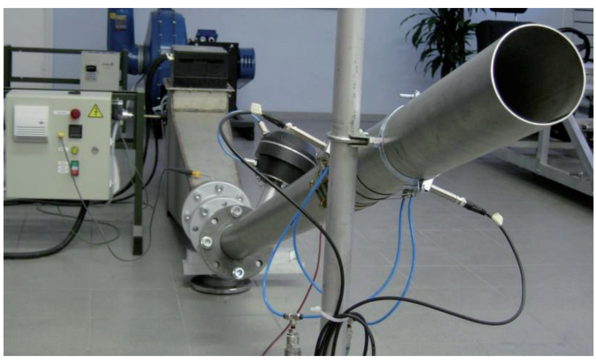

Figure 20. A photo of the experimental set-up used for the measurements of acoustic wave reflection at the duct termination

To further improve the quality of the measured acoustic data, measurements were performed in a room with sound absorbing walls and ceiling. In addition, sound reflection from the floor [35] and duct wall vibrations induced by electro-dynamic driver [15] were considered.

Accuracy of the measured reflection coefficient also depends on the determined state conditions e.g. temperature, speed of sound, flow velocity etc. For the experimental determination of flow profile a Pitot tube with outer diameter of 3 mm and inner diameter of 1 mm together with micro-anemometer (Delta Ohm HD 2164.0) was used. The flow velocity profiles perpendicular to the centre axis of the duct were determined at the transducer reference cross-section, at points evenly distributed over the diameter of the duct. Another thermometer (TES-1312) with a K-type thermocouple was used to determine the room temperature.

If the properties of the gas (e.g. air) are known, simple empirical equations can be used to calculate the speed of sound. In a number of practical applications however, due to unknown or non-stationary gas chemical content, temperature, pressure and humidity, the actual wave numbers are unknown. To obtain the acoustic pressure wave amplitudes and speed of sound, a three-microphone procedure (see equations (13 - 15)) can be used. To evaluate the theory, experiments were performed for three different gas environments (argon, air, helium) [13]. In addition to the speed of sound, the theory can be also applied in flow ducts to determine the flow velocity.

2.1.4 Acquisition and control system

Due to the complexity of the measurement process a purpose built program for data acquisition (DAQ), post processing and measurement control was developed (see Figure 21). Developed programs, for the measurements in *Papers I-IV*, were operated via the National Instruments (NI) measurement hardware and PC based virtual instruments programmed in LabVIEW.

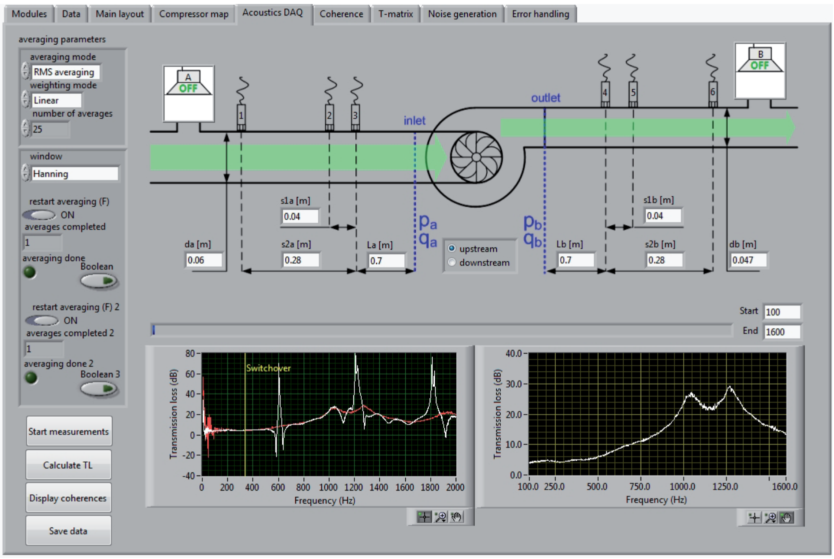

Figure 21. GUI for the turbocharger test-rig

Together with NI cRIO, different modules were used for data acquisition. For acoustic and static pressure signals acquisition NI 9234 and NI 9205 modules were used. The NI 9211 module was used to measure thermocouple signals from K-type thermocouples. In order to monitor rotational speed an eddy-current speed measurement system (DZ135) together with the NI 9401 module was used.

To control the loudspeakers, sine wave and random acoustic excitation was provided by software based signal generators in the NI cRIO through the NI 9263 module. This solution gave the flexibility to entirely control drivers e.g. by applying phase shift technique, source level calibration, parallel excitation technique, MSS technique etc. NI 9263 module was also used to adjust the boost pressure by using an electronically controlled throttle valve.

To increase the accuracy the entire measurement process was computer-based and fully automated. Besides acoustic data, all the parameters were monitored in real time and saved for later analysis. An example of deviation in measurement conditions during the averaging of acoustic data can be seen in Figure 22 and Figure 23. During the measurements all calculated results were plotted in real time - directly after the measured data was available.

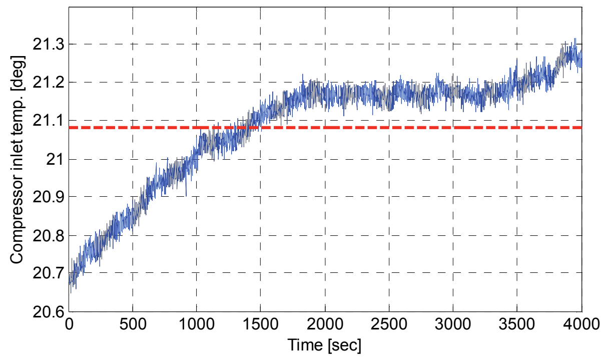

Figure 22. Temperature drift in the turbocharger compressor inlet duct: measured temperature (blue solid line) and averaged temperature (red dashed line)

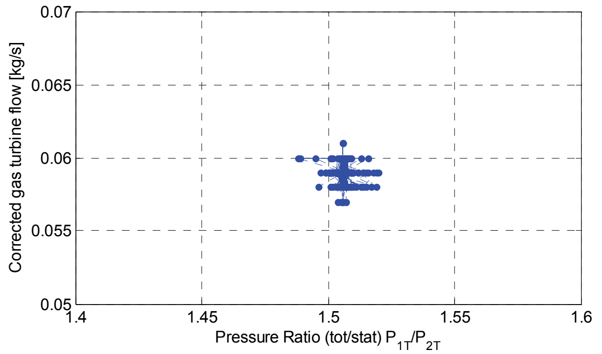

Figure 23. An example of deviation of the turbine operating point during a measurement

2.2 Acoustics of turbochargers

The acoustics of any fluid machine [19], for instance a turbocharger, can be separated in to the active and passive part. The passive properties (reflection and transmission) refer to the scattering of acoustic waves, while the active represents the sound generation of the machine. The reflection and transmission at a fluid machine will be affected both by variations in geometry (area changes) as well as changes in temperature (speed of sound) and density, in addition flow related losses will create acoustics losses. The transmission part of the scattering, often expressed in dB-s as a so called transmission loss (TL), can be directly related to the damping of sound waves passing the machine. For turbochargers one issue of interest is the added damping for pressure waves originating from the engine. This means that for the turbine the TL in the downstream direction and for the compressor in the upstream is of interest. A turbocharger is also a sound source producing high frequency aerodynamic noise. Because of the relatively good damping characteristics of modern silencers on the exhaust side, the noise of the turbocharger is believed to mainly originate from the intake side. Although the noise from the compressor can effectively be reduced by air intake filters, high frequency tones can still radiate from the ducts connected to the compressor.

Relatively few studies have been performed in the field of centrifugal compressors and much of the theory of the sound generation mechanisms comes from the study of axial fans. In the overview of turbocharger acoustics [36] Rämmal and Åbom included a summary of the aerodynamic sound generation mechanisms in rotating machines. In [37] Raitor and Neise performed an experimental study on a larger centrifugal compressor and measured the radiated sound field up to 50.000 RPM. It was concluded, that the main aerodynamic noise generating mechanisms are tonal noise at BPF, buzz-saw noise and blade tip clearance noise. For normal operation the BPF is usually dominating the noise from turbochargers, in particular on the compressor side. This is true for heavy duty vehicles, but for light duty vehicles, because of the high RPM of the turbochargers, the BPF will be above the audible range. The buzz-saw noise appears at supersonic tip speeds and is associated with shock waves moving with the blades. This produces a set of harmonics at multiples of the RPM [37]. Tip clearance noise is associated with secondary flow effects around the blade tip or flow separation at the blade [37]. These effects are in particular important at low mass flow rates and close to the surge line and will cause a broad band peak typically at around 50% of the BPF.

In *Paper I* and *Paper II* an investigation of automotive turbochargers acoustics is presented. In *Paper I* results for the passive acoustic effect are presented for three turbocharger compressors A, B and C (see below in Figure 24 and Table 1) and turbocharger B and C turbines. In *Paper II* analysis of active measurement results of the turbocharger B compressor are also presented.

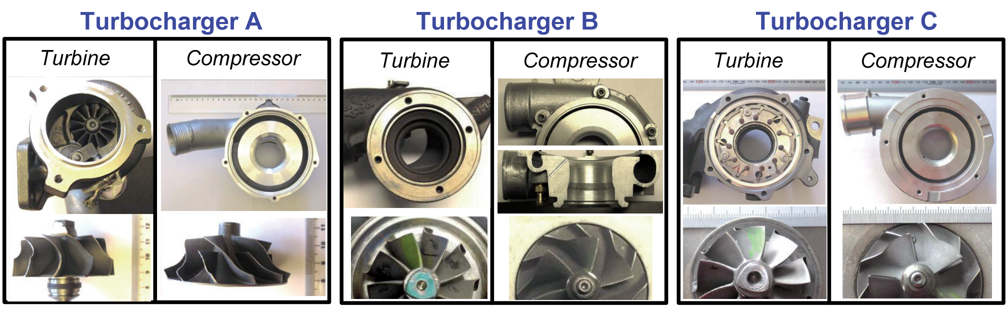

Figure 24. Photos of the turbine and compressor of turbochargers A, B and C

Table 1. Technical data of the three turbochargers investigated

Turbocharger	KKK K24	Garret GT1752	Garret GT1749V
	A	B	C
Turbine			
A/R ratio	0,41	0,47	0,42
Scroll inlet diameter [mm]	52	40	43
Approximate scroll length [mm]	300	285	380
Number of rotor blades	12	9	9
Radius of the rotor [mm]	29	22	21
Rotor length [mm]	21	20	25
Compressor			
Scroll outlet diameter [mm]	41	43	38
Approximate scroll length [mm]	460	358	370
Number of rotor blades	6+6	6+6	5+5
Radius of the rotor [mm]	31	26	25
Rotor length [mm]	25	20	18

Turbocharger A was a Volvo car turbocharger KKK K24, also used for the compressor passive measurements performed by Rämmal [38]. Compared to turbocharger A, turbocharger B was smaller in dimensions (see Table 1).

Turbocharger C was a variable turbine geometry (VTG) type and both compressor and turbine passive properties were characterized. Three different turbine inlet geometry settings (VTG positions) were tested. First, the VTG was kept closed which is used in practice to raise the pressure upstream of the turbine, thus the exhaust gas energy is raised at low engine speeds. Secondly, a fully opened VTG position was used, corresponding to high engine speeds to avoid over-boosting and high engine backpressure. Thirdly, a position was chosen where the VTG was kept 50% open.

2.2.1 Passive part

In order to determine the working conditions of the turbocharger an operating map provided by the manufacturers was followed (see Figure 16). Different static operating points (OP) were selected to systematically cover the region of the map where the turbocharger is normally operated. Transmission loss data up to the cut-on frequency at different operating points for turbocharger B compressor can be seen in Figure 25.

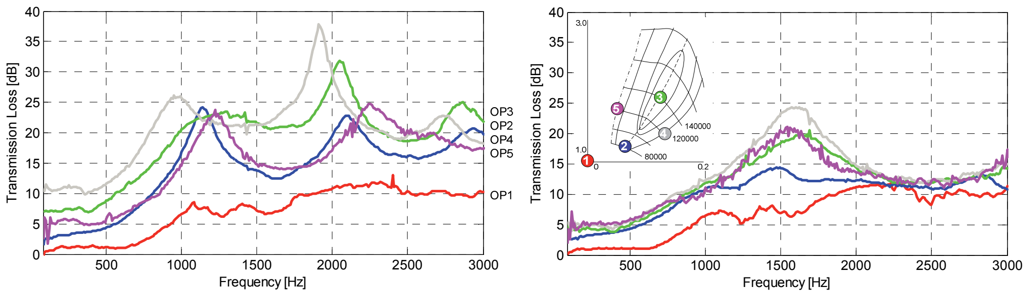

Figure 25. The transmission loss for the turbocharger B compressor where red line represents OP1, blue line is OP2, green line is OP3, grey line is OP4 and purple line is OP5, respectively

All the results for the passive acoustic effect for turbocharger turbines and compressors are presented in *Paper I* and *Paper II*. In order to generalize and make results useful for any turbocharger independent of size (see Figure 26), the results were plotted against the Helmholtz-number $(He = ka = 2\pi fa / c)$. To calculate the Helmholtz number, an average value of the inlet and outlet duct data was used for the radius and the speed of sound.

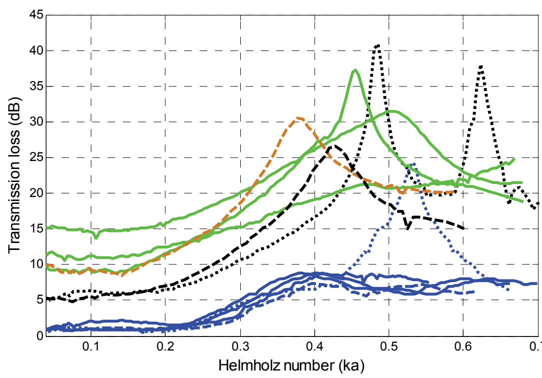

Figure 26. The transmission loss results for different turbocharger compressors (upstream direction) and turbines (downstream direction) as a function of the Helmholtz-number

In *Paper I*, based on Figure 26 it was concluded that for the low frequency region $(He < 0.2)$ the transmission loss (TL) level, which is almost constant, is determined by the losses and the value will increase with mass flow. The mid-frequency region $(0.2 < He < 0.35)$ gives an increase, which is determined by the inner free air volume of the unit that acts as a small expansion chamber silencer. This means, the larger the volume, the faster the increase. In the high frequency range $(He > 0.35)$ TL peaks start to appear, associated with resonances due to open/closed bypass gates and with cancellation associated with different sound paths through the blade sections [39].

2.2.2 Active part

In *Paper II* the sound generated by the compressor was investigated. Experiments were performed on the turbocharger B compressor to obtain the radiated pressure spectra.

In Figure 27, a comparison of sound pressure spectral densities between OP3 and OP4 is shown. Two operating points have been measured by using the same mass flow rate but the RPM level was different. The difference between the results is mainly a shift in the blade passing frequency (BPF) peaks:

$$BPF = n \cdot RPM / 60 \,, \tag{42}$$

where RPM is rotational speed per minute and n is number of blades. Besides the impeller BPF, which was the main source of noise, RPM harmonics can be detected and the second highest mode was at double BPF. The broadband noise is more or less unchanged except for a 5 dB increase for OP3 on the outlet side.

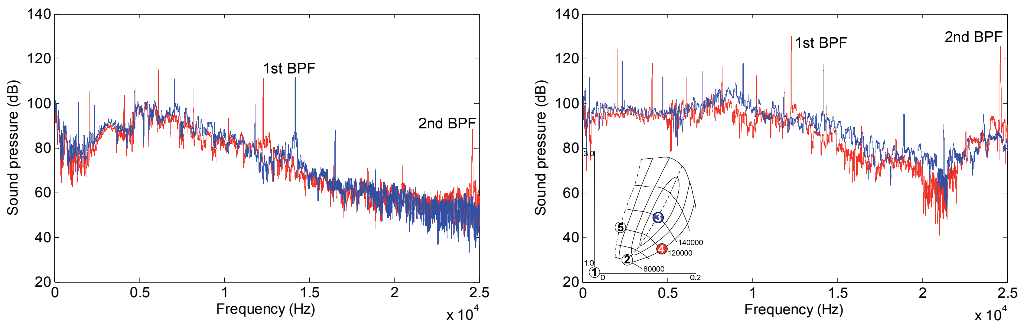

Figure 27. Comparison of sound pressure spectral densities between OP3 (blue line) and OP4 (red line) in inlet side (left) and outlet side (right)

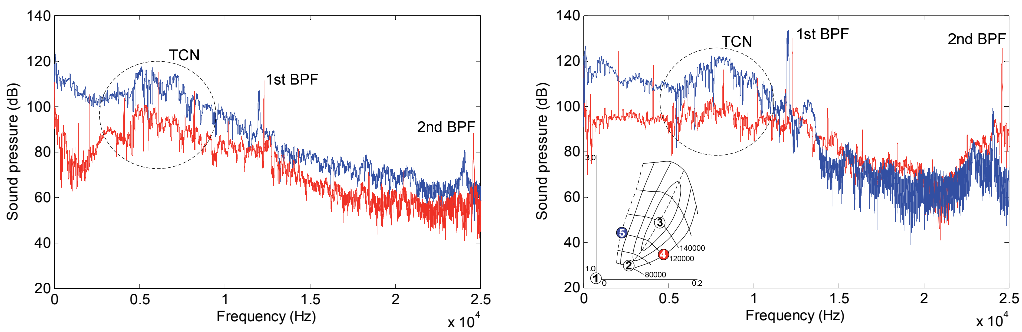

Figure 28. Comparison of sound pressure spectral densities between OP4 (red line) and OP5 (blue line) in inlet side (left) and outlet side (right)

A comparison of sound pressure spectra densities between OP4 and OP5 (constant RPM) is shown in Figure 28. Close to the surge line (OP5) the tip clearance noise becomes more dominant. Up to 10000 Hz the average difference between the OP4 and OP5 auto-spectrum levels is as large as 20 dB.

2.3 Catalytic converters (CC)

In order to correspond to more strict exhaust emission standards, modern IC engine has to be coupled with CC elements. Although the main purpose of CC is to reduce harmful emission by chemical reactions to convert toxic combustion products to less-toxic ones, they will also affect the acoustic emission of the IC engine. To meet legislations for the noise emission it is important to design effective acoustic systems where the knowledge of the sound propagation in these elements is essential.

The purpose of the study in *Paper III* was to develop a measurement technique to provide an accurate data for further numerical studies. Instead of measuring complete unit, the element from the CC was detached and studied separately by giving an opportunity to measure acoustical performance caused by the viscous-thermal losses in the narrow tubes. For the investigation, two different CC honeycomb materials (ceramic and metal core) were used (see Figure 29), both with the same length (76 mm) and cell density (400 CPI). Measurements were carried out up to flow velocity typical for exhaust duct of operating IC-engines. Due to the limited heating capacity, the temperature used for the measurement reached up to 200 °C, representing conditions typical for engine idling.

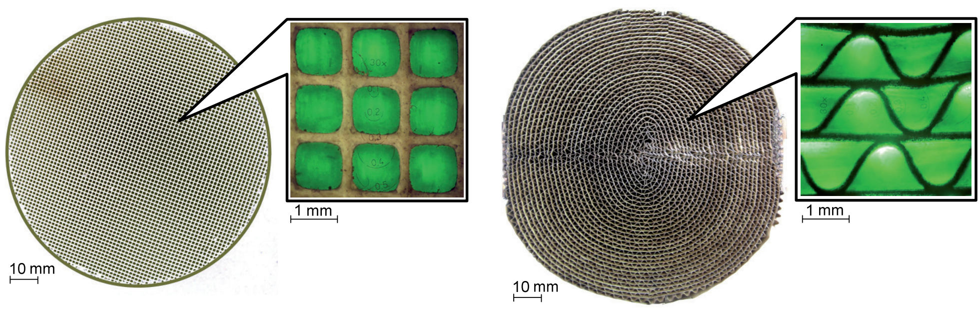

Figure 29. A photo and magnified microscope image of the catalytic converter samples studied; ceramic core (left) and metal core (right)

In *Paper III* the experimentally determined transmission loss results for ceramic and metal core catalytic converter elements are presented (see Figure 30). Compared to the metal core, ceramic CC element offers a relatively higher transmission loss with maximum attenuation up to 7-8 dB around 1000-1200 Hz. By increasing the mean flow velocities, the transmission loss tends to increase over the frequency band for both CC cores, because of the losses in the flow separation in capillary tubes. For ceramic honeycomb a peak shift for higher frequencies by increasing the temperature can be explained by the change of speed of sound in the measurement section.

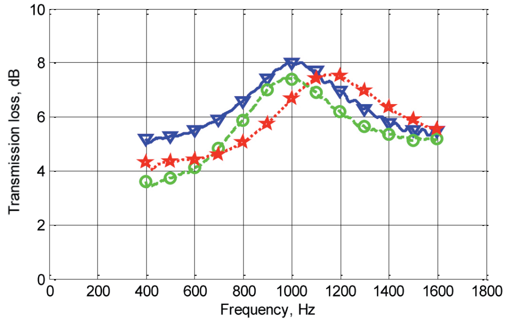

Figure 30. The acoustic transmission loss measured for the ceramic (left) and metal (right) core: 20 °C and 0 m/s (dashed green line, circles), 20 °C and 60 m/s (solid blue line, triangles), 200 °C and 60 m/s (dotted red line, stars)

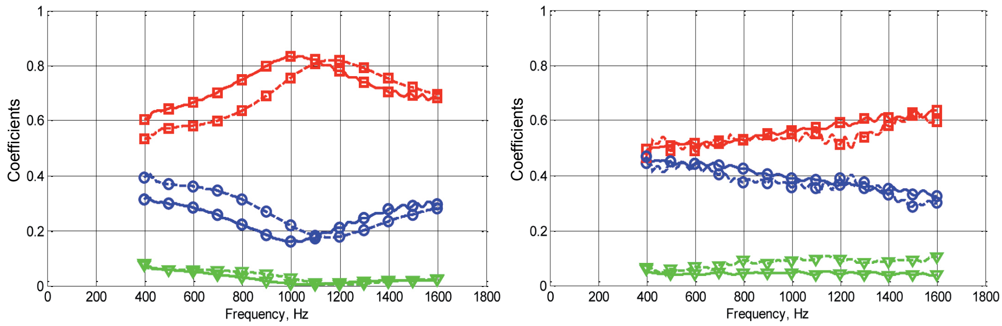

Figure 31. The acoustic coefficients experimentally determined for the ceramic (left) and metal (right) catalytic converter core: 20 °C and 0 m/s (solid line), 20 °C and 60 m/s (dashed line), dissipation (red line, quadrates), reflection (green line, triangles), transmission (blue line, circles)

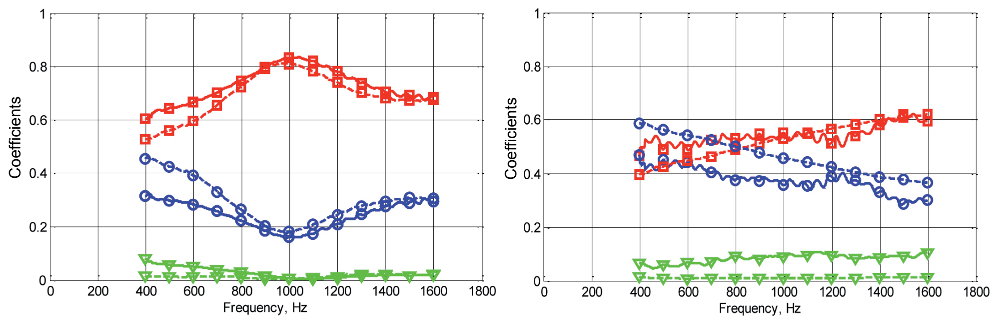

Figure 32. The acoustic coefficients experimentally determined for the ceramic (left) and metal (right) catalytic converter core: 20 °C and 60 m/s (solid line), 200 °C and 60 m/s (dashed line), dissipation (red line, quadrates), reflection (green line, triangles), transmission (blue line, circles)

In Figures 31 and 32, the influence of the flow velocity and temperature to the acoustic coefficients is presented. The dissipation effect tends to be insensitive to the flow speed, but exhibits a frequency shift due to the increased temperature. Small reflection of the pressure waves of the sample elements shows almost a negligible dependency on the flow speed and temperature, referring to the behavior similar to a dissipative type of silencer.

2.4 Open duct terminations

Knowledge of the open end reflection properties is important to determine the acoustic behaviour of systems ranging from wind instruments to exhaust systems of internal combustion engines. In many applications flow and high temperature conditions are involved, adding complexity to the problem.

Despite of several investigations in this field, there is still a lack of experimental data available. In *Paper IV* experimental investigations of the acoustic plane-wave reflection have been carried out for Mach number up to 0.3 for cold jets and up to 0.12 for jet temperature of 200 °C, in order to validate an existing theory on sound reflection from duct openings.

Although there are several analytical models available to calculate the sound reflection at an open duct termination [40-42], the most general is the one proposed by Munt [40], which has been referred to in many investigations [5, 15, 43]. In Munt`s theory [40] the influence of the Mach number on the sound reflection properties at the duct termination was analytically studied by using a linear theory and including a so called Kutta condition. Munt's model was first to predict values for the plane-wave sound reflection coefficient, that exceed unity at low frequencies in a presence of mean flow. Although it is believed that the Munt model [40] is presently the most accurate available and often used for predictions of acoustical properties of duct terminations, it is still only partly validated by published experimental data.

Some earlier experimental investigations show a good agreement with Munt´s model under cold jet conditions, see e.g., Allam and Åbom [5], where reference data was published for mean flow conditions at $M < 0.2$ and $k \cdot a < 1.3$ for the room temperature air flow. In addition, a successful validation of the Munt theory was performed by Rämmal and Lavrentjev [44] up to 500 °C for very low flow speeds $(U < 5\ \mathrm{m/s})$. The purpose of the experimental study in *Paper IV* was to further extend the data range as reported in [5, 44]. A dedicated test facility, described above, was designed to generate hot flow with Mach numbers up to 0.3 and temperature up to 200 °C and to determine accurate reflection coefficient values.

The experiments in *Paper IV* have been performed at different jet temperatures and Mach numbers, as summarized in Table 2. By following the Munt's model [40] the non-dimensional quantities (Ω, *C*) characterising the test conditions are also presented hereby.

Table 2. Physical properties of the experimental cases studied

Case	U_{cl} [m/s]	T [°C]	c [m/s]	M	Ω	C	Fig. marker
1	2	46	359	0.005	1.08	1.04	+ + + —·—·—·
2	65	46	359	0.15	1.08	1.04	☆☆☆ ———
3	130	46	359	0.30	1.08	1.04	○○○ – – –
4	65	200	436	0.12	1.60	1.27	△△△ ·····

In Figure 33 the measurement results for the magnitude and phase of the reflection coefficient for all the flow cases (see Table 2) are plotted as a function of the Helmholtz number $\left(ka = 2\pi fa / c\right)$ and compared with Munt`s theory [40]. To solve the theory of Munt [42] numerically the MATLAB® routine from In `t Panhuis [45] was used.

A good correlation between the measured and calculated values (see Figure 33) was achieved up to cut-on frequency. When the Helmholtz number approaches zero $\left(ka \to 0\right)$, the magnitude of the reflection coefficient becomes unity $\left(|R|=1\right)$, as found by Munt [40]. For intermediate Helmholtz numbers, reflection coefficient values above unity $\left(|R|>1\right)$ are observed. In [40] this phenomenon was explained by the transfer of kinetic energy of the flow to the acoustic field via the interaction of the unstable vortex sheet at the lip of the duct, resulting in increased transmitted sound through the open end. For high Helmholz numbers $(He \to \text{cut-on})$ the magnitude of the reflection coefficient decreases for all the test cases due to the more efficient radiation from the duct opening to the far-field. For higher jet temperatures the maximum of the magnitude of the reflection coefficient is slightly shifted to a lower *ka* value and more efficient radiation from the duct opening for higher *ka* values can be seen.

The value of the end-correction in Figure 33 is strongly dependent on the flow rate. For all flow cases studied, in a small Helmholtz number range $(ka \to 0)$, the value of end-correction approached to the value of $\delta / a = 0.2554\sqrt{1-M^2}$, as predicted by Rienstra [41]. For higher Helmholtz numbers $(ka \to \text{cut-on})$ the values of the end-correction move toward the no flow result predicted by Levine and Schwinger [46]. By increasing the jet temperature compared to the ambient, higher end-correction values for intermediate Helmholtz number range can be seen. For the measurement case 4 (see Table 2), end-correction values above the value of no flow case predicted by Levine and Schwinger [46] can be seen.

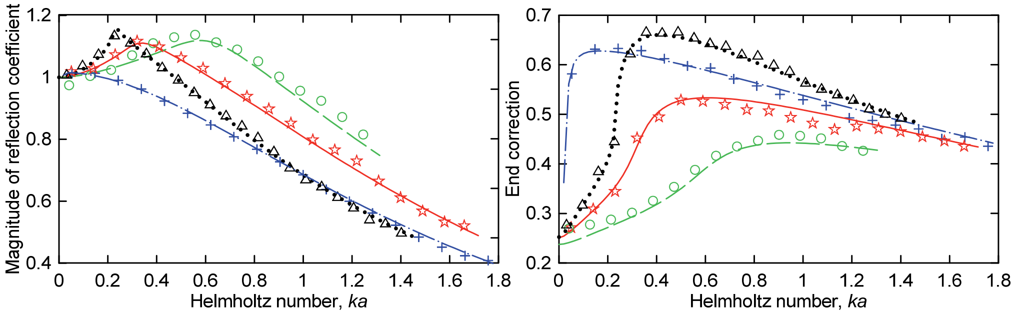

Figure 33. The magnitude and the end-correction of the reflection coefficient for an open duct termination as a function of the Helmholtz number $ka = 2\pi fa/c$ presented for different Mach numbers. Experiments: +, $C = 1.04$ and $M = 0.005$; ☆, $C = 1.04$ and $M = 0.15$; ○, $C = 1.04$ and $M = 0.3$; △, $C = 1.27$ and $M = 0.12$. Munt's theory: —·—·—·, $C = 1.04$ and $M = 0.005$; ———, $C = 1.04$ and $M = 0.15$; – – –, $C = 1.04$ and $M = 0.3$; ·····, $C = 1.27$ and $M = 0.12$

In Figure 34 the results of the reflection coefficient in a Strouhal scale $\left(St = ka/M\right)$ are presented. For all the flow cases the peak value of the magnitude of reflection coefficient appears at $St \approx \pi/2$, which agrees with the theory presented by Munt [40]. For the end-correction, the results tend to collapse into a single curve for a low Strouhal number.

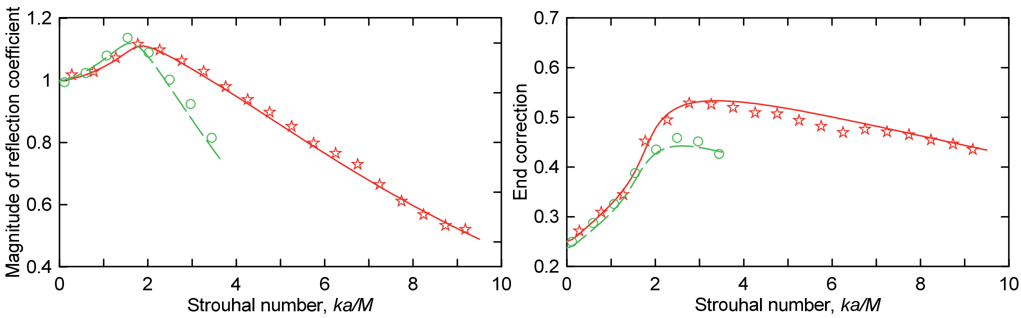

Figure 34. The magnitude and end-correction of the reflection coefficient for an open duct termination as a function of the Strouhal number $St = ka/M$. Experiments: ☆, $C = 1.04$ and $M = 0.15$; ○, $C = 1.04$ and $M = 0.3$. Munt's theory: ———, $C = 1.04$ and $M = 0.15$; – – –, $C = 1.04$ and $M = 0.3$

In Figure 35, the magnitude of the acoustic reflection coefficient is presented as an energy reflection coefficient [47]. For low flow speeds $(M \to 0)$, almost all the sound energy is reflected for low Helmholz numbers $\left(ka \to 0\right)$. This is in accordanece with the theory of Levine and Schwinger [46] where the complete reflection at the duct end without any acoustic radiation from the duct opening to the surrounding is predicted.

The reflection of acoustic energy is strongly dependent on the presence of mean flow. For low Helmholtz numbers the value for the energy reflection coefficient is decreased by increasing the flow velocity. For intermediate Helmholtz number the value of the reflection coefficient increases up to a certain maximum value. This is a clear indication of sound absorption by vorticity shedding described by Bechert [48], Howe [49] and modelled by Munt [40]. After the reflection coefficient maximum value the duct termination starts to radiate acoustic energy more efficiently to the far-field, which can be confirmed by the lower reflection coefficient values for high Helmholtz numbers. It can be also noticed that for the maximum Helmholtz number $(He \to \text{cut-on})$ the value for the reflection coefficient becomes close to 0 $(R_E \to 0)$ for all the cases measured. For the high temperature case a higher energy reflection value at low Helmholtz numbers can be observed, indicating a weaker interaction between the acoustic field and the vorticity.

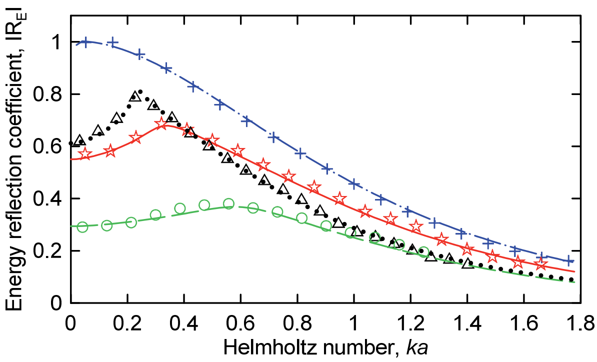

Figure 35. The magnitude of the energy reflection coefficient for an open duct termination as a function of the Helmholtz number $ka = 2\pi fa/c$. Experiments: +, $C = 1.04$ and $M = 0.005$; ☆, $C = 1.04$ and $M = 0.15$; ○, $C = 1.04$ and $M = 0.3$; △, $C = 1.27$ and $M = 0.12$. Munt's theory: —·—·—·, $C = 1.04$ and $M = 0.005$; ———, $C = 1.04$ and $M = 0.15$; – – –, $C = 1.04$ and $M = 0.3$; ·····, $C = 1.27$ and $M = 0.12$

CONCLUSIONS

In this thesis the methods to study sound propagation in automotive duct systems have been in focus where the experimental investigation was performed on automotive turbochargers, catalytic converters and duct termination. The thesis is based on four published papers.

The following are the main conclusions of the current study:

1. The two-port measurement method was improved in order to apply methodology in harsh measurement conditions. To improve the data quality special techniques, such as phase matching the acoustic drivers output, simultaneous driving of two external loudspeakers, multi-step sine method and the three-microphone technique were developed and implemented.
2. A unique acoustic turbocharger test facility was developed, together with the experimental procedures, to determine 2-port data for both the compressor and turbine side. Results from a number of tests on three different automotive turbochargers are given and used to draw general conclusions on the behavior of the transmission loss curves by making it applicable for any operating conditions or turbocharger geometry.
3. Sound generation mechanism from automotive turbochargers has been determined and described. Concerning the measurement of acoustic power the main interest is beyond the plane wave range. For this range an approach based on using the microphone array already installed for the two-port measurements has been proposed and tested. Also the importance of losses to explain the low frequency transmission loss is pointed out and demonstrated by a simple quasi-stationary model.
4. Acoustical properties of ceramic and metal catalytic converter have been presented. Instead of complete catalytic converters, only the honeycomb elements were experimentally investigated. This study represents the first complete acoustic characterization and comparison of catalytic converter honeycomb types in different operating conditions (up to 60 m/s and 200 °C).
5. The magnitude and end-correction of the reflection coefficient, covering the full plane wave range for circular duct termination, was experimentally determined. A dedicated test facility was designed to generate flow up to Mach numbers 0.3. Compared to previous publications the measurement range is considerably extended in terms of temperature $(T = 200\ °C)$ and flow velocity $(M = 0.12)$. It was demonstrated that experimentally obtained reflection coefficient values for hot flow conditions agree with the well-known theoretical model developed by Munt.
6. To improve the accuracy the transducer calibration with flow was proposed and implemented. It was shown that together with the over-determination and method improvements described above, it is possible to carry out precise measurements of the acoustic properties in flow ducts.

Future research

Concerning the investigation of turbocharger acoustics an interesting continuation of the study would be to extend the test range to higher sound pressure levels (> 150 dB) in order to estimate non-linear wave interaction effects. This cannot be done by using electro-dynamic drivers, instead different, more powerful pulsation sources e.g. oscillating valves must be used. For the active part or sound generation from the turbochargers, the thesis described a method based on an average of the pressure cross-spectra, to estimate the auto-spectrum of the modes propagating out from the source. Here, new methodologies can be applied to study in more detail e.g. how phenomena such as surge affects the emitted noise signature.

An interesting continuation of the study of catalytic converters would be to use experimental data in order to validate the existing models of sound propagation in narrow tubes.

The next step for the investigation of reflection at open duct termination would be to experimentally determine the acoustic plane-wave reflection coefficient for high subsonic jet speeds or using different gases with different acoustic properties for jet and the ambient room. Also, an investigation with different duct opening geometries would be an interesting continuation of the research.

REFERENCES

1. ISO 10534-1, Acoustics-Determination of sound absorbing coefficient and impedance in impedance tubes. Part I: Method using standing wave ratio, 1996.
2. Panicker, V. B., Munjal, M. L., Impedance tube technology for flow acoustics. *Journal of Sound and Vibration*, **77** (4), 1981, 573-577.
3. ISO 10534-2, Acoustics-Determination of sound absorption coefficient and impedance method in impedance tubes. Part II: transfer-function method, 1998.
4. Davies, P. O. A. L., Practical flow duct acoustics. *Journal of Sound and Vibration*, **124** , 1988, 91-115.
5. Allam, S., Åbom, M., Investigation of damping and radiation using full plane wave decomposition in ducts. *Journal of Sound and Vibration*, **292**, 2006, 519-534.
6. Dokumaci, E., A note on transmission of sound in a wide pipe with mean flow and viscothermal attenuation. *Journal of Sound and Vibration*, **208** (4), 1997, 653-655.
7. Kirchhoff, G., Uber den Einfluss der Wärmteleitung in Einem Gas Auf Die Schallbewegung. Annalen der Physik, **134** (6), 1868, 177-193, (in German).
8. Mason, V., Some experiments on the propagation of sound along a cylindrical duct containing flowing air. *Journal of Sound Vibration*, **10**, 1969, 208-226.
9. Fahy, F., Sound and Structural Vibration. Academic, New York, 1985, 205-210.
10. Åbom, M., Bodén, H., Error analysis of two-microphone measurements in ducts with flow. *Journal of the Acoustical Society of America*, **83** (6), 1988, 2429-2438.
11. Fujimori, T., Sato, S., Miura, H., An automated measurement system of complex sound pressure reflection coefficients. *InterNoise*, 1984, 1009-1014.
12. Jones, M. G., Parrott, T. L, Evaluation of a multi-point method for determining acoustic impedance. *Mechanical Systems and Signal Processing*, **3** (3), 1989, 15-35.
13. Lavrentjev, J., Tiikoja, H., Investigation of wave propagation and radiation in ducts with arbitrary environment by using the three-microphone method. *InterNoise*, 2008.
14. Jang, S.-H., Ih, J.-G., On the multiple microphone method for measuring in-duct acoustic properties in the presence of mean flow. *Journal of Acoustical Society of America* **103** (3), 1998, 1520-1526.
15. Peters, M. C. A. M., Hirschberg, A., Reijnen, A. J., Wijnands, A. P. J, Damping and reflection coefficient measurements at low Mach and low Helmholtz numbers. *Journal of Fluid Mechanics*, **265**, 1993, 499-534.
16. Pierce, A. D., Acoustics: An Introduction to its Physical Principles and Applications. Mcgraw-Hill, New York, 1981.
17. Munjal, M. L., Acoustics of Ducts and Mufflers. Wiley-Interscience, New York, 1987.
18. Åbom, M., Measurement of the scattering-matrix of acoustical two-ports. *Mechanical Systems and Signal Processing*, **5** (2), 1991, 89-104.

19. Bodén, H., Åbom, M., Modelling of fluid machines as sources of sound in duct and pipe systems. *Acta Acustica*, **3**, 1995, 1-12.
20. Bendat, J. S., Piersol, A. G, Engineering applications of correlation and spectral analysis. John Wiley & Sons Inc, USA, 1980.
21. Allam, S., Bodén, H., Methods for accurate determination of two-port data in flow ducts. *Twelfth International Congress on Sound and Vibration*, Lisbon, 2005.
22. Lavrentjev, J., Åbom, M., Bodén, H., A measurement method for determining the source data of acoustic two-port sources. *Journal of Sound and Vibration* **183** (3), 1995, 517-531.
23. Holmberg, A., Aeroacoustic Characterization Using Multiport Methods. Doctoral Thesis, TRITA-AVE 2012:76, ISSN 1651-7660, KTH, Sweden.
24. Kabral, R., Rämmal, H., Åbom, M., Acoustical methods for investigating turbocharger. *SAE Technical Paper* no: 2013-01-1879, 2013.
25. Tanzosh, J. P., Hayek, S. I., Reflection from an anechoic duct termination. *Journal of the Acoustical Society of America*, **80**, S105, 1986.
26. Neise, W., Arnold, F., On sound power determination in flow ducts. *Journal of Sound and Vibration*, **244** (3), 2001, 481-503.
27. Ross D. F., Crocker M. J., Measurement of the acoustic internal impedance of an internal combustion engine. *Journal of the Acoustical Society of America*, **74**, 1983, 18-27.
28. Munjal, M. L., Analysis and design of mufflers - an overview of research at the Indian Institute of Science. *Journal of Sound and Vibration*, **211**, 1998, 425-433.
29. Munjal, M. L,. Doige, A. G, Theory of a two source-location method for direct experimental evaluation of the four-pole parameters of an aeroacoustic element. *Journal of Sound and Vibration*, **141**, 1990, 323-333.
30. Åbom, M., A note on the the Experimental determination of acoustical two-port matrices. *Journal of Sound and Vibration*, **155** (1), 1992, 185-188.
31. Allam, S., Bodén, H., Åbom, M., Over-determination in acoustic two-port data measurement. *The Thirteenth International Congress on Sound and Vibration*, Vienna, 2006.
32. Johnson, M. E., Fuller, C. R., Creating high level sound in a duct using an axial array of sources. *Journal of Sound and Vibration*, **277**, 2004, 101-122.
33. Pedrosa, A. M., Denia, F. D., Fuenmayor, F. J., Åbom, M., Experimental measurement of acoustic properties by a two-source method with simultaneous excitation, ICSV18, Rio de Janeiro, 2011.
34. Heywood, J. B., Internal Combustion Engine Fundamentals. McGraw-Hill, 1988.
35. Disselhorst, J. H. M., Van Wijngaarden L., Flow in the exit of open pipes during acoustic resonance. *Journal of Fluid Mechanics*, **99** (2), 1980, 293-319.
36. Rämmal, H., Åbom, M., Acoustics of turbochargers. *SAE Technical Paper* no: 2007-01-2205, 2007.
37. Raitor, T., Neise, W., Sound generation in centrifugal compressors. Journal *of Sound and Vibration*, **314**, 2008, 738-756.

38. Rämmal, H., Studies of Flow Duct Acoustics With Application to Turbocharged Engines. Doctoral Thesis, TRITA-AVE 2009:29, KTH, Stockholm.
39. Peat, K. S., Torregrosa, A. J., Broach, A., Fernandez, T., An investigation into the passive acoustic effect of the turbine in automotive turbocharger. *Journal of Sound and Vibration*, **295**, 2005, 60-75.
40. Munt, R. M., Acoustic transmission properties of a jet pipe with subsonic jet flow: 1. The cold jet reflection coefficient. *Journal of Sound and Vibration*, **142**, 1990, 413-436.
41. Rienstra, S. W., A small Strouhal number analysis for acoustic wave-jet flow-pipe interaction. *Journal of Sound and Vibration*, **86**, 1983, 539-556.
42. Cargill, A. M., Low frequency acoustic radiation from a jet pipe - a second order theory. *Journal of Sound Vibration*, **83**, 1982, 339-354.
43. Silva, A. R.,. Scavone, G. P., Lefebvre, A., Sound reflection at the open end of axisymmetric ducts issuing a subsonic mean flow: A numerical study. *Journal of Sound and Vibration*, **327**, 2009, 507-528.
44. Rämmal, H., Lavrentjev, J., Sound reflection at an open end of a circular duct exhausting hot gas. *Noise Control Engineering Journal*, **56** (2), 2008, 107-114.
45. In 't Panhuis, P., Calculations of the acoustic end correction of a semi-infinite circular pipe issuing a subsonic cold or hot jet with co-flow. Report, Marcus Wallenberg Laboratory, KTH, 2003.
46. Levine, H., Schwinger, J., On the radiation of sound from an unflanged circular duct. *Physical Review*, **73**, 1948, 383-406.
47. Ingard, U., Singhal, V. K., Upstream and downstream sound radiation into a moving fluid. *Journal of the Acoustical Society of America*, **54**, 1973, 1343-1346.
48. Bechert, W., Sound absorption caused by vorticity shedding, demonstrated with a jet flow. *Journal of Sound and Vibrations*, **70**, 1980, 389-405.
49. Howe, M. S., The damping of sound by wall turbulent sheer layers. *Journal of Acoustical Society of America*, **98** (3), 1995, 1723-1730.

Acknowledgements

This work has partly been performed at the Department of Machinery, Tallinn University of Technology (TUT) and partly at the Competence Centre of Gas Exchange (CCGEx), the Royal Institute of Technology (KTH). Support to *Paper IV* from the Estonian Science Foundation (Grant nr ETF9441) is acknowledged. The study of automotive turbochargers (*Paper I* and *Paper II*) was financially supported by the Competence Centre for Gas Exchange (CCGEx) through the Swedish Energy Agency, Swedish vehicle industry and KTH. Volvo Car Corporation and GM Powertrain are acknowledged for providing turbochargers for the investigations.

This study would not have been possible without the support of many people. I sincerely thank Prof. Jüri Lavrentjev from TUT for his support and guidance. Many thanks to my colleagues at TUT, Chair of Automotive Engineering: Hans Rämmal, Fabio Auriemma, Risto Kõiv, Raimo Kabral, Janek Luppin and Kristjan Maruste.

I am very grateful to my supervisors Prof. Mats Åbom and Prof. Hans Bodén from KTH for the guidance and help during the work at CCGEx and giving me the opportunity to participate in this work. My third supervisor and also the head of the CCGEx lab Dr. Nils Tillmark is greatly acknowledged for his support. All the seniors at MWL and CCGEx for the courses given are also acknowledged. I would like to thank PhD students from CCGEx and MWL for interesting discussions and invaluable assistance. Many thanks for technical help to Danilo Prelevic, Kent Lindgren, Kim Karlström and Göran Rådberg from MWL and the Mechanics department for their help and advice in building the test-rig. Special thanks to Fredrik Laurantzon, Malte Kjellander, Dr. Ulf Carlsson, Ann Carlsson and Prof. Mats Åbom. I am very glad to have shared the memorable experience of doing the Swedish Classic Circuit with you.

Finally, and most importantly, I would like to thank my wife Kertu for her support and comprehension through the duration of my studies.

ABSTRACT

“Experimental Acoustic Characterization of Automotive Inlet and Exhaust System”

This PhD thesis is based on four original publications which are also presented in the annex. The thesis examines and improves experimental methods for car intake and exhaust systems acoustic research, taking into account the complex physical conditions present in the system. The research was carried out in Tallinn University of Technology (TUT), Chair of Automotive Engineering, in collaboration with the Royal Institute of Technology (KTH), the Competence Centre of Gas Exchange (CCGEx), Sweden.

The main objective of the thesis was to develop experimental acoustic methods, used to determine acoustic properties of induct elements. The aim was to investigate both the passive (sound reflection and attenuation) and active (sound generation) properties of the induct elements. The improved test methods are necessary to obtain acoustic data in high temperature, high flow velocity, high static pressure and high sound pressure level conditions. For the experimental investigation, improved measurement techniques were applied in harsh measurement conditions by using the following car intake and exhaust system components: turbocharger, catalytic converter and duct termination.

The thesis consists of two parts. In the first part of the thesis, an analysis of the acoustic experimental methods used to characterize induct elements is presented and their applicability in harsh measuring conditions in investigated. In order to improve measurement methods, by reducing measurement error and measurement time, a number of modifications e.g. parallel excitation method, improved acoustic sources, multi stepped sine excitation technique and transducer calibration with flow, were proposed.

In the second part of the thesis, the improved measurement techniques were experimentally tested on three different automotive inlet and exhaust system components. First, the unique experimental test facility with automated data acquisition system was designed at KTH CCGEx and used to study sound transmission through automotive turbocharger compressors and turbines at different operating conditions. Experimental procedures to determine the acoustic two-port data, together with techniques such as phase matching of the loudspeaker outputs to improve the quality of data, were introduced. For the passive acoustic effect, results were presented from a number of experiments on three different modern automotive turbochargers. Moreover, the results were re-plotted against the Helmholtz number and general behaviour of the transmission loss curves was drawn in order to make it useful for any turbocharger independent of the size. In *Paper II*, for the passive acoustic effect of the automotive turbocharger a simple quasi-stationary model was proposed to explain the unsymmetrical behaviour of the transmission loss (up-

versus downstream), related to the losses in the system. It was also suggested to apply a power balance in future works to study if there are regions e.g., close to the surge, where the compressor can amplify incident sound waves. The active part or the sound generation was also studied by using an average based measured pressure cross-spectra and the method is applied to study sound produced by a turbocharger compressor at various operating points.

In the experimental investigation of catalytic converters two different elements, ceramic and metal honeycomb cores, were acoustically characterized. The attenuation of sound was determined close to realistic operating conditions. The experiments were carried out with the mean flow velocities (up to 60 m/s) selected to cover a typical flow velocity range from idling to the maximum load of internal combustion engine. Since the heating capacity of the test rig was limited, the maximum temperature of the flow was set to 200 °C, which represents the conditions typical for engine idling. To the authors knowledge, this study represents the first complete acoustic characterization and comparison of catalytic converter honeycomb types in a variety of operating conditions, by using the acoustic coefficients derived from the scattering matrix elements of the two-port.

Finally, an over-determined two-microphone procedure for measurements in hot flow ducts was proposed. Measurements to determine the acoustic plane wave reflection coefficient and phase of the reflected wave for a circular duct were performed for flow velocities up to 130 m/s and jet temperatures up to 200 °C. The results were compared with the theory of Munt and a good agreement was found. This was the first validation of the theoretical model developed by Munt in high flow and high temperature conditions.

The main results of this thesis:

1. Modified acoustic sound sources are developed, which allows them to be used at high temperature and high static pressures conditions. It was shown that measuring with sound sources and using the phase matching outputs, it is possible to significantly increase the power output of sound sources and therefore, their usability for test objects with high background sound pressure levels.
2. It was proved experimentally, that parallel excitation method and multi stepped sine excitation technique can reduce measurement time;
3. For the first time the sensor calibration was performed directly in measurement position and in measurement conditions to reduce measurement error.
4. Complete passive acoustic characterization of automotive turbochargers was performed in a range where turbocharger was designed to work in practice. To make the results useful for any turbocharger, independent of size, a generalized solution in Helmholtz scale for transmission loss was given.
5. Noise radiation from turbocharger beyond the plane wave range was determined by using a method where an average of the pressure spectra was calculated, by using the same three transducers in the inlet and outlet side as for the passive measurements.

6. For the investigation of automotive catalytic converters the results represent the first complete acoustic characterization of catalytic converter honeycomb types in a variety of operating conditions, typical for internal combustion engine.
7. By using the advanced test methods the sound reflection from open duct termination in high flow and high temperature conditions was determined. Experimentally determined result is also the first experimental validation of Munt's theory for hot flow conditions.

Keywords: reflection coefficient, sound scattering, sound source, internal combustion engine, inlet system, exhaust system, flow duct, turbocharger, compressor, turbine, catalytic converter, duct termination.

KOKKUVÕTE

"Autode sisse- ja väljalaskesüsteemi akustilised katsetusuuringud"

Käesolev doktoritöö baseerub neljal publitseeritud artiklil, mis on esitatud ka töö lisas. Doktoritöös uuritakse ja täiustatakse katsetusmeetodeid autode sisse- ja väljalaskesüsteemide akustilisteks uuringuteks, arvestades seal esinevaid keerulisi füüsikalisi tingimusi. Uurimistöö viidi läbi Tallinna Tehnikaülikooli (TTÜ) autotehnika õppetoolis koostöös Rootsi Kuningliku Tehnoloogiainstituudi (KTH) gaasivahetussüsteemide kompetentsikeskusega (CCGEx).

Doktoritöö põhieesmärk on edasi arendada katsetusmeetodeid kanalisüsteemide ja nende elementide akustiliste parameetrite määramiseks. Eesmärgiks oli uurida nii passiivseid (peegeldus, sumbumine) kui ka aktiivseid (heli kiirgamine) parameetreid. Parendatud katsetusmeetodid on vajalikud kasutamaks neid kõrge temperatuuri, suure voolukiiruse, kõrge staatilise rõhu ja kõrge helirõhu taseme korral. Eesmärgiks oli kontrollida täiustatud meetodeid, rakendades neid auto sisse- ja väljalaskesüsteemis turbolaaduri, katalüsaatorseadme ning süsteemi väljundava akustiliste parameetrite uurimisel.

Doktoritöö esimeses osas on analüüsitud kanalites rakendatavaid akustilisi mõõtemeetodeid ja uuritud nende rakendatavust keerukates mõõtetingimustes. Välja on pakutud lahendused meetodite täpsuse suurendamiseks ning mõõteaja vähendamiseks järgmiste täiustuste abil: väliste mõõte-heliallikate samaaegne kasutamine, täiustatud heliallikate ehitus mõõtmiseks rasketes tingimustes, samaaegne mõõtmine erinevates sageduspiirkondades, andurite otsene kalibreerimine mõõtepunktides tegelike mõõtetingimuste korral.

Doktoritöö teises osas on täiustatud katsetusmeetodeid kasutatud ja kontrollitud auto sisse- ja väljalaskesüsteemi komponentide akustilistes uuringutes. Mõõteobjektina on kasutatud kolme sisse- ja väljalaskesüsteemi elementi: turbolaadur, katalüsaatorseade ning süsteemi väljundava.

Turbolaadurite katsetusuuringud viidi läbi nende tegelikele töötingimustele lähedastel füüsikalistel tingimustel. Katsete läbiviimiseks on konstrueeritud mõõtestend ja automatiseeritud andmekogumissüsteem KTH CCGEx laboris. Töötati välja mõõtmismetoodika heli leviku uurimiseks läbi turbolaaduri kompressori ja turbiini eesmärgiga kirjeldada turbolaaduri akustilisi omadusi. Töö tulemusena on läbi viidud kolme erineva turbolaaduri passiivsete akustiliste parameetrite määramine erinevates tööpunktides. Helmholtzi skaalal esitatud tulemused võimaldavad välja tuua üldistatud järeldused turbolaaduri akustilistest omadustest, sõltumata selle geomeetriast ja suurusest. On välja töötatud teoreetiline mudel päri- ja vastuvoolu suunaliste akustiliste kadude ebasümmeetria uurimiseks turbolaadurites ning soovitatud kasutada akustilisel võimsusbilansil baseeruvat mudelit, millega on võimalik kirjeldada heli võimendumist turbolaaduris teatud piirrežiimis. Lisaks akustiliste kadude kirjeldamisele on uuritud ka meetodeid turbolaaduri poolt kiiratava müra mõõtmiseks kuuldavas helisageduspiirkonnas.

Katalüsaatorseadmete akustilistes katsetusuuringutes mõõdeti kahte katalüsaatoritüüpi: keraamilise ja metallist elemendiga katalüsaatorit. Mõõtmised on teostatud füüsikalistes tingimustes, mis on lähedased katalüsaatorseadme tegelikele töötingimustele. Uuringutes kasutatud õhuvoolu kiirus ulatus kuni 60 m/s ja temperatuur kuni 200 °C, mis vastab minimaalsele katalüsaatorseadme tööks vajalikule väärtusele. Tegemist on esimese katseuuringuga, kus katalüsaatorelementi uuriti eraldi ilma seadme ümbrise ja ühendustorudeta. Katalüsaatori elementidi akustiliste omaduste iseloomustamiseks kasutati energiapõhiseid akustilisi parameetreid, mis arvutati akustilise hajuvusmaatriksi elementidest.

Väljalaskesüsteemi väljundava akustiliste omaduste uurimisel vaadeldi helilaine peegeldumist erinevate voolukiiruste ja temperatuuride korral. Mõõtevea vähendamiseks moodustati helilainete levikut kirjeldavatest võrranditest ülemääratud maatriks, mis lahendati numbriliselt vähimruutude meetodil. Katseteks loodi unikaalne mõõtestend ning läbi viidi katsetused voolukiirusel kuni 130 m/s ja temperatuuril kuni 200 °C. Mõõtetulemusi on võrreldud Munt`i teoorial põhineva matemaatilise mudeliga, mis on esmakordne teooria kontroll nimetatud tingimustel. Mõõtmismeetodi täiustusena on välja arendatud tehnika erineva sagedustega helisignaalide rakendamiseks, mis võimaldab mõõtmise ajalist kokkuhoidu. Lisaks on tõestatud mõõtetäpsuse suurendamine juhul, kui mõõteandureid kalibreeritakse vahetult mõõtetingimustes.

Töö peamised tulemused on järgmised:

1. On arendatud välja ja katseliselt kontrollitud modifitseeritud heliallikad akustilisteks mõõtmisteks, mis võimaldavad neid kasutada kõrgetel temperatuuridel ja suurte staatilite rõhkude korral. Tõestati, et kasutades heliallikate faasi ja võimsuse vastastikku kohandamist, on võimalik oluliselt tõsta heliallikate summaarset võimsust ja seega nende kasutatavust uurimisobjekti kõrge helirõhutaseme korral.
2. Katseliselt näidati, et mitme siinus-signaali samaaegne kasutamine mõõte-heliallikas võimaldab oluliselt vähendada mõõteaega.
3. Esmakordselt kalibreeriti mõõteandureid vahetult mõõtekohal tegelikes töötingimustes ja tõestati, et see võimaldab saavutada täpsemaid mõõtetulemusi.
4. Mõõdeti turbolaaduri (turbiin ja kompressor) müra passiivsed akustilised omadused tegelikele töötingimustele lähedases olukorras. Esmakordselt võimaldavad mõõtetulemused Helmholtzi skaalal esitada üldistatud tulemusi kõigi turbolaadurite kohta.
5. Mõõdeti turbolaaduri poolt kiiratud müra tasalaine levikust kõrgematel sagedustel. Parim tulemus saadi meetodiga, kus arvutati müraspektri kesktase, kasutades selleks samu andureid kui turbolaaduri passiivsete akustiliste parameetrite määramisel.
6. Esmakordselt on mõõdetud väljalaskegaaside katalüsaatorseadme elementide akustilised omadused sisepõlemismootori väljalaskesüsteemile iseloomulikes tingimustes, kasutades energiapõhiseid akustilisi meetodeid.

7. Kasutades täiustatud katsetusmeetodeid, uuriti heli peegeldumist kanali väljundavast kiire õhuvoolu ja kõrge temperatuuri tingimustes. Saadud tulemusi on võrreldud Munt'i teoreetilise mudeliga. Tegemist on esmakordse mudeli vastavuse kontrolliga samaaegse kõrge temperatuuri ja suure voolukiiruse korral.

Märksõnad: akustiline peegeldus, akustiline sumbuvus, heliallikas, sisepõlemismootor, sisselaskesüsteem, väljalaskesüsteem, voolukanal, turbolaadur, kompressor, turbiin, katalüsaatorseade, kanali väljundava.

APPENDIXES

Paper I

Tiikoja, H., Rämmal, H., Åbom, M., Bodén, H.,
Sound Transmission in Automotive Turbochargers
SAE Technical Paper Series, Paper 2011-01-1525

2011-01-1525

Sound Transmission in Automotive Turbochargers

Heiki Tiikoja, Hans Rämmal, Mats Åbom and Hans Bodén
KTH-Competence Centre for Gas Exchange Research, The Marcus Wallenberg Laboratory, SE-10044 Stockholm, SWEDEN

ABSTRACT

Turbochargers are common parts of a modern automotive engine. This paper presents an overview of the recent studies performed in the competence center for gas exchange studies at KTH on the sound transmission in turbochargers. The compressor and turbine of the turbochargers are treated as acoustic 2-ports and the scattering matrix for these devices are determined. A unique experimental facility established in the competence center for gas exchange research at KTH has been utilized to study the turbochargers at a variety of operating conditions systematically selected from compressor and turbine charts. A description of the experimental procedures to determine the acoustic 2-port data including techniques implemented to improve the quality of the results is presented. Results from a number of experiments on various modern automotive turbochargers including a unit with variable turbine geometry (VTG) are included. By plotting the up- and downstream transmission loss data against a dimensionless (He-number) frequency scale general characteristics for the sound transmission of turbochargers is found.

INTRODUCTION

Nowadays almost all the automotive and industrial diesel engines produced and the vast majority of high performance SI engines are turbocharged. Naturally, the acoustics of turbochargers has currently become an important issue.

Exhaust gas driven turbochargers consisting of turbine and compressor are used to increase the thermodynamic efficiency of an IC-engine. It is achieved by supplying air to the engine at higher pressure and therefore allowing cylinders to be filled with more combustible mixture by using the energy available in the exhaust gas (see Fig. 1). Modern turbochargers are typically equipped with variable geometry turbines (VTG), which offer adaptability and higher efficiency for a variety of operating conditions.

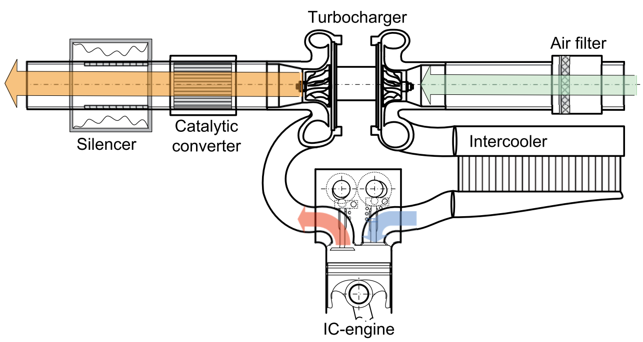

Figure 1 – Illustration of exhaust gas (red arrows) driven turbocharger charging fresh air (blue arrows) into an IC-engine.

During the investigations [1-4] on turbocharger acoustics in KTH it has been found that the turbine and compressor of the turbocharger can have a strong influence on the propagation of sound in the intake and exhaust systems. This influence is referred to as the passive acoustic effect of the turbocharger and it describes the interaction between the turbocharger and the low frequency engine pressure pulsations.

The knowledge about the passive acoustic effect of turbochargers is important for the effective tuning of the acoustical performance for the turbocharged engine. For the complete characterization of the passive acoustic effect of an in-duct device the acoustic 2-port data represented by the scattering matrix or the transfer matrix [5] is required. Since the 2-port model is linear and time invariant use of this model is only valid for sufficiently small amplitudes say less than 0.1 of the mean pressure. The exact amplitude limit for the model when applied to turbochargers is however not known and should be investigated further.

In [1] a review about the previous investigations in the field of turbocharger acoustics was published by Rämmal and Åbom. This paper was followed by the first systematic investigation [2] on the sound transmission in a turbo-compressor working at realistic operating conditions by the same authors. In [3] the experimental results presented in [2] for automotive turbo-compressors were compared to the simulated 2-port data obtained from a 1-D wave model with a good agreement in the low frequency region.

Recently the first successful efforts to experimentally characterize the complete turbocharger were published [4]. Both the turbine and the compressor were studied in up- and downstream directions under various operating conditions. The transmission loss of the turbine was in general found to be considerably higher than that of the compressor. For both units the TL was concluded to be highly dependent on the mass flow.

The aim of the present paper is describe the most recent developments and improvements in the experimental procedure as well as to present an effort to generalize the trends found for the damping (transmission) loss of turbocharger units.

EXPERIMENTAL PROCEDURES

EXPERIMENTAL FACILITY

In the following sections a brief overview together with the latest modifications of the experimental procedures to determine the sound transmission through a working automotive turbocharger compressor and -turbine is given.
In the KTH an experimental facility dedicated to acoustic characterization of automotive turbochargers has been set up. The current layout of the rig is illustrated by a photo in Fig. 2 and schematically presented in Figs. 3-4.

The air mass flow (up to 0.5 kg/s) used to drive the turbocharger turbine originates from two remotely located industrial compressors. The installation has been designed to provide stable inflow conditions (up to 6 bars and pressure fluctuation less than 1%). In order to provide higher inflow temperatures into the turbocharger turbine, an 18kW custom made electrical heater is used, capable of raising the air temperature up to 100°C for the highest mass flows. The turbine inflow as well as the boost pressure in the compressor outlet pipeline is regulated from the operators control module (LabView virtual instrument) by electronically controlled and pneumatically operated ball-valves (SOMAS A13-DA). An autonomous portable lubrication rig is used to supply pressurized oil flow to the turbochargers tested at the acoustics facility. The oil flow is required to provide optimal lubrication and cooling of the turbocharger bearings.

In order to simulate the operating conditions of the turbocharger the compressor and turbine map has to be followed respectively. In Figs. 8 and 9 the performance maps of all the compressors and turbines used in this study together with the operating points (OP) investigated are presented. The characteristic data of the operating points studied for the compressors and turbines are specified in Table 2. In order to define the operating point during the acoustic experiments and to locate it on the compressor map at least two of the three dynamic parameters (the pressure ratio, the mass or volume flow rate and the shaft rotational speed) have to be determined. The compressor pressure ratio is hereby defined as the absolute total outlet (discharge) pressure of the compressor divided by the absolute total inlet pressure. The corrected mass or volume flow rates through the compressor and turbine were determined by using centrally mounted Pitot tubes and a mass flow meter (ABB FMT500-IG). The static pressure values were determined by using pressure transducers (Gems and MPX) mounted at the inlet and outlet cross-sections. Temperature readings in the four cross-sections (see Figs. 3-4) were taken by using NI 9211 thermocouple input module and K-type thermocouples, fixed to the centre of the ducts. The measured flow velocity, pressure and temperature readings were used to determine the density and the speed of sound values in the inlet and outlet pipes and used for calculation of the transmission loss data. To perform the monitoring of the turbocharger shaft rotational speed during the test sessions an eddy-current type speed sensor (Micro-epsilon turbo speed DZ135) pointed onto the compressor wheel blades was used.

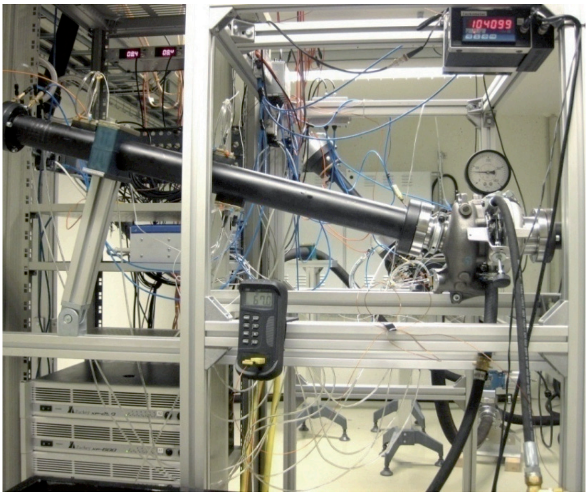

Figure 2 – Photo of the turbocharger test facility in the KTH competence centre for gas exchange research.

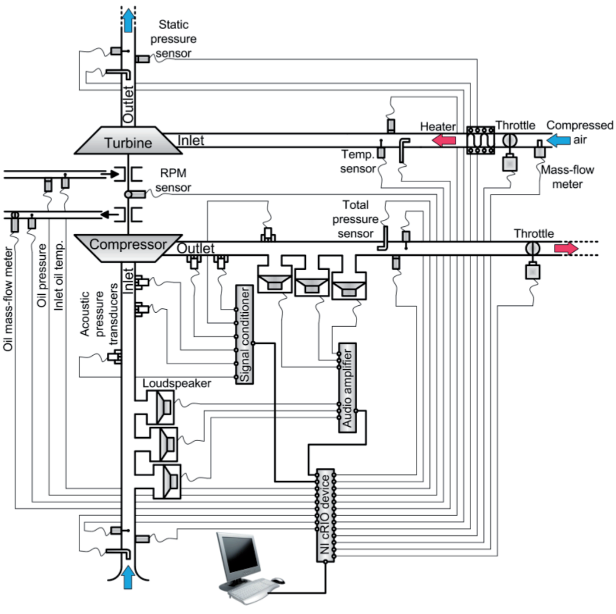

Figure 3 – Figure describing the turbocharger test facility in KTH set up for experiments on the compressor side.

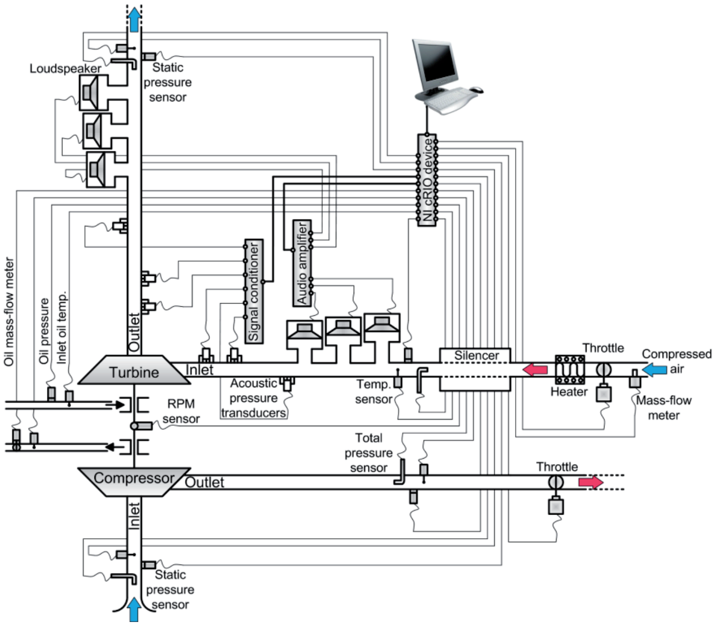

Figure 4 – Figure describing the turbocharger test facility in KTH set up for experiments on the turbine side.

EXCITATION LEVEL MAXIMIZATION

Performing sound transmission experiments on a turbocharger working at realistic operating conditions is a demanding task with turbo-charger wheels rotating at 100 kRPM and pipe flow speeds of 100 m/s. The high background levels encountered are believed to be caused by the flow generated noise, mechanical noise and turbulent pressure fluctuations at the transducers, As the quality of the results was found to be highly dependent on the strength of the acoustic excitation a number of steps were taken to ensure a high excitation level.

Three professional series electro-dynamic audio drivers (DAS ND-8 and K-8) with titanium membrane and neodymium magnets are used on both sides of the compressors and turbines (see Figs. 3-4). By amplifying the excitation signal to the drivers by professional audio amplifiers (Zachry XP600) the drivers were capable of producing sound pressure levels in the test sections (pure tones) reaching up to around 140dB. To concentrate all the generated acoustic energy into a single frequency stepped sine excitation is also used. Considering the quality of results and the time required for performing the experiments 20 averages is used for the data presented here and the frequency resolution was set at 10Hz for most of the test cases.

To stand the high pressure (up to 300 kPa) conditions and high temperatures (up to 160 degrees Celsius), the excitation drivers were modified by reinforcing the body components and gaskets, adding pressure equalization channels and mounting them to the test sections via Bakelite temperature isolation washers and water cooling units (see Fig. 5).

Another technique to enhance the acoustic excitation level used phase-tuning of the drivers, aiming to achieve maximum constructive interference by synchronizing their output to the same phase. This was performed by applying individual control (NI cRIO control unit through the amplifier NI 9263 and analog output module) to all the active drivers using the common LabVIEW virtual instrument control board. The input voltage (e) to the acoustic drivers is used as a reference signal and the transfer function between this signal and the acoustic pressure in the wave propagating in the positive direction p+ is measured. The phase of these transfer functions for the three drivers is then compared and used to phase shift the voltage e. This phase adjustment to ensure a maximum p+ level is done automatically for each operating point and frequency step.

In Fig. 6 the results exhibiting the advantage of using the phase tuning technique are presented. As can be seen the output from the phase-tuned drivers is clearly more uniform over the frequency range treated, offering up to 15 dB improvement compared to the performance of a single driver. It can be noted that in the case of no phase-tuning the output level varies a lot over the frequency range as the output waves from the drivers encounter destructive interference at certain frequencies.

In order to suppress the standing waves and external disturbances the test ducts were equipped with dissipative terminations at the test section inlets and outlets. Extra acoustic damping in the duct system was achieved by mounting 5-10m long flexible pressure resistant rubber hoses to all the inlets and outlets of the test sections.

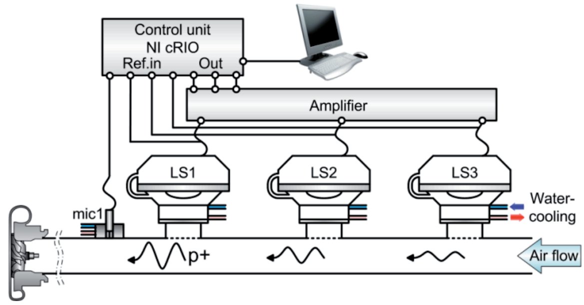

Figure 5 – A schematic representation of the loudspeaker section with acoustically phase-matched loudspeakers.

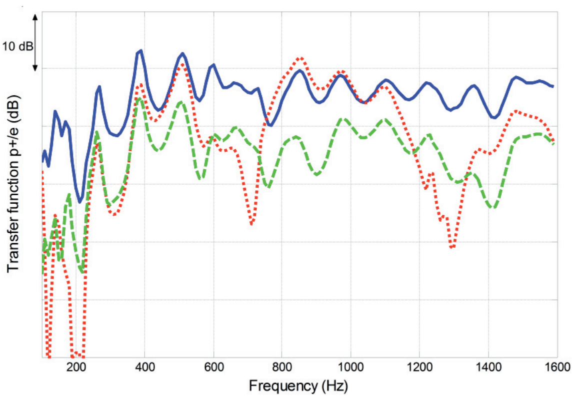

Figure 6 – The sound pressure level generated by the loudspeaker section towards the turbocharger. Three phase tuned drivers (blue solid line), three drivers without phase tuning (red dotted line), single active driver (green dashed line).

DETERMINATION OF THE 2-PORT DATA

Six flush mounted water-cooled piezoelectric pressure transducers (Kulite WCT-312M-25A via Dewetron signal conditioner) were used simultaneously to perform acoustic wave decomposition. The acoustic data acquisition was performed by using National Instruments CompactRIO signal analyzer controlled by a purpose built virtual control module (LabVIEW). The electrical signal from the output channel of the analyzer driving the acoustical excitation (the drivers) is correlated to the pressure signals from the six transducers. For the data analysis plane waves are assumed which requires a sufficient distance between the electro-dynamic driver and the pressure transducers. To avoid the interaction of the non-plane waves present close to the drivers the distance between the driver and the closest microphone is chosen to be at least ten diameters.

To determine the sound transmission the automotive turbocharger is treated as an acoustic 2-port. This implies the following relationship in the frequency domain:

$$\underbrace{\begin{bmatrix} p_{a+} \\ p_{b+} \end{bmatrix}}_{p_+} = \underbrace{\begin{bmatrix} S_{11} & S_{12} \\ S_{21} & S_{22} \end{bmatrix}}_{S} \cdot \underbrace{\begin{bmatrix} p_{a-} \\ p_{b-} \end{bmatrix}}_{p_-} + \underbrace{\begin{bmatrix} p_{a+}^S \\ p_{b+}^S \end{bmatrix}}_{p_+^S}, \tag{1}$$

where S_{11}, S_{22} and S_{12}, S_{21} describe the reflection and transmission of the incoming waves respectively, a and b refer to two sides of the two-port, the plus and minus signs indicate propagation outwards and into the two-port respectively and the superscript s refers to source generated sound. As the dominating noise generated by the turbocharger typically appears beyond the plane wave region, the source strength vector $\mathbf{p}^s_+$ can be neglected. By forming the transfer functions between the measured signals and the external signal driving the external sources e, the scattering matrix can be determined. To obtain the scattering matrix we also need two different acoustic test states, which can be created by using acoustic excitation on both sides of the test object. Eq. 1 can then be expressed as:

$$\begin{bmatrix} H^{I}_{ea+} & H^{II}_{ea+} \\ H^{I}_{eb+} & H^{II}_{eb+} \end{bmatrix} = \begin{bmatrix} S_{11} & S_{12} \\ S_{21} & S_{22} \end{bmatrix} \begin{bmatrix} H^{I}_{ea-} & H^{II}_{ea-} \\ H^{I}_{eb-} & H^{II}_{eb-} \end{bmatrix}, \qquad (2)$$

where the superscript indicates the different test states (I – upstream drivers "on" and downstream "off" ", II – downstream drivers "on" and upstream "off"). H_{ex} is the transfer function taken between the microphone signal x and the voltage e exciting the drivers which can be expressed as [6]:

$$H_{ea+} = F_a\left[H_{ea1}\exp(ik_{a-}s) - H_{ea2}\right], \qquad (3)$$

$$H_{ea-} = F_a\left[-H_{ea1}\exp(-ik_{a+}s) + H_{ea2}\right], \qquad (4)$$

$$H_{eb+} = F_b\left[H_{eb1}\exp(-ik_{b-}s) - H_{eb2}\right], \qquad (5)$$

$$H_{eb-} = F_b\left[-H_{eb1}\exp(-ik_{b+}s) + H_{eb2}\right], \qquad (6)$$

where F can be calculated from:

$$F = \left[\exp(ik_{\_}s) - \exp(-ik_{+}s)\right]^{-1}, \qquad (7)$$

where k+ and k- are wavenumbers in the up- and downstream direction and s is the separation between pressure transducers.

By knowing the S-matrix elements, we have the complete information about the passive acoustic effect of the two-port device tested, including the transmission loss (TL) which can be calculated as follows:

$$TL_u = 10\cdot\log\left(\frac{W_{in}}{W_{tr}}\right) = 10\cdot\log\left(\frac{(1+M_b)^2 A_b\cdot\rho_a\cdot c_a}{(1+M_a)^2 A_a\cdot\rho_b\cdot c_b\left|S_{12}\right|^2}\right), \qquad (8)$$

$$TL_d = 10\cdot\log\left(\frac{W_{in}}{W_{tr}}\right) = 10\cdot\log\left(\frac{(1+M_a)^2 A_a\cdot\rho_b\cdot c_b}{(1+M_b)^2 A_b\cdot\rho_a\cdot c_a\left|S_{21}\right|^2}\right), \qquad (9)$$

where TL_u is the transmission loss in upstream direction and TL_d is the transmission loss in downstream direction, W_{in} and W_{tr} are the incident and transmitted acoustic powers respectively, M is the Mach number, A is the cross-sectional area of the pipe, ρ is the air density and c is the speed of sound and M the Mach-number.

THE TURBOCHARGERS TESTED

TECHNICAL DESCRIPTION OF THE TURBOCHARGERS TESTED

Technical information about the three turbochargers investigated is given in Table1. In Fig. 7 photos describing the geometry of the turbochargers wheel and housing for compressor and turbine side are presented.

Table 1 – Technical data of the three turbochargers investigated. Type C is the VTG turbine.

Turbocharger	KKK K24	Garret GT1752	Garret GT1749V
	A	B	C
Turbine			
A/R ratio	0.41	0,47	0,42
Scroll inlet diameter [mm]	52	40	43
Approximate scroll length [mm]	300	285	380
Number of rotor blades	12	9	9
Radius of the rotor [mm]	29	22	21
Rotor length [mm]	21	20	25
Compressor			
Scroll outlet diameter [mm]	41	43	38
Approximate scroll length [mm]	460	358	370
Number of rotor blades	6+6	6+6	5+5
Radius of the rotor [mm]	31	26	25
Rotor length [mm]	25	20	18

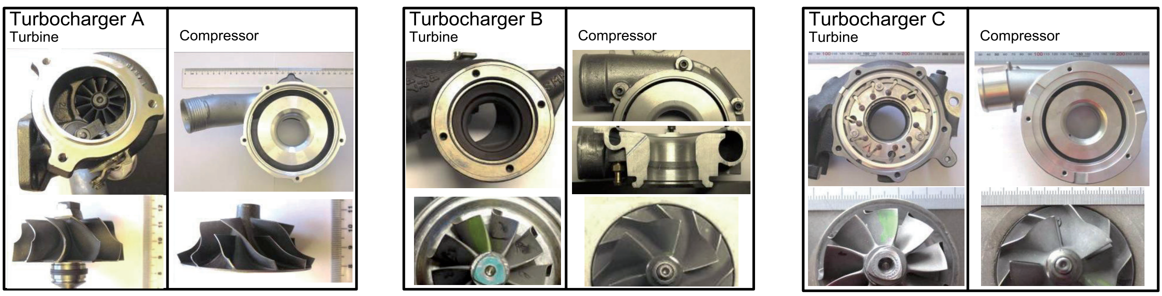

Figure 7 – Photos of the turbine and compressor of turbochargers A, B and C.

OPERATING CONDITIONS

The operating points measured on the compressor- and turbine maps are illustrated in Figs. 8-9 for all three turbocharger tested. Operating conditions of the turbochargers in which the experiments were carried out are summarized in Table 2.

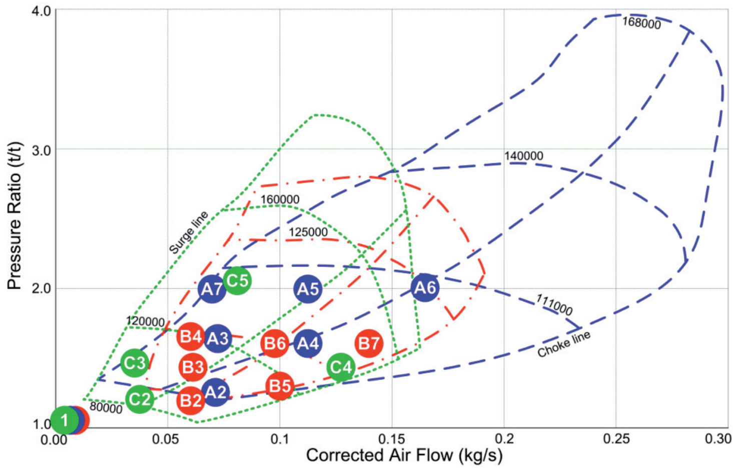

Figure 8 – Comparison of simplified compressor charts for all three turbochargers investigated. The experimentally studied operating points are shown as A1…A4 (turbocharger A), B1…B4 (turbocharger B) and C1…C4 (turbocharger C).

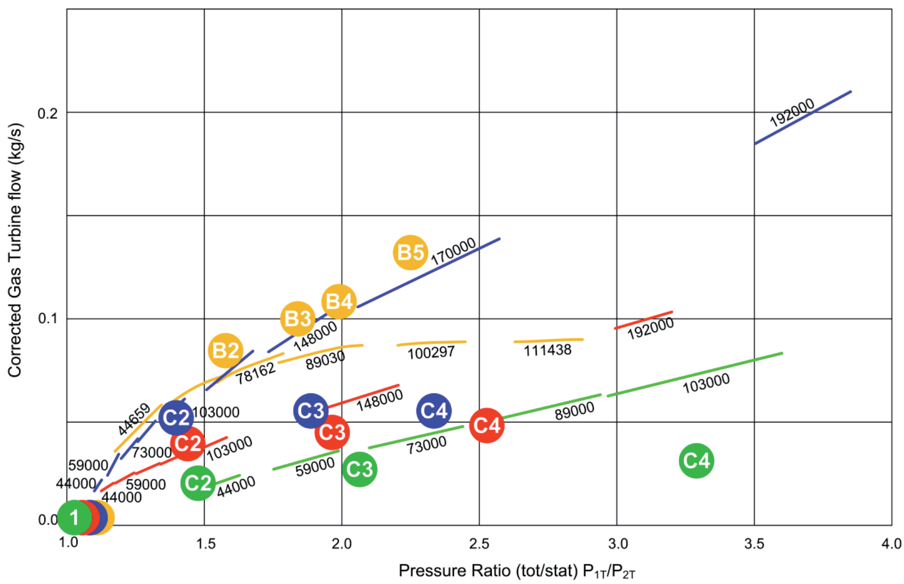

Figure 9 – Comparison of simplified turbine charts for all three turbochargers investigated. The experimentally studied operating points are shown as A1…A4 (turbocharger A), B1…B4 (turbocharger B) and C1…C4 (turbocharger C). The three points for the C (VTG) turbine correspond to three different valve settings 0, 50 and 100%, where 0 is closed and 100% is fully open.

Table 2 – The operating conditions of the turbocharger compressors (right) and turbines (left) investigated. It should be noted that the RPM and mass flow in this table are corrected values (regarding the actual conditions).

Operating point	Turbocharger part tested	Line type in Figs. 11 and 12	RPM [1/min]	Mass-flow [kg/s]	Pressure ratio
C-A1	Compressor (A)	dotted blue line	0	0	1
C-A2	Compressor (A)	dotted green line	45800	0.08	1,1
C-A3	Compressor (A)	dotted black line	81600	0.08	1,5
C-A4	Compressor (A)	dotted magenta line	88200	0.135	1.52
C-A5	Compressor (A)	dotted grey line	107600	0.135	1.89
C-A6	Compressor (A)	dotted brown line	115000	0.192	1.91
C-A7	Compressor (A)	dotted yellow line	104400	0.08	1.89
C-B1	Compressor (B)	dashed blue line	0	0	1
C-B2	Compressor (B)	dashed green line	80000	0,062	1,24
C-B3	Compressor (B)	dashed black line	100000	0,062	1,45
C-B4	Compressor (B)	dashed magenta line	120000	0,062	1.72
C-B5	Compressor (B)	dashed grey line	100000	0.11	1.28
C-B6	Compressor (B)	dashed brown line	120000	0.11	1.62
C-B7	Compressor (B)	dashed yellow line	140000	0.15	1.66
C-C1	Compressor (C)	solid blue line	0	0	1
C-C2	Compressor (C)	solid green line	65000	0,044	1,21
C-C3	Compressor (C)	solid black line	83400	0,038	1.42
C-C4	Compressor (C)	solid magenta line	117000	0,135	1.3
C-C5	Compressor (C)	solid grey line	124700	0,091	2
C-C6	Compressor (C)	solid brown line	90500	0,07	1.42
C-C7	Compressor (C)	solid yellow line	160900	0.14	2.85

Operating point	Turbocharger part tested	Line type in Figs. 11 and 12	RPM [1/min]	Mass-flow [kg/s]	Pressure ratio
T-B1	Turbine (B)	dashed blue line	0	0	1
T-B2	Turbine (B)	dashed green line	80000	0,086	1,53
T-B3	Turbine (B)	dashed black line	100000	0,1	1,75
T-B4	Turbine (B)	dashed magenta line	100000	0.12	1.86
T-B5	Turbine (B)	dashed grey line	120000	0.14	2.25
T-C1 0	Turbine (C)	solid blue line	0	0	1
T-C1 50	Turbine (C)	solid blue line	0	0	1
T-C1 100	Turbine (C)	solid blue line	0	0	1
T-C2 0	Turbine (C)	solid green line	101900	0.021	1.49
T-C2 50	Turbine (C)	solid green line	124600	0.042	1.45
T-C2 100	Turbine (C)	solid green line	102000	0.051	1.4
T-C3 0	Turbine (C)	solid black line	153900	0.026	2.16
T-C3 50	Turbine (C)	solid black line	172300	0.048	1.93
T-C3 100	Turbine (C)	solid black line	137300	0.056	1.8
T-C4 0	Turbine (C)	solid magenta line	206900	0.028	3.28
T-C4 50	Turbine (C)	solid magenta line	207300	0.047	2.57
T-C4 100	Turbine (C)	solid magenta line	171100	0.054	2.37

RESULTS AND ANALYSIS

The experimentally determined transmission loss results in up- and downstream directions for all the turbo-compressors and turbines tested are presented in Figs. 10 and 11 respectively.

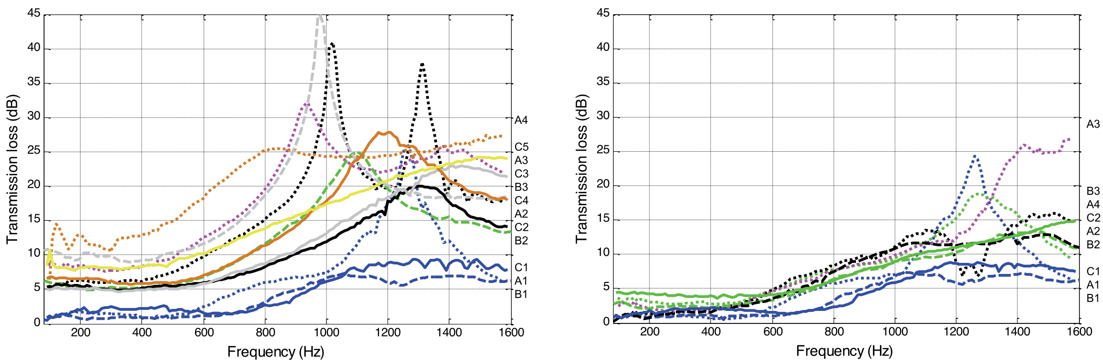

Figure 10 – The transmission loss results for different turbo-compressors in upstream (left) and downstream (right) direction.

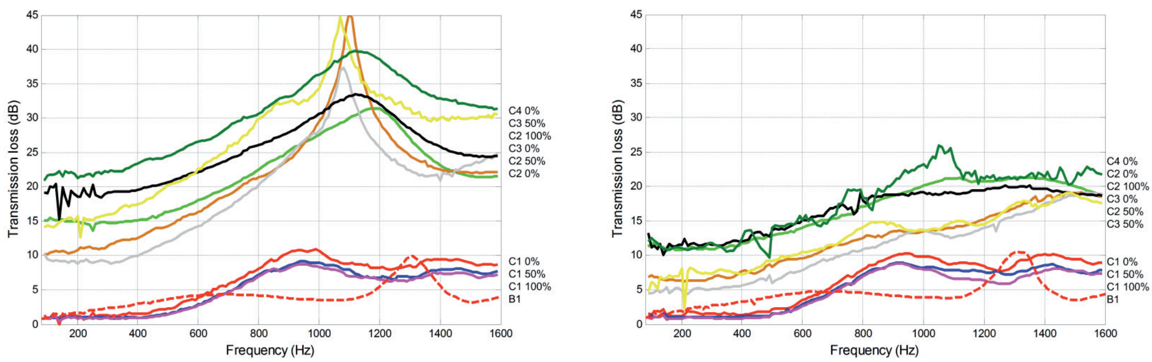

Figure 11 – The transmission loss results for different turbocharger turbines in upstream (left) and downstream (right) direction.

For the stationary turbocharger (RPM=0) the transmission loss (TL) is not dependent on the direction of the sound propagation. Also the TL curves for the no flow case approach a small value at low frequencies which is related to the area change of the pipes across the unit. If these areas are equal then the no flow TL will approach zero at low frequencies. When the unit is rotating the low frequency TL will be affected by reflections caused by the change in both area and characteristic impedance (density*speed of sound) across the device.

Computing these effects for the tested cases typically give TL values less than 1 dB. Also if only changes in acoustic impedance across the device would matter for the low frequency behaviour, it is straightforward to prove that the TL values would be the same in the up- and downstream directions. It is therefore clear that the main part of the low frequency TL values must be caused by dissipation, e.g., due to flow acoustic interaction in particular at regions with flow separation. Of course for supersonically rotating wheels shock waves can create both reflections and also dissipation of incident sound waves. The importance of losses is also clear from the fact that the TL values for a given unit tend to increase with the mass flow. After the low frequency plateau there is an upward slope that is determined by the inner free air volume of the unit that acts as a small expansion chamber muffler. This means that the larger the volume the steeper the slope will point upwards. For the small automotive turbo-chargers tested this low frequency TL region, with a plateau and a slope upwards, typically extends up to 600-800 Hz. Higher up peaks can occur in the TL and are either associated with resonances in a side-branch, e.g., from a closed/open bypass valve or as reported by Peat et al. [7] correspond to inner resonances in the devices itself.

An example of a closed by pass valve peak can be seen in Figure 12 giving a TL peak up to 25 dB in the stationary case. It can also be noticed that the effect of the resonator decreases by adding a flow, which creates more damping.

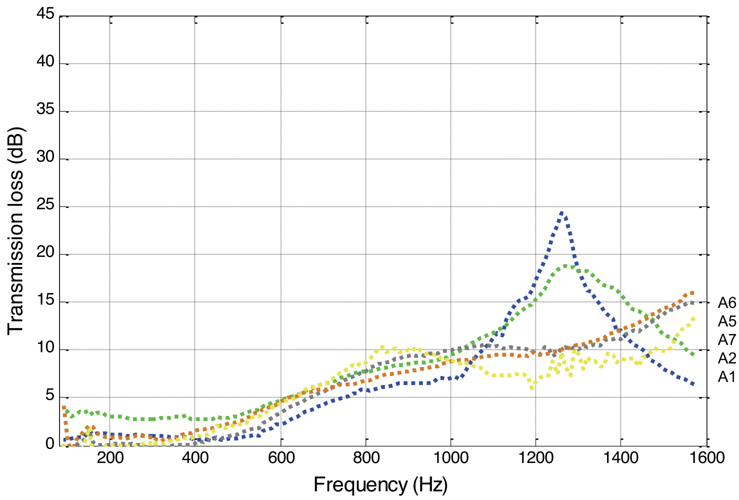

Figure 12 – The transmission loss results for the turbocharger A compressor in downstream direction.

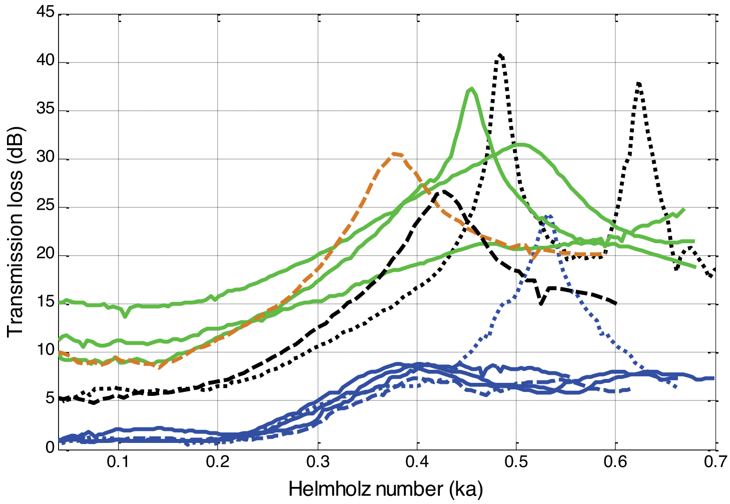

Figure 13 – The transmission loss results for different turbocharger compressors and turbines as a function of the Helmholtz-number.

In order to generalize the above statements and make them useful for any turbocharger independent of size one can replot Figs. 10-11 against the Helmholtz-number (He):

$$He = \frac{2\pi f\, a}{c}, \tag{10}$$

where f is the frequency, a the radius and c the speed of sound. In Fig. 13 the TL data for selected cases from Figs. 10-11 have been plotted using this scale based on the average (for d and c) of the inlet/outlet data. From this figure the following general conclusions can be drawn: **i)** The low frequency plateau region with a level determined by losses and increasing with mass flow extends up to $He < 0.2$; **ii)** This is followed by an upward slope which increases with larger inner volume in the range $0.2 < He < 0.35$; **iii)** In the range $He > 0.35$ TL peaks starts to appear associated with resonances due to open/closed bypass gates and with cancellation associated with different sound paths through the blade sections as suggested in Ref. [7]. The first type of peaks will not change their position with flow but will due to flow induced damping often be reduced with increasing mass flow, see Fig. 12. The second type of peaks associated with cancellation effects will move when the mass flow varies and is less affected by damping.

SUMMARY AND DISCUSSION

The unique acoustic turbocharger test facility at KTH has been presented together with the experimental procedures to determine 2-port data for both the compressor and turbine side. Special techniques to improve the data quality are also described, such as phase matching the loudspeaker outputs in order to create a maximum constructive interference and input level. Results from a number of tests on automotive turbochargers are shown and used to draw general conclusions on the behavior of the transmission loss curves. The next step in the rig development will be to also measure the sound generation from the turbocharger. In the plane wave range this can be done by including the source strength in Eq. 1 as described for instance in Ref. [8]. Beyond the plane wave range one can either use standard (e.g. ISO) methods to estimate the propagating sound power which require reflection free terminations. These methods are based on spatial averaging of the sound field and normally involve some assumption that the power is equally distributed over the propagating modes. Since most of the noise emission [1] will lie well above the plane wave range it is essential to include such methods in the testing. Other interesting developments are to increase the excitation level in the rig, i.e., go beyond the < 1% relative pressure amplitudes created by the acoustic drivers. This can be done by using compressed air sources such as a siren or a pulse generator consisting of a valve with a time varying opening.

REFERENCES

1. Rämmal, H., Åbom, M., “Acoustics of Turbochargers,” SAE Technical Paper no. 2007-01-2205, 2007.
2. Rämmal, H., Åbom, M., “Experimental Determination of Sound Transmission in Turbo-Compressors,” SAE Technical Paper no. 2009-0101, 2009.
3. Rämmal, H., Galindo, J., “The Passive Acoustic Effect of Turbo-Compressors,” presented at the 9th International Conference on Turbochargers and Turbocharging, UK, May 19-20, 2010.
4. Rämmal, H., Tiikoja, H., Åbom, M., Bodén, H., “Experimental Facility for the Complete Determination of Sound Transmission in Turbochargers,” SAE Technical Paper no. 2010-01-1424, 2010.
5. Bodén, H., and Åbom, M., “Modelling of Fluid Machines as Sources of Sound in Duct and Pipe Systems,” *Acta Acustica,* **3**: 1-12, 1995.
6. Åbom, M., “Measurement of the Scattering-Matrix of Acoustical Two-Ports,” *Mech. Systems and Signal Proc* **5**(2): 89-104, 1991.
7. Peat, K. S., Torregrosa, A. J., Broach, A. and Fernandez, T, “An Investigation into the Passive Acoustic Effect of the Turbine in Automotive Turbocharger,” *Journal of Sound and Vibration,* **295**: 60-75, 2005.
8. Lavrentjev, J., Åbom, M., and Bodén, H.,“A Measurement Method for Determining the Source Data of Acoustic Two-Port Sources,” *Journal of Sound and Vibration* **183**(3): 517-531, 1995.

CONTACT INFORMATION

Mats Åbom: email: matsabom@kth.se,
phone: +46 8 7907944

Hans Rämmal: email: hansra@kth.se,
phone: +37 256 465738

ACKNOWLEDGMENTS

The authors acknowledge the support from Dr. Nils Tillmark (KTH Mechanics Dept.) for the development of the rig and in particular for help in setting up the data acquisition for the fluid dynamics.

Paper II

Tiikoja, H., Rämmal, H., Åbom, M., Bodén, H.,
Investigations of Automotive Turbocharger Acoustics
Printed in: *SAE International Journal of Engines* 4(2):2531-2542

Investigations of Automotive Turbocharger Acoustics

2011-24-0221
Published
09/11/2011

Heiki Tiikoja, Hans Rämmal, Mats Abom and Hans Boden
KTH-CCGEx, Marcus Wallenberg Laboratory

doi:10.4271/2011-24-0221

ABSTRACT

In this paper an overview of recent experimental studies performed at KTH on the sound transmission and sound generation in turbochargers is presented. The compressor and turbine of the turbochargers are treated as acoustic active 2-ports and characterized using the unique experimental test facility established at KTH. The 2-port model is limited to the plane wave range so for higher frequencies the propagating acoustic power is estimated using an average based on pressure cross-spectra. A number of automotive turbochargers have been studied for a variety of operating conditions systematically selected from the compressor and turbine charts. The paper discusses the experimental procedures including special techniques implemented to improve the quality of the data. Results from a number of experiments on various modern automotive turbochargers including a unit with variable turbine geometry (VTG) are presented.

1. INTRODUCTION

Turbochargers are an important part of most modern automotive high efficiency engines. Nowadays almost all the automotive and industrial diesel engines produced and the vast majority of high performance SI engines are turbocharged. Naturally, the acoustics of turbochargers has therefore also become an issue.

Exhaust gas driven turbochargers consisting of turbine and compressor are used to increase the thermodynamic efficiency of an IC-engine. It is achieved by supplying air to the engine at higher pressure and therefore allowing cylinders to be filled with more combustible mixture by using the energy available in the exhaust gas (see Fig. 1). Modern turbochargers are typically equipped with variable geometry turbines (VTG) which offer adaptability and higher efficiency for a variety of operating conditions.

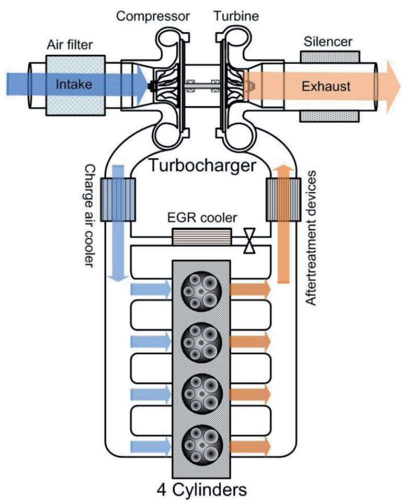

Figure 1. A simplified schematic representation of the turbocharged IC-engine.

Turbocharger compressors are generally centrifugal compressors consisting of a wheel, diffuser and housing. As the compressor wheel rotates, ambient air is drawn in axially through a filter-silencer system, accelerated to high speed and then expelled in a radial direction to the outlet which normally leads to an intercooler.

Both the turbine and the compressor have an influence on how the low frequency engine pulsations propagate in the intake/exhaust system i.e., the scattering of incident pressure pulses or waves from the unit. This is referred to as the *passive acoustic* property of the turbocharger. If linear acoustic models are applied the passive properties can in the plane wave range be described using two parameters: the reflection coefficient and the transmission coefficient or alternatively the transmission loss.

A turbo-unit also produces high frequency aerodynamic sound, which is referred to as its *active* ("sound generating") *acoustic* properly. The sound field in a duct system coupled to a turbocharger depends on both the passive and active properties of the device.

According to Lighthills classical theory there are three basic mechanisms that can create sound in a fluid: i) fluctuating volume flow - monopole type of source; ii) fluctuating surface pressures - dipole type of source and iii) free turbulence - quadrupole type of source.

In a rotating machine, such as a turbocharger, the blades will generate a monopole type of source only when the blades move close to the speed of sound or supersonically. In the supersonic case there will also be rotating shock waves attached to the blades. The spectrum of the monopole contribution will in the supersonic case be harmonics of the rotation frequency f_0. This type of rotating shock wave noise is referred to as buzz-saw noise and exists for instance on modern aero-engines. Supersonic tip speeds are also common for modern high speed turbo compressors.

A number of dipole or fluctuating pressure sources can be found in rotating machines. One is the blade pressure. The most important contribution to time varying blade pressures is inflow disturbances. These can be of two types: stationary and non-stationary flow distortions, e.g., turbulence. The stationary distortions will lead to periodic acoustic signals and the turbulence to a broad band signal. The periodic signals will consist of harmonics of the blade passing frequency (BPF). Without inflow disturbances these tones are referred to as rotor-alone tonal noise. A second source of dipole noise on rotating machines is rotor-stator interaction, e.g., fluctuating pressure fields created by interaction between inlet/outlet guide vanes and the rotor. This noise is also periodic in time and consists of harmonics of the BPF. Finally the turbulence in the flow will act as a broad band acoustic source but normally this source is not important unless the flow forms a jet with a Mach-number close to 1. This quadrupole type of source is normally important only at the outlet of jet engines and high pressure valves, but for turbochargers it is of little interest. In general the influence of turbocharger noise has been reported to be more important on the intake, i.e., compressor side, mainly because of the relatively good damping characteristics by modern mufflers on the exhaust side.

Based on the above discussion the main aerodynamic noise generating mechanisms in turbo-compressors are: tonal noise at blade passing frequencies, buzz-saw noise and blade tip clearance noise.

In [1] a review about the major fundamental investigations in the field of turbocharger acoustics was published by Rämmal and Åbom. This paper was followed by the first systematic experimental investigation [2] on the sound transmission in a turbo-compressor working at realistic operating conditions by the same authors. In [3] the experimental results presented in [2] for automotive turbo-compressors were compared to the simulated 2-port data obtained from a 1-D wave model with a good agreement in the low frequency region. To the authors knowledge it was the first effort to implement a simple 1-D wave model for prediction of the acoustic two-port data of an automotive turbo-compressor working at realistic operating points.

Recently the first successful experimental characterization of the complete turbocharger was published [4]. Both the turbine and the compressor side were studied in up- and downstream directions under various operating conditions for a 3 different automotive units. General conclusions for the behavior of the transmission loss as a function of frequency were presented based on the results.

The aim of the present paper is offer an overview of the most important findings from the investigations of automotive turbocharger acoustics carried out at KTH including the recent developments and improvements in the experimental procedures. In particular measurement of active data or sound power spectra will be discussed and some results presented. Also for the passive part the possibility to develop quasi-stationary models is discussed. An important part of such models are the losses that occur in the turbocharger unit. Methods to estimate such losses using acoustic 2-port data are also addressed.

2. INVESTIGATION METHODS

This section presents an overview of the state of the art methods recently tested and developed in KTH for experimental investigations of turbocharger acoustics. To the authors knowledge the unique turbocharger acoustics test rig described in section 2.1 represents the currently most advanced experimental setup for the complete acoustic characterization of automotive turbochargers.

2.1. THE EXPERIMENTAL FACILITY

The turbocharger characterization facility has been established at the research competence centre for investigations on IC-engine gas management at KTH in Stockholm. The ambition was to develop accurate experimental procedures for the determination of the scattering data for automotive turbochargers at realistic operating conditions selectable from the compressor and turbine charts. Additionally to the measurements for the passive data, the facility can also be implemented to measure the sound generation by the turbo unit (the active properties).

Hereby an overview together with the latest modifications for the experimental procedures to determine the sound transmission through and sound generation from a working automotive turbocharger compressor and -turbine is given. The current layout of the rig is schematically presented in Fig. 2 and illustrated by photo composition in Fig. 3 and. The rig has two distinct sides: the compressor side and the turbine side, which can both be investigated at any operating conditions selectable from the manufacturers operating charts.

The air mass flow (up to 0.5 kg/s) used to drive the turbocharger turbine originates from two remotely located industrial compressors. The installation has been designed to provide stable inflow conditions (up to 6 bars and pressure fluctuation less than 1%). In order to provide higher inflow temperatures into the turbocharger turbine, an 18kW custom made electrical heater is used, capable of raising the air temperature at least up to 100°C for the highest mass flows. The turbine inflow as well as the boost pressure in the compressor outlet pipeline is regulated from the operators control module (LabVIEW virtual instrument, see Fig. 4) by implementing electronically controlled and pneumatically operated ball-valves (SOMAS A13-DA). An autonomous portable lubrication rig is used to supply pressurized oil flow to the turbochargers tested at the acoustics facility. The oil flow is required to provide optimal lubrication and cooling for the turbocharger bearings.

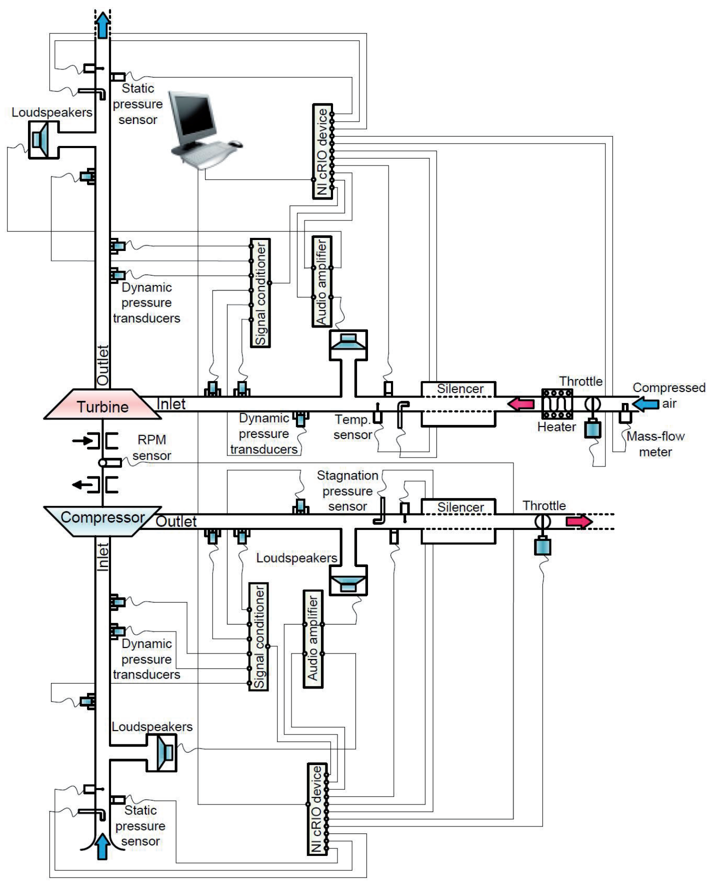

Figure 2. A schematic representation of the test facility in KTH designed for investigations of automotive turbocharger acoustics.

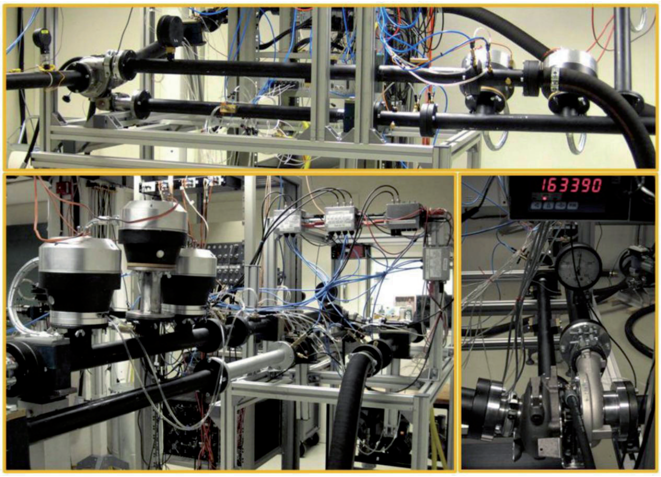

Figure 3. Photos of the test facility in KTH implemented for investigations of automotive turbochargers.

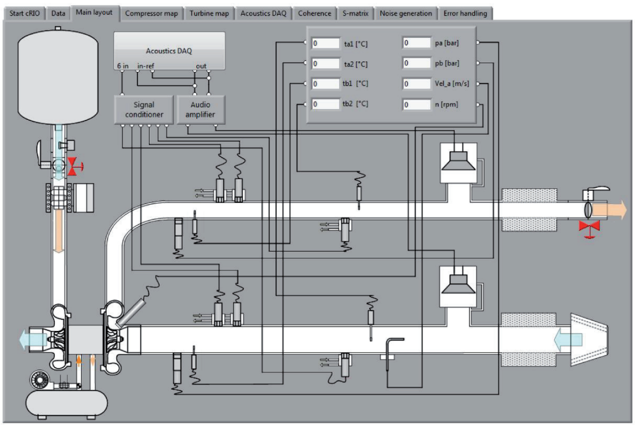

Figure 4. An example screenshot of the custom built data acquisition and control board programmed in LabVIEW.

In order to simulate the operating conditions of the turbocharger the compressor and turbine map has to be followed respectively. In section 3 the performance maps of all the compressors and turbines used in this study together with the operating points (OP) investigated are presented. The characteristic data of the operating points studied for the compressors and turbines are specified in Table 2. In order to define the operating point during the acoustic experiments and to locate it on the compressor map at least two of the three dynamic parameters (the pressure ratio, the mass or volume flow rate and the shaft rotational speed) have to be determined. The compressor pressure ratio is hereby defined as the absolute total outlet (discharge) pressure of the compressor divided by the absolute total inlet pressure. The corrected mass or volume flow rates through the compressor and turbine were determined by using centrally mounted Pitot tubes and a mass flow meter (ABB FMT500-IG). The static pressure values were determined by using pressure transducers (Gems and MPX) mounted at the inlet and outlet cross-sections. Temperature readings in the four cross-sections (see Figs. 2-3) were taken by using NI 9211 thermocouple input module and K-type thermocouples, fixed to the centre of the ducts. The measured flow velocity, pressure and temperature readings were used to determine the density and the speed of sound values in the inlet and outlet pipes and used for calculation of the transmission loss data. To perform the monitoring of the turbocharger shaft rotational speed during the test sessions an eddy-current type speed sensor (Micro-epsilon turbo speed DZ135) pointed onto the compressor wheel blades was used.

2.2. ACOUSTIC CHARACTERIZATION OF TURBO-UNITS

Here a summary of the theory is presented with focus on some aspects not earlier reported such determination of sound power data beyond the plane wave range. Concerning details for measurement of the passive plane wave data, i.e., the scattering-matrix, a full account of this can be found in [4].

2.2.1. DETERMINATION OF THE PASSIVE 2-PORT DATA

To determine the sound transmission the automotive turbocharger is treated as an acoustic 2-port. This implies the following relationship in the frequency domain [5]:

$$\underbrace{\begin{bmatrix} p_{a+} \\ p_{b+} \end{bmatrix}}_{p_+} = \underbrace{\begin{bmatrix} S_{11} & S_{12} \\ S_{21} & S_{22} \end{bmatrix}}_{S} \cdot \underbrace{\begin{bmatrix} p_{a-} \\ p_{b-} \end{bmatrix}}_{p_-} + \underbrace{\begin{bmatrix} p_{a+}^S \\ p_{b+}^S \end{bmatrix}}_{p_+^S}, \qquad (1)$$

where S_{11}, S_{22} and S_{12}, S_{21} describe the reflection and transmission of the incoming waves respectively, a and b (or 1 and 2) refer to two sides of the two-port (up- to downstream side), the plus and minus signs indicate propagation outwards and into the two-port respectively and the superscript s refers to source generated sound.

By forming the transfer functions between the measured signals and the external signal driving the external sources e, the scattering matrix can be determined. To obtain the scattering matrix we also need two different acoustic test states which can be created by using acoustic excitation on both sides of the test object. Eq. 1 can then be expressed as:

$$\begin{bmatrix} H_{ea+}^{I} & H_{ea+}^{II} \\ H_{eb+}^{I} & H_{eb+}^{II} \end{bmatrix} = \begin{bmatrix} S_{11} & S_{12} \\ S_{21} & S_{22} \end{bmatrix} \begin{bmatrix} H_{ea-}^{I} & H_{ea-}^{II} \\ H_{eb-}^{I} & H_{eb-}^{II} \end{bmatrix}, \qquad (2)$$

where the superscript indicates the different test states (I - upstream drivers "on" and downstream "off", II - downstream drivers "on" and upstream "off"). H_{ex} is the transfer function taken between the travelling wave amplitude x and the voltage e exciting the drivers which can be related to the pressure transducer signals using the two-microphone technique [6].

By knowing the S-matrix elements, we have the complete information about the passive acoustic effect of the two-port device tested, including the transmission loss (TL) which can be calculated as follows:

$$TL_u = 10 \cdot \log\left(\frac{W_{b-}}{W_{a-}}\right) = 10 \cdot \log\left(\frac{(1+M_b)^2 A_b \cdot \rho_a \cdot c_a}{(1+M_a)^2 A_a \cdot \rho_b \cdot c_b |S_{12}|^2}\right), \qquad (3)$$

$$TL_d = 10 \cdot \log\left(\frac{W_{a+}}{W_{b+}}\right) = 10 \cdot \log\left(\frac{(1+M_a)^2 A_a \cdot \rho_b \cdot c_b}{(1+M_b)^2 A_b \cdot \rho_a \cdot c_a |S_{21}|^2}\right), \qquad (4)$$

where TL_u is the transmission loss in upstream direction and TL_d is the transmission loss in downstream direction, W_+ and W_- are the incident acoustic powers from the up- and downstream side, respectively, M is the Mach number, A is the cross-sectional area of the pipe, ρ is the air density and c is the speed of sound.

2.2.2. ESTIMATION OF THE POWER LOST

Here a suitable state variable is the acoustic energy x [7], which is simply related to the time averaged power as $W_\pm = \hat{x}_\pm^* \hat{x}_\pm$. Now, denoting the scattering matrix in energy form $\mathbf{S}_P$ the time averaged acoustic power loss for a given incident acoustic field is

$$W_{loss} = \hat{\mathbf{x}}_-^* \hat{\mathbf{x}}_- - \hat{\mathbf{x}}_-^* \left(\mathbf{S}_P^* \mathbf{S}_P\right) \hat{\mathbf{x}}_-, \qquad (5)$$

where * is the Hermitian transpose. If the flow-acoustic interaction result in an amplification of the incident sound this equation is positive. One way of using this result is to assume excitation at only one port *n* at the time. Although a multi-port in practice is likely to experience incident sound at more than one port at the time this approach can give valuable insight into the systems characteristics. Normalizing the incident power at the port of interest to unity (that is, $\hat{\mathbf{x}}_{n-}^{*}\hat{\mathbf{x}}_{n-}=1$ this can be expressed as

$$W_{loss}=1-\hat{\mathbf{x}}_{n-}^{*}\left(\mathbf{S}_{P}^{*}\mathbf{S}_{P}\right)\hat{\mathbf{x}}_{n-}. \tag{6}$$

Using this result the acoustic losses in a turbo-charger unit can be computed for up- or downstream excitation using the measured two-port data.

2.2.3. A QUASI-STATIONARY MODEL OF THE SOUND TRANSMISSION

Assuming low pulsation frequencies the acoustic wavelength will be much larger than the size of the turbo unit and wave propagation effects can be neglected. A model can then be derived using a quasi-stationary approach. The starting point in this case is the set of equations governing the flow based on enthalpy and mass flow. For the enthalpy *h* there is a decrease or increase between the inlet (1) and outlet (2) for the turbine and compressor (see Fig. 5), respectively.

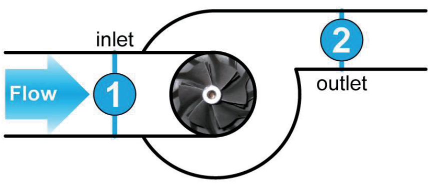

Figure 5. A simplified schematic layout illustrating the model set up for a turbocharger.

The following equation can be written:

$$h_1=h_2+\Delta h. \tag{7}$$

For the mass flow *m* we get:

$$m_1=m_2. \tag{8}$$

Adding now a fluctuating part on the steady flow part we get: $h = h_0 + h'$ and $m = m_0 + m'$, where the subscript 0 denotes the steady flow part and the prime the fluctuating part. Inserting this into Eqs. (7) and (8) and subtracting the steady flow part gives:

$$\begin{cases} h'_1 = h'_2+\Delta h' \\ m'_1=m'_2 \end{cases}. \tag{9}$$

The fluctuating change in enthalpy $\Delta h'$ is now split into two parts. The first part $\Delta h'_{loss}$ is associated with losses and is assumed to be proportional to the fluctuating mass flow, i.e., it represents a linear loss term. The second part $\Delta h'_{source}$ is a source term which in accordance with Lighthill is independent of the fluctuating fields and only depends on the steady flow. Based on these ideas one rewrite eq. (9) in the form of a two-port:

$$\begin{pmatrix} h'_1 \\ m'_1 \end{pmatrix}=\begin{bmatrix} 1 & R \\ 0 & 1 \end{bmatrix}\begin{pmatrix} h'_2 \\ m'_2 \end{pmatrix}+\begin{pmatrix} \Delta h'_{source} \\ 0 \end{pmatrix}. \tag{10}$$

Equation (10) represents the TC two-port in so called transfer (**T**) matrix form and the scattering of sound is related to the passive part of this equation or the **T**-matrix. Expressing the fluctuating enthalpy and mass flow in propagating pressure wave amplitudes results in:

$$\begin{pmatrix} \frac{1}{\rho_1}[1-(1-r)M1] & -\frac{1}{\rho_2}(1+M2) \\ \frac{A1}{c_1}(1-M1) & \frac{A2}{c_2}(1+M2) \end{pmatrix}\begin{pmatrix} p'_{1-} \\ p'_{2+} \end{pmatrix}=\begin{pmatrix} -\frac{1}{\rho_1}[1+(1-r)M1] & \frac{1}{\rho_2}(1-M2) \\ \frac{A1}{c_1}(1+M1) & \frac{A2}{c_2}(1-M2) \end{pmatrix}\begin{pmatrix} p'_{1+} \\ p'_{2-} \end{pmatrix}, \tag{11}$$

which can be written as:

$$\boldsymbol{S}_l\begin{pmatrix} p'_{1-} \\ p'_{2+} \end{pmatrix}=\boldsymbol{S}_r\begin{pmatrix} p'_{1+} \\ p'_{2-} \end{pmatrix}\Rightarrow\begin{pmatrix} p'_{1-} \\ p'_{2+} \end{pmatrix}=\boldsymbol{S}_l^{-1}\boldsymbol{S}_r\begin{pmatrix} p'_{1+} \\ p'_{2-} \end{pmatrix}, \tag{12}$$

where the last expression gives the scattering-matrix: $\boldsymbol{S}=\boldsymbol{S}_l^{-1}\boldsymbol{S}_r$. The factor *r* represents the losses normalized to the inlet conditions:

$$\Delta h'_{loss}=rU1u'_1. \tag{13}$$

Solving these equation for the elements S_{12} and S_{21} it is found that the up and down- and upstream TL are the same for a system with no losses. In other words any difference seen between these two TL measures for low frequencies is entirely due to the losses we have in the system. Using the approach described in sec. 2.2.2 these losses can be investigated.

2.2.4. SOUND GENERATION

In this section the focus is on the aerodynamically generated sound, which always dominates for high RPM and when there is a negligible contribution from unbalances.

In the plane wave range the sound generation can be obtained by including the source strength in Eq. 1 as described for instance in Ref. [8]. It can be noted that this approach eliminates the effect of reflections in the test rig. Beyond the plane wave range one can either use standard (e.g. ISO) methods to estimate the propagating sound power which require reflection free terminations. The KTH rig is equipped with terminations which are damped (rubber hoses not shown in Fig.2) and have dissipative silencers. This arrangement gives some reflections in the plane wave range but should give very small reflections for high frequencies. The standard methods are based on spatial averaging of the sound field and normally involve some assumption that the power is equally distributed over the propagating modes. Since most of the noise emission [1] will lie well above the plane wave range it is essential to include such methods in the testing. In the present investigation it was decided to use the same transducer array (3 on each side) as used for the plane wave range two-microphone approach. The spatial averaging needed to obtain an estimate of the strength of the propagating modes was achieved by using cross-spectra between the transducers. This also has the advantage of reducing turbulence noise at the transducers. The estimate for the propagating mode strength G_{++} used can then be written:

$$G_{++} = \mathrm{Re}\left[(G_{12} + G_{13} + G_{23}) / 3 \right], \tag{14}$$

where G_{12},G_{13} and G_{23} are the cross-spectrums between the microphone pairs. This auto-spectrum can be related to the sound power by assuming e.g. a semi-diffuse sound field.

3. THE TURBOCHARGERS TESTED

3.1. TECHNICAL DESCRIPTION OF THE TURBOCHARGERS TESTED

Technical information about the three turbochargers investigated is given in Table 1. In Fig. 6 photos describing the geometry of the turbochargers wheel and housing for compressor and turbine side are presented.

Table 1. Technical data of the three turbochargers investigated. Type C is the VTG turbine.

Turbocharger	KKK K24	Garret GT1752	Garret GT1749V
	A	B	C
Turbine			
A/R ratio	0.41	0,47	0,42
Scroll inlet diameter [mm]	52	40	43
Approximate scroll length [mm]	300	285	380
Number of rotor blades	12	9	9
Radius of the rotor [mm]	29	22	21
Rotor length [mm]	21	20	25
Compressor			
Scroll outlet diameter [mm]	41	43	38
Approximate scroll length [mm]	460	358	370
Number of rotor blades	6+6	6+6	5+5
Radius of the rotor [mm]	31	26	25
Rotor length [mm]	25	20	18

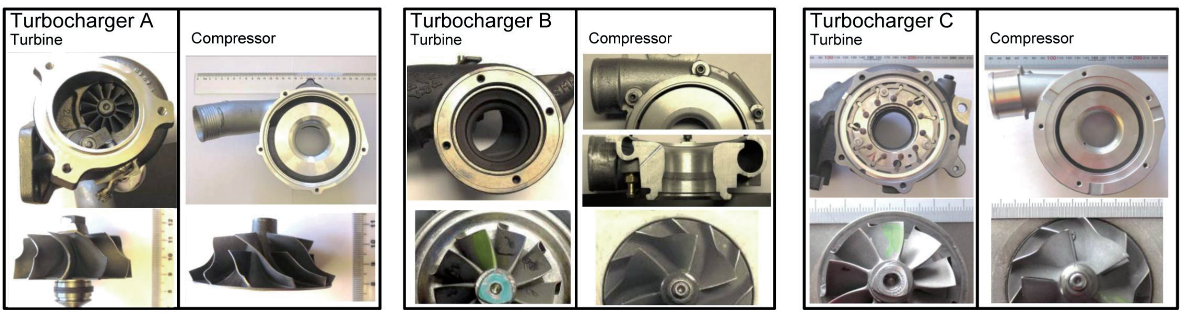

Figure 6. Photos of the turbine and compressor of turbochargers A, B and C.

3.2. OPERATING CONDITIONS

The operating points measured on the compressor- and turbine maps are illustrated in Figs. 7-8 for all three turbocharger tested. Details of the operating conditions of the turbochargers at which the experiments were carried out are summarized in Ref. 4. It should be noted here that for turbocharger A only the compressor was investigated.

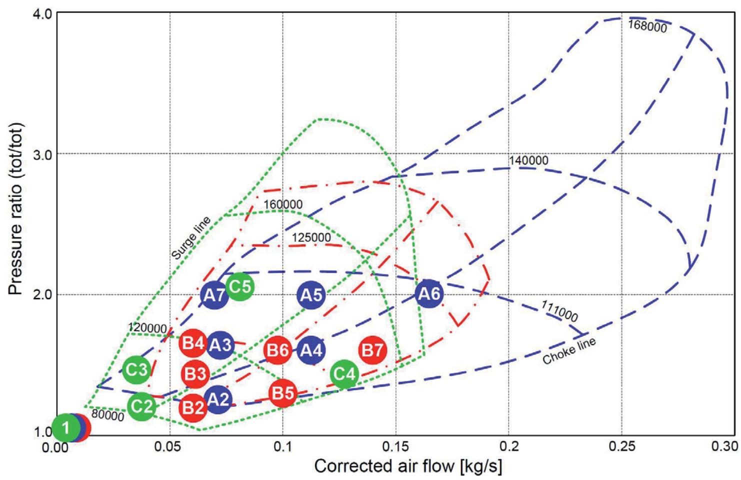

Figure 7. Comparison of simplified compressor charts for all three turbochargers investigated. The experimentally studied operating points are shown as A1…A7 (turbocharger A), B1…B7 (turbocharger B) and C1…C5 (turbocharger C).

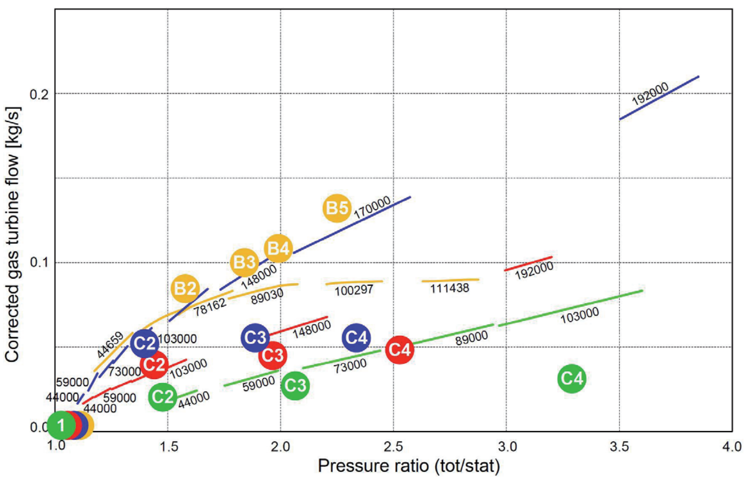

Figure 8. Comparison of simplified turbine charts for all three turbochargers investigated. The experimentally studied operating points are shown as B1…B5 (turbocharger B) and C1…C4 (turbocharger C). The three groups of data for the turbine C (VTG) distinguished by different colors correspond to three guide-vane positions of the VTG actuator tested: 100% open (blue), 50% open (red) and 0% open (green). The turbine of the turbocharger A was not studied in this paper.

4. RESULTS AND ANALYSIS

4.1. PASSIVE RESULTS

4.1.1. TRANSMISSION LOSS DATA

The experimentally determined transmission loss results in up- and downstream directions for all the turbo-compressors and turbines tested are presented in Figs. 9 and 10 respectively.

For the stationary turbocharger (RPM=0) the transmission loss (TL) is not dependent on the direction of the sound propagation. Also the TL curves for the no flow case approach a small value at low frequencies which is related to the area change of the pipes across the unit. If these areas are equal then the no flow TL will approach zero at low frequencies. When the unit is rotating the low frequency TL will be affected by the change in both area and characteristic impedance across the device. Computing these effects for the tested cases typically give TL values less than 1 dB. Also if only changes in acoustic impedance across the device would matter for the low frequency behaviour, it is straightforward to prove that the TL values would be the same in the up- and downstream directions (see sec. 2.3). It is therefore clear that the main part of the low frequency TL values must be caused by dissipation, e.g., due to flow acoustic interaction in particular at regions with flow separation. Of course for supersonically rotating wheels shock waves can create both reflections and also dissipation of incident sound waves. The importance of losses is also clear from the fact that the TL values for a given unit tends to increase with the mass flow.

4.1.2. SCATTERING MATRIX DATA-AN EXAMPLE

In Fig. 11 an example of four scattering matrix elements (magnitude) are plotted for the GT1752 turbo compressor in

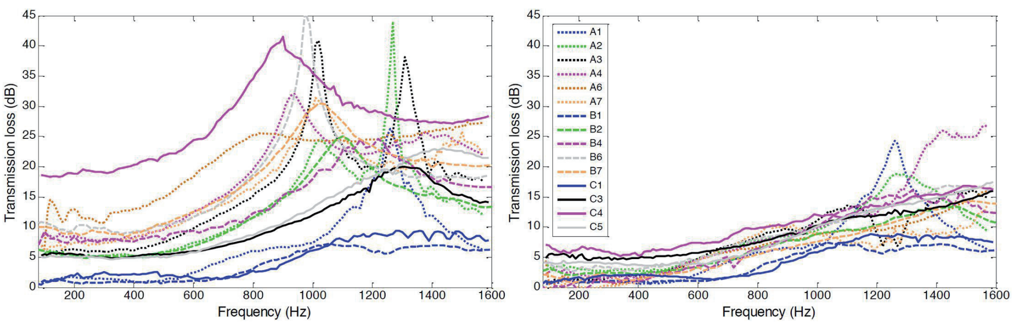

Figure 9. The transmission loss results for all three turbo-compressors in upstream (left) and downstream (right) direction. For clarity, only selected results have been plotted in this figure. A legend valid for both figures is shown on the left side.

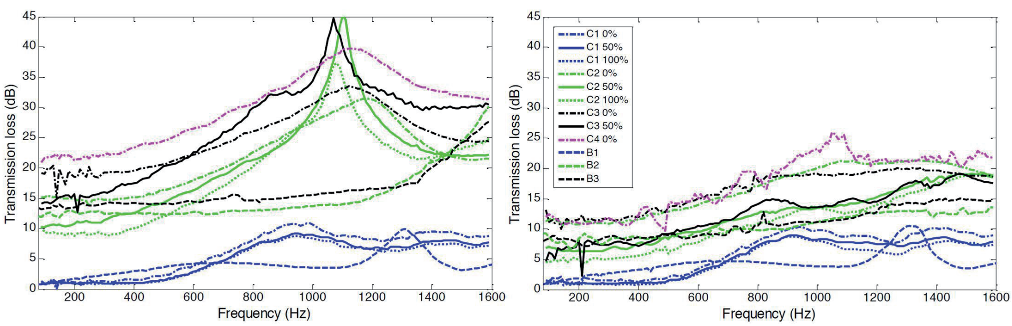

Figure 10. The transmission loss results for turbocharger B and C (VTG) turbines in upstream (left) and downstream (right) direction. The turbine of the turbocharger A was not studied in this paper. For clarity, only selected results have been plotted in this figure. A legend valid for both figures is shown on the left side.

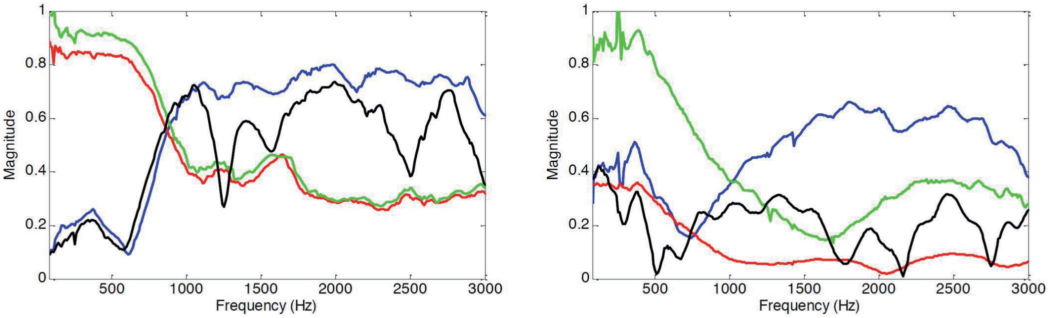

Figure 11. The scattering matrix results for Garret GT1752 turbocharger compressor in OP1 (left) and OP3 (right). Blue line is S11, red line is S12, green line is S21 and black line is S22 respectively.

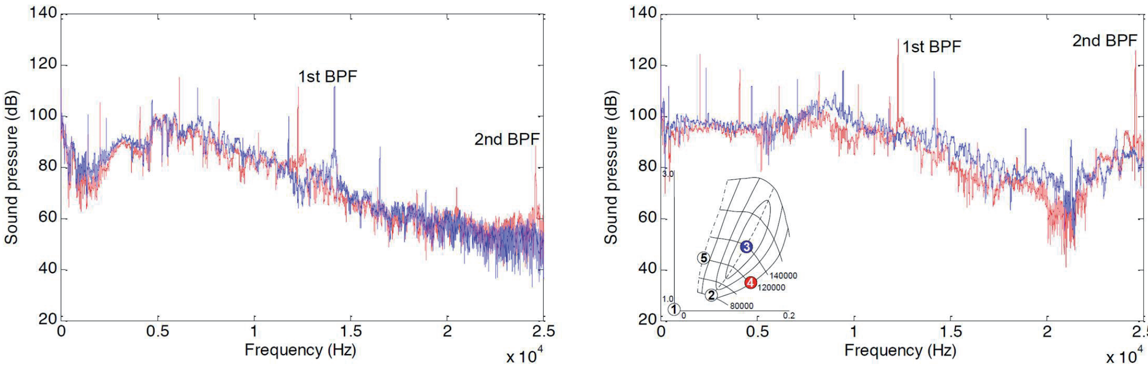

Figure 12. Comparison of sound pressure spectral densities between OP3 (blue line) and OP4 (red line) in inlet side (left) and outlet side (right).

OP1 (static) and working in OP3 where the elements S11 and S22 define the reflection from and the elements S12 and S21 represent the transmission of the incident waves through the object. As noted in sec. 2.2.2 these data can be used to in more detail analyse the losses occurring in the unit to better understand the low frequency TL behaviour.

4.2. SOUND GENERATION RESULTS

The method (Eq. 13) described in section 2.2.4 has been tested on the compressor side for turbocharger B (see table 1). It was found that the method had a noise floor in the range of 60-80 dB. The operating points investigated were: OP3, OP4 and OP5 (see compressor map included on Fig. 12 and Fig. 13).

A comparison of sound pressure spectral densities between OP3 and OP4 (constant pressure ratio) is shown in Fig. 12. From the compressor map we see that the mass flow for OP3 and OP4 are close to each other but the RPM:s are different. As can be seen from the figure, for both sides, the difference between the results from OP3 and OP4 is mainly a shift in the BPF peaks, while the broad band is more or less unchanged except for a 5 dB increase for OP3 outlet side.

A comparison of sound pressure spectra densities between OP4 and OP5 (constant RPM) is shown in Fig. 13. It can be noticed that close to the surge line (OP5) the tip clearance noise becomes more dominant. When we focus on the frequency range up to 10000 Hz the average difference between OP4 and OP5 auto-spectrum levels is as large as 20 dB.

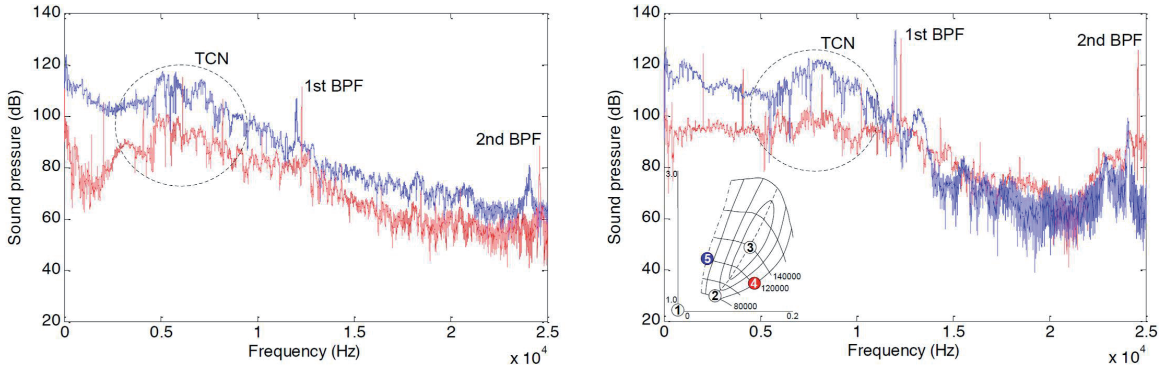

Figure 13. Comparison of sound pressure spectral densities between OP4 (red line) and OPS (blue line) in inlet side (left) and outlet side (right).

5. CONCLUDING REMARKS

The unique acoustic turbocharger test facility at KTH has been presented together with the experimental procedures to determine the scattering and generation of sound from automotive turbochargers. The scattering data is obtained in the plane wave range as acoustic two-ports that can be used to compute the typical damping or transmission loss of turbo units. A summary of trends found for the transmission loss based on measurements on a number of units is given. As shown in our recent SAE paper [4] these trends can generalized by plotting the data as function of the Helmholtz-number, which makes the trends applicable for any operating conditions or turbo-charger diameters. Also the importance of losses to explain the low frequency transmission loss is pointed out and demonstrated by a simple quasi-stationary model. In order to better understand the mechanisms that create these losses, it is suggested to study the two-port data in more detail. This will be addressed in future works using the power balance formulation described in section 2.2.2. Concerning the measurement of acoustic power the main interest is beyond the plane wave range. For this range an approach based on using the microphone array already installed for the two-port measurements is proposed and tested. Here a more detailed investigation of the accuracy of this method is required in a future work.

REFERENCES

1. Rämmal, H. and Åbom, M., "Acoustics of Turbochargers," SAE Technical Paper 2007-01-2205, 2007, doi:10.4271/2007-01-2205.

2. Rämmal, H. and Åbom, M., "Experimental Determination of Sound Transmission in Turbo-Compressors," SAE Technical Paper 2009-01-2045, 2009, doi: 10.4271/2009-01-2045.

3. Rämmal, H., Galindo, J., "The Passive Acoustic Effect of Turbo-Compressors," presented at the 9th International Conference on Turbochargers and Turbocharging, UK, May 19-20, 2010.

4. Tiikoja, H., Rämmal, H., Abom, M., and Boden, H., "Sound Transmission in Automotive Turbochargers," SAE Technical Paper 2011-01-1525, 2011, doi: 10.4271/2011-01-1525.

5. Bodén, H., and Åbom, M., "Modelling of Fluid Machines as Sources of Sound in Duct and Pipe Systems," *Acta Acustica*, **3**: 1-12, 1995.

6. Åbom, M., "Measurement of the Scattering-Matrix of Acoustical Two-Ports," *Mech. Systems and Signal Proc* **5**(2): 89-104, 1991.

7. Aurégan, Y. and Starobinski, R., "Determination of acoustical dissipation/production potentiality from the acoustical transfer function of a multiport", *Acta Acustica* 85:788-792, 1999.

8. Lavrentjev, J., Åbom, M., and Bodén, H., "A measurement Method for Determining the Source Data of Acoustic Two-Port Sources," *Journal of Sound and Vibration* **183**(3): 517-531, 1995.

9. Karlsson, M., "Aeroacoustic Studies of Duct Branches - with Application to Silencers," Ph.D. Thesis, Aeronautical and Vechicle engineering Department, The Royal Institute of Technology, Stockholm, 2011.

10. Auregan, Y., Starobinski, R., "Determination of Acoustical Dissipation/Production Potentiality from the Acoustical Transfer Function of a Multiport," *Acta Acustica* **85**: 788-792, 1999.

11. Watson, N., Janota, M. S., "Turbocharging the Internal Combustion Engine," Macmillan Publishers Ltd., London, 1982.

CONTACT INFORMATION

Mats Åbom
matsabom@kth.se
phone: +46 8 7907944

Hans Rämmal
hansra@kth.se
phone: +37 256 465738

ACKNOWLEDGMENTS

The authors acknowledge master student Zhenrui Wang (KTH) for processing measured turbocharger sound radiation data and Volvo Car Corporation and GM Powertrain for providing turbochargers for the investigations. Support from Estonian Science Foundation (No 7913) is also acknowledged.

Paper III

Lavrentjev, J., Rämmal, H., Tiikoja, H.,
The Passive Acoustic Effect of Automotive Catalytic Converters
SAE Technical Paper Series, Paper 2011-24-0219

SAE International

The Passive Acoustic Effect of Automotive Catalytic Converters

2011-24-0219
Published
09/11/2011

Jüri Lavrentjev, Hans Rämmal and Heiki Tiikoja
Tallinn University of Technology

doi:10.4271/2011-24-0219

ABSTRACT

For the last couple of decades, catalytic converters (CC) have become a standard part of the internal combustion engine exhaust systems. Besides reducing toxic components in exhaust gases, catalytic converters can have a certain effect on the acoustic performance of the exhaust system. In this paper the sound transmission and attenuation in the catalytic converters has been investigated. A catalytic converter is known to have two distinct acoustic effects: the reactive effect originating from the acoustic wave reflections caused by cross-sectional area changes within the unit and the resistive effect which results in the acoustic wave dissipation caused by visco-thermal losses. The flow resistance in the narrow tubes in the catalytic converter element results in frequency dependent dissipative effects on the transmitted sound. An experimental investigation on engine catalytic converters treated as acoustic two-ports is carried out. The acoustic behavior of the catalytic converters is investigated in detail by analyzing the scattering matrix elements.

INTRODUCTION

Catalytic converters (CC) are commonly used in motor vehicle exhaust systems. Their main purpose is to provide an environment for chemical reactions to convert toxic combustion products to less-toxic ones. The catalytic converter as an integral part of the modern exhaust system makes a notable contribution to the acoustical performance of the complete system. Therefore, the knowledge of the acoustical properties of the catalytic converters is essential for efficient design of the exhaust systems as well as for the development of predictive tools for IC-engine exhaust systems [1].

Most of the investigations on the CC-s have typically considered the relevant chemical reactions in the unit. Despite of the fact that today almost every automotive IC-engine produced is equipped with CC and a large variety of CC types has been designed, relatively few papers related to the acoustic performance of the devices are available. Peat [2] and Astley with Cummings [3] implemented FEM analysis, based on equations for waves in a visco-thermal fluid in the quadratic cross-section capillary tubes, to study the acoustics of CC. An acoustic two-port model for the CC was derived by Dokumaci [4], assuming a plug flow in the capillary tubes. In [5] analytical solutions for the sound propagation in capillary cylindrical tubes with a parabolic mean flow were developed by Ih et al. In a later work Dokumaci [6] extended his earlier studies [4] for the conditions of rectangular narrow tubes with a plug flow. An investigation, implementing both the CFD and experimental approach, was performed by Jeong and Kim [7] for unsteady three-dimensional flow inside a monolith catalytic converter. Transmission loss (reduction of acoustic power) and back pressure (pressure loss across the device) characteristics of three different CC types composed of metal and ceramic substrate converters were experimentally determined by Lavrentjev and Rämmal [8] in a variety of mean flow conditions.

In this paper the passive acoustic effect that treats the sound transmission, reflection and absorption inside the catalytic converters is investigated by performing the complete acoustic two-port analysis. Hereby, the scattering matrix elements are presented for all the CC-s studied together with the absorption coefficients computed.

There are two common types of catalytic converters determined by the core material of the unit: ceramic core type and metal core type. In the modern mufflers the metal core (also known as the metal matrix) CC-s are frequently used.

This type of CC offers improved resistance to shock, vibration and physical impact compared to the ceramic core type. Also, engine rich running, which can melt and deteriorate the ceramic core, are less harmful for the metal CC-s. As one of the major hindrances, the metal CC-s are more expensive to produce. In this paper both the CC types are investigated experimentally and quantitative acoustic data for the particular CC-s are presented to characterize the acoustical behavior.

In order to determine the acoustical characteristics, the CC-s are typically treated by focusing on the following two parts: the casing and the catalytic converter honeycomb. Today, the acoustical behavior of the surrounding casing has been investigated thoroughly and the relevant two-port models exist. The acoustic characteristics of the honeycombs are less investigated, partly due to more complex gas dynamic phenomena related to the narrow capillary tubes. The ambition of this paper is to experimentally investigate the honeycomb part of the CC-s by studying prepared samples. The acoustic characteristics of ceramic and metal honeycombs are investigated in a variety of operating conditions (mean flow temperature and velocity).

EXPERIMENTS

A DEDICATED EXPERIMENTAL FACILITY was used to determine the acoustic two-port data of the catalytic converters in a variety of flow velocity and temperature conditions. A sketch and a photo of the set-up implemented in the experimental work are presented in Figs. 1 and 2. The design of the test-rig together with the technical solutions developed and implemented for the improvement of the quality of the results is described in details in earlier works by the authors, for instance in [8,9]. Thus, only a few relevant issues are briefly described hereby.

In order to focus on the acoustic effect of the honeycomb, the CC-s studied were first decomposed by extracting the honeycomb core material and mounting it into the test section of the rig (see Fig. 1). The extracted samples of the CC honeycomb elements were fixed between two flanged steel pipes, which formed the test section with uniform active diameter (42mm) for all the samples studied. The classical two-microphone approach [10] was used to obtain complex pressure amplitudes of the traveling acoustic waves at the inlet and outlet cross-sections of the test-section. Two water-cooled piezo-resistive pressure transducers were used on both sides of the test section to perform acoustic wave decomposition. The pressure signals were conditioned and amplified for dynamic signal analyser. White noise was found to be an adequate choice for acoustic excitation provided by electro-dynamic drivers equipped with neodymium magnets, titanium membranes and custom-built pressure equalization channels. The drivers were fitted into a side-branch upstream and downstream of the test section (see Fig. 1). The acoustic excitation and the signal acquisition were controlled by PC based custom-built virtual instrument (LabView). Air-flow in the test section, partly simulating the acoustical conditions of exhaust gas flow the CC-s are designed for, was generated by a two-stage high pressure blower, integrated with an electric heater unit (see Fig. 1).

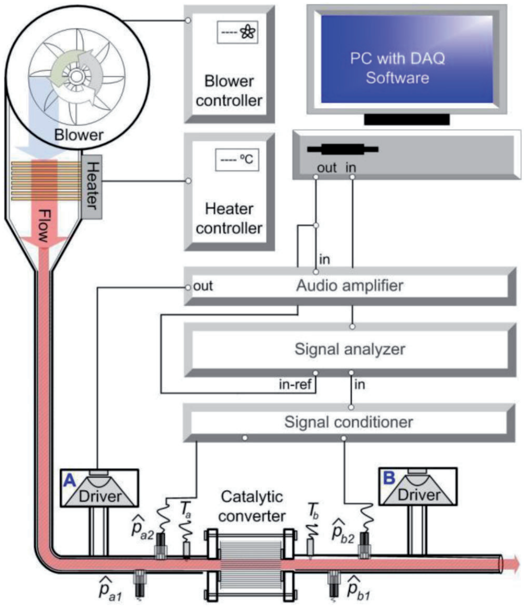

Figure 1. Experimental set-up designed for the complete determination of acoustic two-port data for catalytic converter samples in hot and cold mean flow conditions

THE CATALYTIC CONVERTERS STUDIED are shown in Figs. 3-4, where magnified sections illustrate the design of the catalytic converter cells. The selected honeycomb samples with common cell density (400CPI) were prepared for equal length (76 mm).

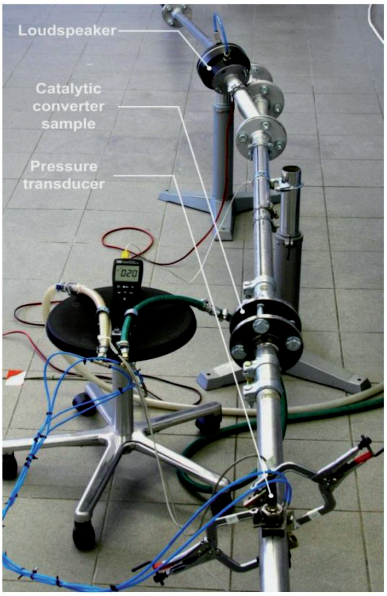

Figure 2. A photo presenting the test-section of the experimental facility.

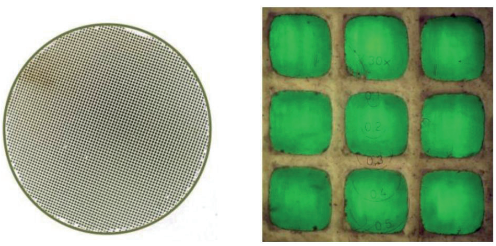

Figure 3. A photo of the first type of catalytic converter sample studied; ceramic core, 76 mm element length and 400 CPI cell density (left side), a 30x magnified microscope image of the honeycomb (right side).

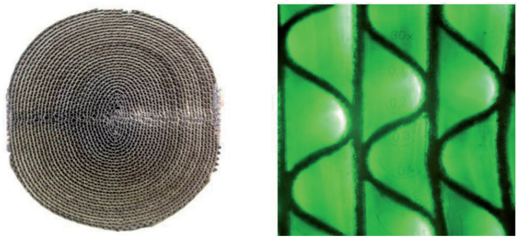

Figure 4. A photo of the second type of catalytic converter sample studied; metal core, 76 mm element length and 400 CPI cell density (left side), a 30x magnified microscope image of the honeycomb (right side).

MEASUREMENT METHOD is based on transfer matrix representation of the two-port element represented in the frequency domain as the relationship between the acoustic states at the inlet (a) and outlet (b) sections (see Fig. 5):

$$\begin{bmatrix} p_{\mathrm{a}+} \\ p_{\mathrm{b}+} \end{bmatrix} = \begin{bmatrix} S_{11} & S_{12} \\ S_{21} & S_{22} \end{bmatrix} \begin{bmatrix} p_{\mathrm{a}-} \\ p_{\mathrm{b}-} \end{bmatrix}, \tag{1}$$

or

$$\mathbf{p}_{+} = \mathbf{S}\mathbf{p}_{-} \tag{2}$$

where p denotes the complex plane wave acoustic pressure, **S** is the two-port scattering matrix, representing the acoustic characteristics of the 2-port. Matrix element $S_{11}=p_{\mathrm{a}+}/p_{\mathrm{a}-}$ represents reflection properties of the 2-port, seeing from *a* side and matrix element $S_{21}=p_{\mathrm{b}+}/p_{\mathrm{a}-}$ represents transmission properties of the 2-port element seeing from *a* side. Therefore, the scattering matrix elements S_{11} and S_{21} can be suitably used for the complete acoustic characterization of the 2-port element in the downstream direction (see Fig. 5).

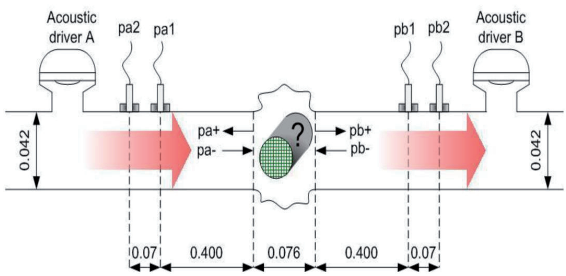

Figure 5. A schematic representation of the measurement set-up used for determination of the acoustic two-port data for catalytic converter samples studied.

In order to compute the four elements of **S** from the equation (1) two independent test states must be created. This can be done by activating two external sources (electro-dynamic drivers) up- and downstream the test section, as illustrated in Fig. 5. By combining the results from the two independent test states the following equation can be derived:

$$\begin{bmatrix} p^{\mathrm{I}}_{\mathrm{a+}} & p^{\mathrm{II}}_{\mathrm{a+}} \\ p^{\mathrm{I}}_{\mathrm{b+}} & p^{\mathrm{II}}_{\mathrm{b+}} \end{bmatrix} = \begin{bmatrix} S_{11} & S_{12} \\ S_{21} & S_{22} \end{bmatrix} \begin{bmatrix} p^{\mathrm{I}}_{\mathrm{a-}} & p^{\mathrm{II}}_{\mathrm{a-}} \\ p^{\mathrm{I}}_{\mathrm{b-}} & p^{\mathrm{II}}_{\mathrm{b-}} \end{bmatrix} \tag{3}$$

where the superscripts denote the test states: I -loudspeaker A “on” and loudspeaker B “off, II -loudspeaker B “on” and loudspeaker A “off”. In order to suppress disturbing flow noise in the measurement section it is preferable to use transfer functions taken between the microphone signals and a reference signal correlated with the sound field in the duct but uncorrelated with flow noise and with the sound field from the source under test. Hereby, the electrical signals *e*, driving loudspeakers A and B are a convenient choice for the reference. Thus, equation (3) can be rewritten into the following form:

$$\begin{bmatrix} H^{\mathrm{I}}_{\mathrm{ea+}} & H^{\mathrm{II}}_{\mathrm{ea+}} \\ H^{\mathrm{I}}_{\mathrm{eb+}} & H^{\mathrm{II}}_{\mathrm{eb+}} \end{bmatrix} = \begin{bmatrix} S_{11} & S_{12} \\ S_{21} & S_{22} \end{bmatrix} \begin{bmatrix} H^{\mathrm{I}}_{\mathrm{ea-}} & H^{\mathrm{II}}_{\mathrm{ea-}} \\ H^{\mathrm{I}}_{\mathrm{eb-}} & H^{\mathrm{II}}_{\mathrm{eb-}} \end{bmatrix} \tag{4}$$

or

$$\mathbf{H}_{+} = \mathbf{S}\mathbf{H}_{-} \tag{5}$$

where $H_{\mathrm{ex}} = p_{\mathrm{X}} / e$, $e=e_{\mathrm{a}}$ implies for the test state I and $e=e_{\mathrm{b}}$ for test case II. The transfer functions required in equation (4) can be expressed by following the description in [12]. By using equations (4-5) it is possible to express the **S** matrix. Now, the transmission loss of the two-port (CC honeycomb in this paper) can be calculated in the downstream (from (a) to (b) side) direction:

$$TL = 10\log\left(\frac{1}{|S_{21}|^2}\frac{d_a^2(1+M_a)^2\rho_b c_b}{d_b^2(1+M_b)^2\rho_a c_a}\right), \tag{6}$$

where M_{a} is a Mach number, ρ is a density of the media and c is the speed of sound. Regarding the equal cross-sections of the duct at (a) and (b) sides of the test section, assuming similar acoustic conditions at both sides of the 2-port and considering energy flow through the 2-port investigated the following coefficients characterizing the passive acoustic effect of the CC can be determined for the downstream direction:

1). power reflection coefficient

$$|R|^2 = \frac{(1-M_a)^2}{(1+M_a)^2}|S_{11}|^2 \tag{7}$$

2). power transmission coefficient

$$|T|^2 = \frac{(1+M_b)^2}{(1+M_a)^2}|S_{21}|^2 \tag{8}$$

3). dissipation coefficient

$$|A|^2 = 1 - |R|^2 - |T|^2. \tag{9}$$

MEASUREMENT RESULTS - the experiments were carried out with the mean flow velocities selected to cover a typical flow velocity range from idling to the maximum load and RPM expected for the type of engines the catalytic converters had been designed for. For comparison a stationary case in the absence of mean flow was added. Since the heating capacity of the test-rig was limited the maximum temperature of the flow was set to 200 °C, which represents the conditions typical for engine idling. It should also be noted that 200 °C is typically the initiation combustion temperature for most of the modern catalytic converters. Results measured in room temperature conditions (20 °C) were added for comparison.

All the results in this paper are presented for the frequency range from 400 to 1600 Hz, which is determined by the microphone separation *s* used for the two-microphone approach. The experimentally determined transmission loss results for the catalytic converter samples plotted for different flow speeds and flow temperatures are shown in Figs. 6, 7, 8. As can be seen in Fig. 6 the ceramic core CC offers a relatively higher transmission loss over the frequency range investigated with maximum attenuation at 7-8 dB-s around 1000-1200 Hz frequency region. In case of higher mean flow velocities the transmission loss tends to increase all over the frequency range for both the CC types studied (see Fig. 6 and 7), clearly indicating the effect of visco-thermal losses induced by the flow separation in the capillary tubes of the honeycomb element.

Expectedly, a shift towards the higher frequencies can be observed for the ceramic honeycomb (see Fig. 6) in case of measurements in increased temperature conditions. This can be explained by the change of the speed of sound in the air-flow passing through the CC element.

The transmission loss in Fig. 7 presented for the metal core CC on the contrary is relatively less sensitive to the variation of flow speed and temperature. The higher values of the ceramic converter compared to the metal one exhibited in Fig. 8 can be explained by four times higher porosity of the unit leading to increased dissipation of acoustic waves.

In Figs. 9, 10, 11, 12 the influence of the flow velocity and the temperature on the acoustic coefficients of the catalytic converters, computed by following the equations (7),(8),(9), is presented. In Figs. 9-10 it can be clearly noticed that the acoustic attenuation in the ceramic CC is mostly determined by the dissipation effect inside the converter. The reflection of pressure waves at the inlet cross-section of the sample presents a relatively minor effect in this case. It can be concluded that the catalytic converter core clearly behaves similarly to a dissipative type of muffler. The dissipation effect tends to be insensitive to the flow speed but exhibits a frequency shift due to the increasing temperature. While being affected by the flow speed, the reflection coefficient at the element does not show a noticeable dependency on the temperature. The resonant peak seen on the dissipation curves correlates well with the TL peaks in Fig. 6.

Since the dissipation inside the metal core is lower and less frequency dependent than in the ceramic element the resulting curves are almost flat across the frequency range. The dissipation inside the metal CC tends to decrease in increased flow speed and decreased temperature conditions. The reflection coefficient at the elements shows almost a negligible dependency on the flow speed and temperature.

In Fig. 13 a comparison between the acoustic coefficients of two CC honeycomb types is presented. The figure shows that both the CC types offer very little acoustic reflection across the frequency range studied. This is expectable, by considering the dominant resistive character of the units described earlier. To generalize, it can be interpreted from the results that acoustically both the CC-s behave similarly to a dissipative type of muffler in which the absorption of sound caused by the visco-thermal effects typically dominates.

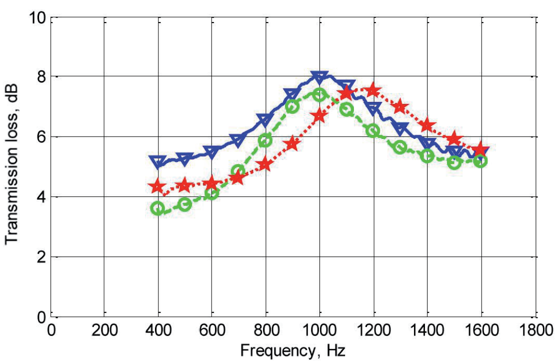

Figure 6. The acoustic transmission loss measured for the ceramic core: 20°C and 0m/s (dashed green line, circles), 20°C and 60m/s (solid blue line, triangles), 200°C and 60m/s (dotted red line, stars).

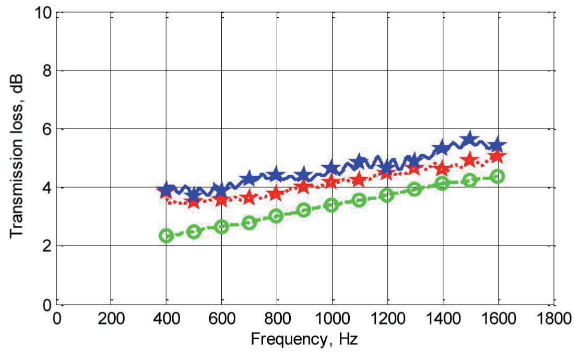

Figure 7. The acoustic transmission loss measured for the metal core: 20°C and 0m/s (dashed green line, circles), 20°C and 60m/s (solid blue line, stars), 200°C and 60m/s (dotted red line, stars).

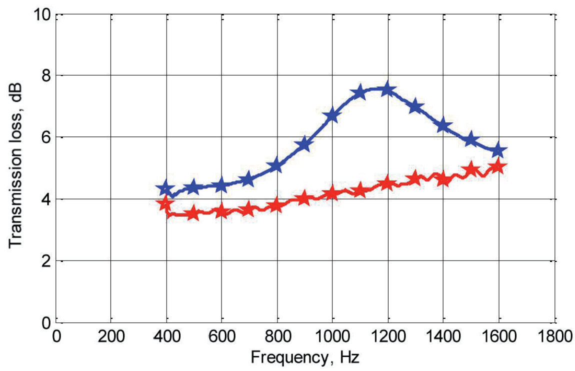

Figure 8. The acoustic transmission loss measured for the catalytic converters at 200°C and 60m/s: ceramic core (dashed blue line, stars), metal core (solid red line, triangles).

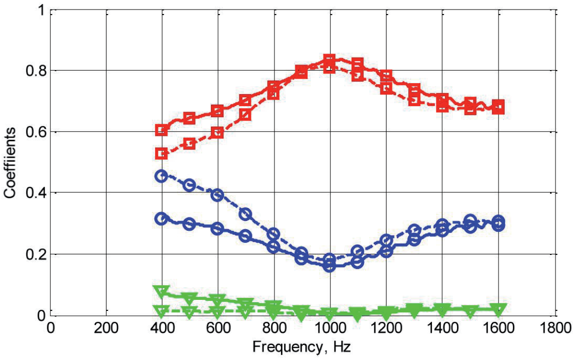

Figure 9. The acoustic power coefficients experimentally determined for the ceramic catalytic converter: 20°C and 0 m/s (dashed line), 20°C and 60 m/s (solid line), dissipation (red line, quadrates), reflection (green line, triangles), transmission (blue line, circles).

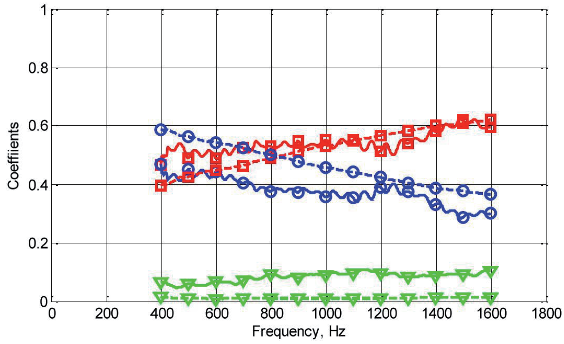

Figure 11. The acoustic power coefficients experimentally determined for the metal catalytic converter: 20°C and 0 m/s (dashed line), 20°C and 60 m/s (solid line), dissipation (red line, quadrates), reflection (green line, triangles), transmission (blue line, circles).

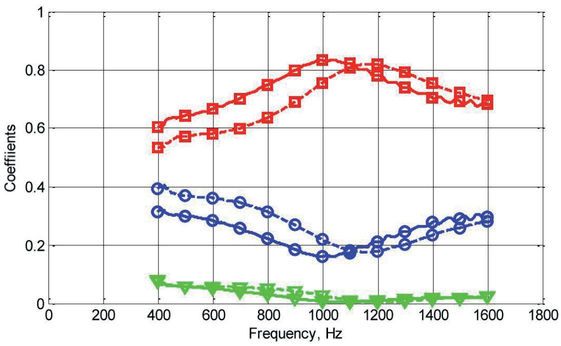

Figure 10. The acoustic power coefficients experimentally determined for the ceramic catalytic converter: 20°C and 60 m/s (solid line), 200°C and 60 m/s (dashed line), dissipation (red line, quadrates), reflection (green line, triangles), transmission (blue line, circles).

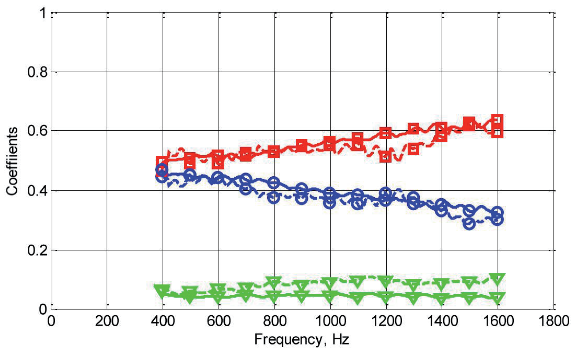

Figure 12. The acoustic power coefficients experimentally determined for the metal catalytic converter: 20°C and 60 m/s (dashed line), 200°C and 60 m/s (solid line), dissipation (red line, quadrates), reflection (green line, triangles), transmission (blue line, circles).

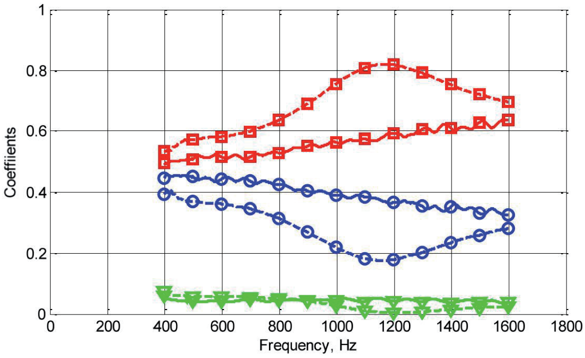

Figure 13. The acoustic power coefficients experimentally determined for the catalytic converters at 200°C and 60m/s: ceramic core (dashed line), metal core (solid line), dissipation (red line, quadrates), reflection (green line, triangles), transmission (blue line, circles).

CONCLUSIONS

In this paper an experimental study on the complete acoustic characterization of different catalytic converter types has been presented. Test samples prepared of two typical catalytic converter honeycomb core types have been characterized by analyzing the acoustic transmission loss results and the scattering matrix elements.

It has been demonstrated that the attenuation of sound in both the catalytic converter element types is dominantly determined by the visco-thermal dissipation effects occurring inside the element. Both the honeycomb types offer a relatively little acoustic reflection in the frequency range investigated.

The catalytic converter cores exhibit a relatively flat transmission loss results in the frequency range studied. The transmission loss of the units tested was low, especially compared to a typical commercial exhaust silencer used in the exhaust systems, and the maxima did not exceed 6-8 dB depending on the honeycomb type. This is natural considering the relatively small dimensions of the honeycomb elements compared to the wavelength of the acoustic excitation, as well as the non-reflective behavior of the units.

It has also been experimentally proven that the attenuation of sound inside the catalytic converter honeycombs is not remarkable affected by the operating conditions of the device.

To the authors knowledge, this paper represents the first complete acoustic characterization and comparison of catalytic converter honeycomb types in a variety of operating conditions by using the acoustic coefficients derived from the scattering matrix elements of the two-port.

ACKNOWLEDGMENTS

The authors acknowledge the support from the Estonian Science Foundation (No 7913).

REFERENCES

1. Munjal, M.L., Acoustics of ducts and mufflers with application to exhaust and ventilation system design, Wiley-Interscience, 328 p (1987).

2. Peat, K. A first approximation to the effects of mean flow on sound propagation in capillary tubes, Journal of Sound and Vibration 175 (1994) 475-489.

3. Astley, R.J., Cummings, A., Wave propagation in catalytic converter: formulation of the problem and finite element scheme, Journal of Sound and vibration 188 (5) (1995) 635-657.

4. Dokumaci, E. Sound transmission in narrow pipes with superimposed uniform mean flow and acoustic modeling of automobile catalytic converters, Journal of Sound and vibration 182 (1995) 799-808.

5. Ih, J.-G. Park, C.M., Kim, H.-J. A model for sound propagation in capillary ducts with mean flow, Journal of Sound and Vibration 190 (2) (1996) 163-175.

6. Dokumaci, E. On transmission of sound in circular and rectangular narrow pipes with superimposed mean flow, Journal of sound and vibration 210 (3) (1998) 375-389.

7. Jeong, S. and Kim, T., "CFD Investigation of the 3-Dimensional Unsteady Flow in the Catalytic Converter," SAE Technical Paper 971025, 1997, doi: 10.4271/971025.

8. Lavrentjev, J. and Rämmal, H., "On Experimental Techniques to Determine Acoustic Performance of Small Exhaust Silencers," SAE Technical Paper 2009-32-0015, 2009, doi:10.4271/2009-32-0015.

9. Lavrentjev, J. and Rämmal, H., "Acoustic Analysis of Small Engine Catalytic Converters," SAE Technical Paper 2010-32-0022, 2010, doi:10.4271/2010-32-0022.

10. Chung, J. Y. and Blaser, D. A., Transfer function method for measuring in-duct acoustic properties. I. Theory, II Experiments, Journal of Acoustical Society of America, **68** (3), 907-921 (1980)

11. Munjal, M.L., Doige, A.G., Theory of a two source-location method for direct experimental evaluation of the four-pole parameters of an aeroacoustic element, Journal of Sound and Vibration, **141**, pp 323-333, (1990)

12. Lavrentjev, J. Åbom, M Bodén, H. A measurement method for determining the source data of acoustic two-port sources, Journal of Sound and Vibration 1830 (3) (1995) 517-531.

CONTACT INFORMATION

Jüri Lavrentjev
juri.lavrentjev@ttu.ee
phone: +372 620 3262.

The Engineering Meetings Board has approved this paper for publication. It has successfully completed SAE's peer review process under the supervision of the session organizer. This process requires a minimum of three (3) reviews by industry experts.

ISSN 0148-7191

SAE Customer Service:
Tel: 877-606-7323 (inside USA and Canada)
Tel: 724-776-4970 (outside USA)
Fax: 724-776-0790
Email: CustomerService@sae.org
SAE Web Address: http://www.sae.org
Printed in USA

SAE International®

Paper IV

Tiikoja, H., Lavrentjev, J., Rämmal, H., Åbom, M.,
Experimental investigations of sound reflection from
hot and subsonic flow duct termination.
Journal of Sound and Vibration, Vol. 333, Issue 3, pp. 788-800, 2014

Journal of Sound and Vibration 333 (2014) 788–800

Contents lists available at ScienceDirect

Journal of Sound and Vibration

journal homepage: www.elsevier.com/locate/jsvi

Experimental investigations of sound reflection from hot and subsonic flow duct termination

Heiki Tiikoja [a,b,*], Jüri Lavrentjev [a], Hans Rämmal [a], Mats Åbom [b]

[a] Department of Machinery, Tallinn University of Technology, Ehitajate tee 5, Tallinn 19086, Estonia
[b] KTH CCGEx, The Marcus Wallenberg Laboratory, Teknikringen 8, SE-10044 Stockholm, Sweden

A R T I C L E I N F O

Article history:
Received 13 March 2012
Received in revised form
19 September 2013
Accepted 20 September 2013
Handling Editor: R.E. Musafir
Available online 30 October 2013

A B S T R A C T

The knowledge of the reflection properties of open end jet ducts is important for different applications, where the flow and high temperature conditions are involved and add complexity to the problem. In this paper, the magnitude of the reflection coefficients together with the respective end-corrections is experimentally determined for hot flow duct openings. A Mach number range up to 0.3 for cold jets and up to 0.12 for a jet temperature of 200 °C is treated. The experimental results are compared with the numerical model proposed by Munt (Acoustic transmission properties of a jet duct with subsonic jet flow: 1. The cold jet reflection coefficient, *Journal of Sound and Vibration* 142 (1990) 413–436) and a good correlation in plane-wave region is demonstrated. To reduce experimental uncertainty, the sound reflection properties at the duct opening are obtained by using an overdetermined two-microphone technique with the implementation of a three pressure transducer array. By introducing a modified multistep version of the stepped sine excitation, the accuracy of data acquisition process is improved without compromising the measurement time.

1. Introduction

To comply with tougher legislations on noise pollution, noise radiation from duct systems has become a significant problem; practical examples of technical applications are found in tailpipes of internal combustion engine exhaust systems, industrial pipeline openings and burner stacks. If noise transmission through the system is to be estimated, knowledge of the acoustical boundary conditions at the duct openings is essential.

The reflection of sound at the boundaries separating two media in relative motion was originally examined by Rayleigh [1]. In the classical theoretical work by Levine and Schwinger [2] the problem of sound reflection at and radiation from an open unflanged duct termination has been solved for no-flow condition by the Wiener–Hopf technique. One of the early investigations to study the axial propagation of sound through duct opening in the presence of mean flow was performed by Tsien [3] for a rocket motor exhaust nozzle. The acoustic transmission and reflection for plane waves propagating from a moving medium, impinging on a plane shear discontinuity into a cold stationary region was theoretically analyzed by Miles [4] and Ribner [5]. The effects of the velocity discontinuity on the transmission and reflection, the possibility of resonance, amplification and instability of the interface were treated. Candel [6] demonstrated that a discontinuity of temperature has a major effect on the propagation directivity of the transmitted waves.

* Corresponding author at: Department of Machinery, Tallinn University of Technology, Ehitajate tee 5, 19086 Tallinn, Estonia. Tel.: +372 5153464.
E-mail addresses: tiikoja@kth.se, tiikoja@gmail.com (H. Tiikoja).

0022-460X/$ - see front matter
http://dx.doi.org/10.1016/j.jsv.2013.09.030

It was shown by Carrier [7] and Munt [8] that in case the jet exhausts out of a duct opening, the acoustic field sheds a vortex sheet from the trailing edge, which has to be taken into account when estimating the sound field around the opening. A complete theory based on the Wiener–Hopf technique for the radiation from a semi-infinite cylindrical flow duct submerged in a subsonic coaxial uniform mean flow was presented by Munt [9]. Because this paper took a long time to publish, it was referred to and used by other authors before being finally published in 1990. Rienstra [10] and Cargill [11] studied the solutions proposed by Munt by using the approximations of low Strouhal numbers and low frequencies. In accordance with experimental investigations, Munt's model [9] was the first to predict values for the plane-wave reflection coefficient that exceed unity at low frequencies and different flow velocities of the jet and ambient gas. An important aspect of the model proposed by Munt [9] is the application of a full Kutta condition at the duct termination. This condition is assumed to be the same as the one for the steady-flow, i.e., the flow leaving the duct remains parallel to the duct wall also when acoustic perturbations are added. The first experimental investigations in the presence of mean flow, exhibiting values of the reflection coefficient above unity, were performed by Mechel [12] and Ronneberger [13].

Measurements for acoustical damping and reflection coefficient for an open duct at low Mach and Helmholtz numbers were performed by Peters et al. [14] by implementing a multimicrophone approach. It was concluded that in the presence of mean flow the reflection coefficient and acoustical damping in a duct are strongly influenced by the Mach number. By testing several duct opening geometries it was found that, for low Helmholtz numbers and subsonic flows, the magnitude of the reflection coefficient is not considerably influenced by the geometry of the termination, whereas the end correction showed significant influence.

The experimental work performed by Allam and Åbom [15] showed a good agreement with Munt's theoretical model for cold jets and Mach numbers up to 0.2. In addition, this paper also gave experimental validation of the acoustic turbulence damping model proposed by Howe [16]. Successful validation of Munt's theory was performed by Rämmal and Lavrentjev [17] for a high temperature jet (up to 500 °C) exhausting into a relatively cold (20 °C) surrounding air. The aim in [17] was to focus on the influence of the jet temperature effects on the sound reflection from the duct opening and to exclude the flow effects; the Mach number was kept below 0.007 during these tests.

A number of studies are available where the implementation of numerical simulations to predict the acoustic properties of the circular flow duct is treated. To test the applicability of an FEM model, analysis of the high temperature effect on the sound propagation through an open duct termination in a quiescent flow was carried out by the Rämmal and Lavrentjev [18]. The simulation results were in good agreement with Munt's theory [9] and the experimental results presented in [17]. Silva et al. [19] used a numerical technique based on an axi-symmetrical lattice Boltzmann scheme to predict the parameters associated with the acoustic reflection at the open end issuing a cold subsonic ($M \le 0.15$) mean flow. The results agreed well with the theoretical model [9] and the experimental data published earlier [15]. In addition, simulations with a duct terminated by circular horns of curvature radii $R=2a$ and $R=4a$ were carried out. Because there are no theoretical models available, the results were compared to the experimental data by Peters et al. [14].

In this paper the influence of the mean flow and the temperature on the acoustic reflection properties of an open ended duct will be experimentally investigated. Compared to previous publications the measurement range is considerably extended in terms of hot flow velocity. A dedicated test facility is designed to generate hot flow with Mach numbers up to 0.3 and temperature up to 200 °C. This experimental investigation is performed in the plane-wave region up to the cut-on frequency.

2. Method

2.1. Experimental approach

With the two-microphone wave decomposition method (WDM) [20], the in-duct acoustic properties can be determined over a wide frequency range. The number of microphones in WDM is often extended by using more than two microphone locations to extend the frequency range [25], to obtain the wave numbers of traveling waves [14,15] or to increase the measurement accuracy by overdetermining the equation system [21]. The procedure used in the current paper to experimentally determine the reflection coefficient of the duct opening follows the overdetermined WDM [21]. This approach has an advantage over the classical two-microphone method where accurate measurements are required in more demanding measurement conditions, e.g., in turbulent duct flows with temperature gradients.

By following the overdetermined WDM the plane-wave acoustic pressures at the three transducers mounted into different cross-sections of the duct (see Fig. 1) can be expressed as:

$$p_1(f) = p_{1+}(f) + p_{1-}(f) \tag{1}$$

$$p_2(f) = p_{1+}(f)\exp(-\mathrm{i}k_+x_2) + p_{1-}(f)\exp(\mathrm{i}k_-x_2) \tag{2}$$

$$p_3(f) = p_{1+}(f)\exp(\mathrm{i}k_+x_3) + p_{1-}(f)\exp(-\mathrm{i}k_-x_3) \tag{3}$$

where p_1, p_2 and p_3 are the Fourier transforms of the acoustic pressure at transducer cross-sections, $-$ and $+$denote the wave propagation in negative and positive x-direction and k is the wavenumber. The cross-section at the pressure transducer 1 is considered as reference cross-section ($x_1=0$). To improve the accuracy of the method, the effect of visco-thermal damping was

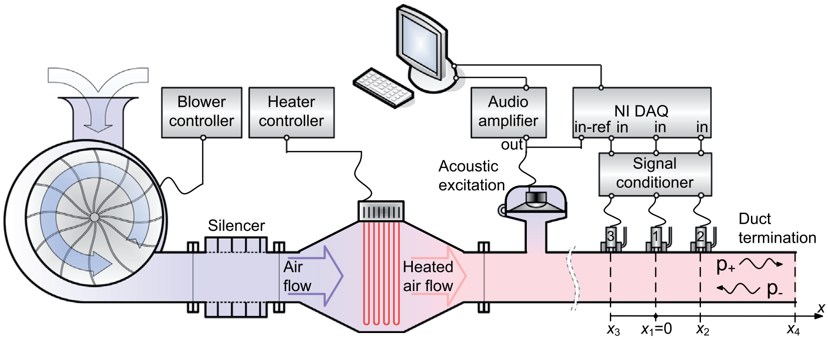

Fig. 1. A sketch of the experimental set-up for the measurements.

included, and the wave numbers in Eqs. (1)–(3) were obtained from a model proposed by Dokumaci [22]:

$$k_{\pm} = \frac{2\pi f}{c} \frac{K_0}{1 \pm K_0 M} \tag{4}$$

where f is the frequency, c is the speed of sound, $M = U/c$ is the Mach number and U is the cross-sectional averaged mean flow velocity. In Eq. (4) the coefficient K_0 is the classical Kirchhoff solution and determined from the relationship:

$$K_0 = 1 + \frac{(1-\mathrm{i})}{\sqrt{2}S}\left(1 + \frac{(\gamma-1)}{Pr}\right) - \frac{\mathrm{i}}{S^2}\left(1 + \frac{\gamma-1}{Pr} - \frac{\gamma}{2}\frac{\gamma-1}{Pr^2}\right) \tag{5}$$

where $\gamma = (C_p/C_v)$ is the ratio of specific heats, the suffix p and v refer to constant pressure and constant volume conditions, respectively, $Pr = \mu C_p/\kappa_{th}$ is the Prandtl number, $S = a\sqrt{\rho_0 \omega/\mu}$ is the shear wave, κ_{th} is the thermal conductivity, a is the duct radius, ρ_0 is the gas density in the duct and μ is the dynamic viscosity.

To reduce random flow noise in the recorded signals, it is preferable to use transfer functions in Eqs. (1)–(3) instead of the acoustic pressures. The transfer functions H were taken between the transducer signals and the reference electric signals supplying voltage to the acoustic drivers. Hereby, Eqs. (1)–(3) form an overdetermined system of equations and can be expressed as:

$$\begin{pmatrix} \exp(-\mathrm{i}k_+ s_1) & \exp(\mathrm{i}k_- s_1) \\ \exp(-\mathrm{i}k_+ s_2) & \exp(\mathrm{i}k_- s_2) \\ \exp(-\mathrm{i}k_+ s_3) & \exp(\mathrm{i}k_- s_3) \end{pmatrix} \begin{pmatrix} H_+ \\ H_- \end{pmatrix} = \begin{pmatrix} H_1 \\ H_2 \\ H_3 \end{pmatrix} \tag{6}$$

or in matrix formulation as:

$$\mathbf{Eh} = \mathbf{H} \tag{7}$$

where $s_1 = 0$, $s_2 = x_2 - x_1$, $s_3 = x_1 - x_3$ are the transducer separations. This system can be solved by using Moore–Penrose pseudoinverse as:

$$\mathbf{h} = \mathbf{E}^{-1}\mathbf{H} \tag{8}$$

As the unknowns H_+ and H_- can be determined at the reference cross-section, the sound field in the duct becomes completely described. The reflection coefficient at the reference cross-section ($x=0$) is defined as:

$$R_0(f) = \frac{H_{1-}(f)}{H_{1+}(f)} \tag{9}$$

where subscript 0 denotes the values determined at the reference cross-section. The reflection coefficient R_0 is finally transferred to the duct termination cross-section. This is performed by using the following equation:

$$R_l = R_0 \exp(\mathrm{i}(k_+ + k_-)l) \tag{10}$$

where l is the distance from the reference cross-section to the duct termination: $l = x_4 - x_1$ (see Fig. 1). The phase of the reflection coefficient R_l can be related to the end-correction. The end-correction can be interpreted as the extra length δ added to the duct to obtain a reflection coefficient R_δ with a phase equal to π:

$$R_\delta = |R_l|\exp(-\mathrm{i}\theta + \mathrm{i}(k_- + k_+)\delta) = |R_l|\exp(-\mathrm{i}\pi) \tag{11}$$

where θ represents the phase of the reflection coefficient. The normalized end-correction can be expressed as:

$$\frac{\delta}{a} = \frac{\theta - \pi}{\mathrm{Re}[(k_- + k_+)]a} \tag{12}$$

Alternatively, the reflection properties of the duct termination can be expressed as the energy reflection coefficient R_E, introduced by Ingard and Singhal [23]. It can be defined as the ratio of the incident and the reflected acoustic power:

$$R_E = |R|^2 \frac{(1-M)^2}{(1+M)^2} \tag{13}$$

2.2. Description of the measurement set-up

A test facility has been developed for the experimental determination of accurate reflection coefficient data in an extended range of jet velocities and temperatures (see Figs. 1 and 2). The measurements have been carried out in a 2.0 m long circular test duct with a wall roughness less than 1 μm. As reported by Peters et al. [14] the reflection coefficient, especially the end-correction, is affected by geometrical imperfections close to the duct termination. Considering the assumption of infinitely thin wall thickness in Munt's theoretical model [9], a circular stainless steel duct with inner radius $a=0.021$ m and 1.5 mm wall thickness was used for the experiments.

To minimize the effect of the reflected sound on the acoustic field at the duct termination and inside the duct, the measurements were performed in a room with sound-absorbing walls and ceiling. The duct termination was positioned at least 1 m above the rigid floor and more than 3 m away from the closest wall. The influence of the rigid floor at the open duct end can be taken into account by assuming a mirror image point source below the floor. By neglecting the reflections at the ceiling and the side walls as well as multiple reflections, the correction for the reflection coefficient and the end-correction are found by following the Disselhorst and Van Wijngaarden model [24]:

$$|R_{fl}| - |R_{ff}| = -\frac{(ka)^2}{4kh} \sin(2kh) \tag{14}$$

$$\delta_{fl} - \delta_{ff} = \frac{a^2}{8h} \cos(2kh) \tag{15}$$

where $|R_{fl}|$, $|R_{ff}|$ and δ_{fl}, δ_{ff} are the reflection coefficient and the end-correction values in the presence of floor and free field, respectively. According to the distance h from the duct end to the floor, the correction for low Helmholtz numbers is less than 0.2 percent and therefore it can be neglected.

For this particular test duct the plane-wave region cut-on frequency, determined for a circular duct by $f_c=1.841c/(2\pi a)$, is approximately 5000 Hz. To obtain reliable experimental data in the plane-wave region up to the cut-on frequency, the two-microphone separation criteria $0.1\pi(1-M^2) < ks < 0.8\pi(1-M^2)$, suggested by Åbom and Bodén [25] was followed. To cover a wider frequency range two-microphone separations, one for the low ($s_L=0.21$ m) and one for the high ($s_H=0.024$ m) frequency range, were used. This gives the frequency range from 80 Hz up to the cut-on frequency for duct used in the experiments.

Generally, at least 30 duct diameters after the area constriction are considered to be enough to assume a fully developed turbulent flow profile [26]. Thus, the transducers were positioned more than 2.1 m away from the loudspeaker cross-sections.

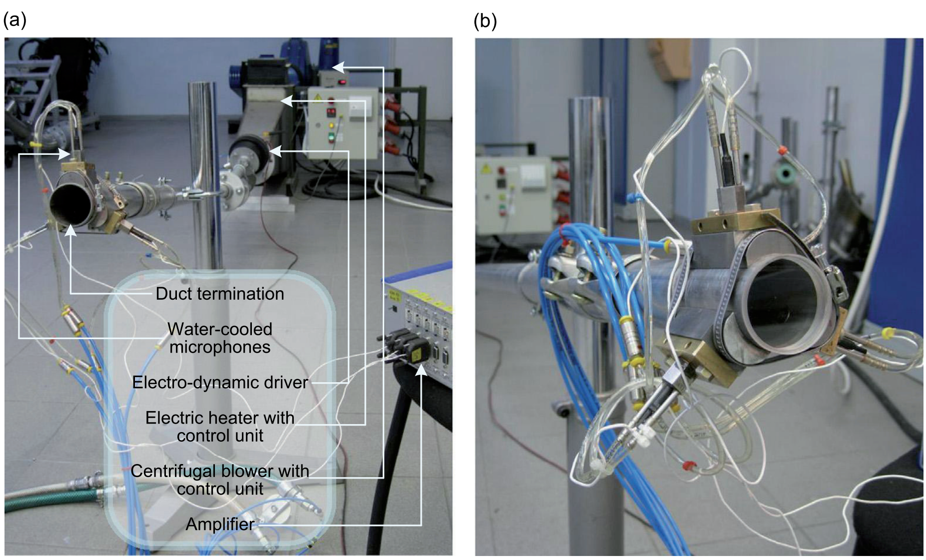

Fig. 2. Photos of the experimental set-up (a) and transducer mounting for calibration (b).

The distances $l_L = 0.256$ m and $l_H = 0.07$ m from the reference cross-section to the duct termination were selected to minimize the temperature gradient between the transducer cross-sections and the duct termination.

A Pitot tube with a micro-anemometer (Delta Ohm HD 2164.0) was used to determine the flow velocity, taking into account the actual air density via a temperature measurement at the same cross-section. A Pitot tube with outer diameter of 3 mm and inner diameter of 1 mm was placed temporarily to the transducer cross-sections and the flow profile was measured by moving the Pitot tube radially. The average flow velocity $U = 0.82 \cdot U_{cl}$ was determined by using the centreline velocity and by assuming axi-symmetrical fully developed turbulent flow. The Mach number $M = U/c$, used to calculate the wave numbers (see Eq. (4)) and to plot the data, was calculated based on the speed of sound and the average cross-sectional flow velocity. The temperatures measured by a K-type thermocouple inserted into the duct were used to calculate the speed of sound and to monitor the temperature of the jet. Another thermometer (TES-1312) with a K-type thermocouple was used to determine the room temperature just outside the jet at the duct termination.

A high speed jet exhausting out of the open termination was generated by a PC-controlled high pressure centrifugal blower (Kongskilde 300TRV). The blower was driven by a 22 kW electric motor and the flow velocities studied were obtained by regulating the speed of the motor via an electronic control unit. The outlet from the blower was equipped with a vibro-damper to minimize vibrations at the test section. Additionally, a commercial ventilation silencer (see Fig. 1) was mounted to suppress the flow fluctuations. A stagnation chamber, with a volume of approximately 0.15 m^3, incorporating a 22.5 kW electric heater unit (see Figs. 1 and 2), was designed to heat the airflow and suppress the pulsating flow originating from the blower. The temperature of the exhausting jet was automatically set and maintained by a custom-built proportional-integral-derivative (PID) controller module.

The acoustic excitation was provided by an electrodynamic driver (DAS ND-8) mounted into a side-branch of 0.2 m and diameter of 0.042 m (see Fig. 1). The electrodynamic driver was driven by a software-based signal generator via a power amplifier (Velleman VPA2100MN). As the excitation strength has been found to be an important factor influencing the quality of the results, it is crucial to find a source capable of dominating over the background noise apparent in high velocity flow ducts. In this study an electrodynamic driver with neodymium magnet and titanium membrane with the output of more than 135 dB SPL in free field was found to be an adequate source. The driver equipped with titanium diaphragm offered increased resistance to mechanical and thermal loads in a duct exhausting a high-velocity hot jet. The neodymium magnet reduces the weight of the driver and guarantees negligible magnetic strength loss at the highest operating temperatures. To avoid sudden overpressure damage to the membrane the electrodynamic driver was pressure equalized by a bypass tube, connecting the front and the rear volumes of the unit.

To investigate the effect of duct wall vibrations induced by electrodynamic driver, a routine described by Peters et al. [14] was applied. High-amplitude measurements were performed in no-flow conditions where 5 mm distance and damping layer was applied to avoid direct contact between the duct and the acoustic driver. It was noticed that the influence of the source-induced vibrations on the measured data was negligible.

Due to the high temperature conditions during the tests, water cooled piezo-resistive type of pressure transducers (Kulite WCT-312 M-25 A) and signal conditioners (Dewetron) were found to be the most appropriate set of transducers for measuring the acoustic and static pressures. Three 1/4 inch pressure transducers were flush mounted to the inner duct walls to simultaneously record the acoustic pressure signals (see Figs. 1 and 2). The pressure transducers were evenly distributed around the duct cross-section to suppress the uncorrelated flow disturbances.

The acquisition of the sound pressure signals and the computation of the transfer functions were performed by a four-channel dynamic signal analyser (National Instruments NI PCI-4474). The analyser and the signal generator were controlled by a purpose built PC-based virtual instrument (LabVIEW).

According to the cut-on frequency and Nyquist criterion, the sampling speed for data acquisition was chosen as 12.8 kS/s and 1 s long data records (12800 samples). To increase the measurement quality, the stepped sine method was used. By using a stepped sine instead of a broadband excitation, improved signal to noise ratio properties were achieved, which was vital in this case because the pressure transducers used have a relatively low sensitivity.

In harsh measurement conditions where the signal to noise ratio is relatively low, the stepped sine method is improving the measurement quality but is time-consuming. To reduce measurement time, a multistepped sine (MSS) excitation technique was developed. A number of sine waves (5) were excited simultaneously, equally distributed over the frequency region (see Fig. 3), thus considerably reducing the measurement time. By using the MSS technique, a reasonable compromise between the signal to noise ratio and the measurement time can be achieved. A custom-made program in LabVIEW enabled to easily determine the start and stop frequencies, the frequency step and the number of simultaneous sine signals. By using the source correlation technique and the MSS excitation method, the tests revealed that 24 was a sufficient number of averages for the measurements. Using a frequency step of 10 Hz, the measurement in a range between 80 and 5000 Hz took approximately 40 minutes.

As stated by Peters et al. [14] the accuracy of the measurement is mainly limited by the accuracy of the calibration of the pressure transducers. By using a single pressure transducer for all measurement positions, the calibration procedure is not necessary. For the majority of the measurement procedures this is however unacceptable due to the increased measurement time. For the calibration, the pressure transducers were positioned at the same duct cross-section (see Fig. 2b) with an accuracy of 0.1 mm. The transfer functions H_{en} between the electrical signal driving the acoustic driver and the transducer signals were measured. Thereafter, the transfer functions between the transducer signals were used to determine the calibration curves. To avoid pressure nodes at the calibration cross-section, it is usually appropriate to use a closed end

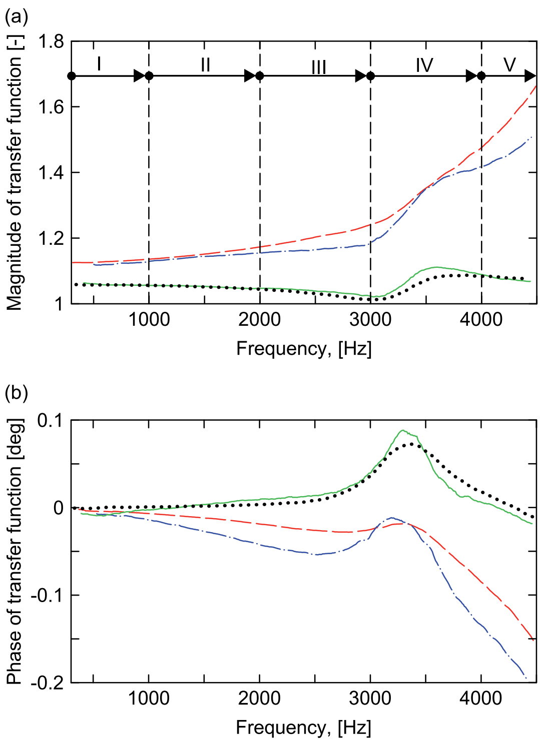

Fig. 3. The magnitude and the phase recorded during the pressure-transducer calibration:…, H_{21} measured at $M=0$; ——— H_{21} measured at $M=0.15$; — — —, H_{31} measured at $M=0$; — · — · —, H_{31} measured at $M=0.15$. MSS technique with five frequency regions I–V, excitation direction indicated by the arrows.

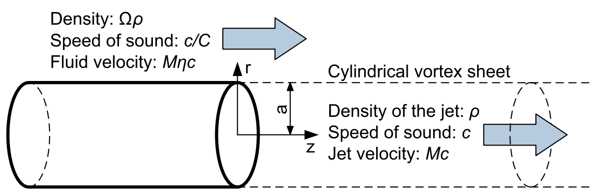

Fig. 4. A simplified schematic representation of the model proposed by Munt [9].

calibration duct with pressure transducers positioned at the duct termination. It was found that for the Kulite transducers used, the calibration curve was considerably affected by the measurement conditions. Therefore, the transducer calibration was performed for all measurement cases with different flow velocities and the open end calibration duct was inevitable. The discrepancy between the calibration curves apparent for different flow cases (see Fig. 3) can be explained by the absence of pressure equalization of the Kulite transducer membrane. The influence of the temperature on the calibration curves was found to be negligible.

2.3. The analytical model by Munt

Although there are several analytical models available to calculate the sound reflection at an open duct termination [9–11], the most general is the one proposed by Munt [9], which has been referred to in many investigations [14,15,19].

The classical solution to the reflection of the acoustic waves at the open end of a circular duct with a thin rigid wall into a free space was given by Levine and Schwinger [2]. In Munt's model [9] (see Fig. 4) this solution was extended by including the effect of a mean flow ($M<1$). In Munt's model the jet leaving the duct termination was assumed to be separated from the ambient fluid by an infinitely thin vortex sheet. The properties of the fluid inside the duct are described by the density ρ, the speed of sound c and the fluid velocity Mc. The surrounding media outside the thin shear layer are described by the fluid density $\Omega\rho$, the speed of sound c/C and fluid velocity $M\eta c$, where the nondimensional quantities Ω, C and η determine the ratio between the inner and the outer jet parameters, respectively.

In Munt's theory the coupling between the acoustic and vorticity fields is controlled entirely by the Kutta or edge condition applied at the duct opening. The Kutta condition implies a finite velocity and absence of pressure discontinuity across the shear layer at the edge and determines the strength of the coupling between the acoustic disturbances in the jet and the disturbances in the vortex sheet. This coupling transfers the energy from the acoustic field to the flow and induces a dissipation of acoustic energy. The jet flow outside the duct is assumed to be uniform and is delimited by an infinitely thin shear layer. This implies that the expansion and merging of the jet with the surroundings and its effect on the sound radiation is neglected.

For low Mach and Helmholtz numbers, an approximate solution has been derived by Cargill [11] and Rienstra [10] both for the case with and without the Kutta-condition applied. Despite the complexity of the model of Munt [9], it gives the solution for higher order modes and for all subsonic velocities. In the current study, reflection coefficient R_{000} in [9], restricted to a plane-wave range, was used. To solve the theory of Munt [9] numerically, the MATLAB® routine from In 't Panhuis [27] was used here.

3. Results and discussion

As the motivation of this work was to provide experimental data for high velocity hot jets, the experiments have been performed at different jet temperatures and Mach numbers, as summarized in Table 1. By following Munt's model, the nondimensional quantities (Ω, C) characterizing the test conditions are also presented hereby (see Table 1).

3.1. Flow profile measurements

The flow velocity profiles were determined at the transducer reference cross-section by measuring the centreline velocities (U_{cl}). Although numerous empirical velocity profiles can be found in literature for turbulent duct flows, the simplest and the best way to get such profiles is based on the empirical power law equation. Accordingly, the velocity at any point in the cross-section of cylindrical duct is proportional to the $1/n$ power of the distance from the wall, which can be expressed as:

$$\frac{U_x}{U_{\text{cl}}} = \left(1 - \frac{Y}{D}\right)^{1/n} \tag{16}$$

where the exponent n is a constant depending on the Reynolds number ($Re = 2aMc/\nu$) and ν is the kinematic viscosity. The velocity profile for the range of $1.39 \times 10^5 < Re < 2.88 \times 10^5$ approximately follows a 1/7 power law (Prandtl one-seventh law), which is known to give a good agreement with experimental data in a smooth duct.

Table 1
Physical properties of the experimental cases studied.

Case	U_{cl} [m/s]	T [°C]	c [m/s]	M	Ω	C
1	2	46	359	0.005	1.08	1.04
2	65	46	359	0.15	1.08	1.04
3	130	46	359	0.30	1.08	1.04
4	65	200	436	0.12	1.60	1.27

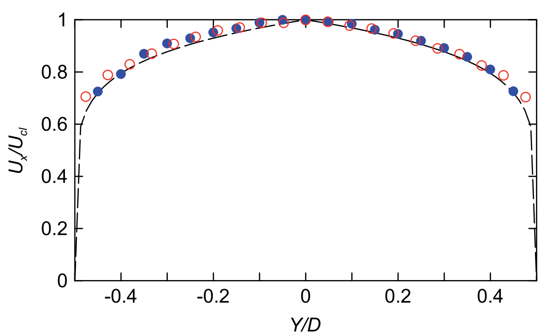

Fig. 5. The measured and modeled flow profile: ●, flow profile at $U_{\text{cl}} = 65$ m/s; ○, flow profile at $U_{\text{cl}} = 130$ m/s; – – –, modeled flow profile.

As mentioned above, a Pitot tube was used to measure the flow velocity U_x at 21 points, evenly distributed over the diameter D of the duct (see Fig. 5). The variable Y in (Fig. 5) was determined as coordinate along an axis, originating from and perpendicular to the centre axis of the duct. Although there were small imperfections close to the measurement section, such as flush mounted transducers, the experimental mean velocity values agreed remarkably well with the theory. The result provided in Fig. 5 indicates that for $n=7$ the bulk velocity can be calculated from the relation $U \approx 0.82 \cdot U_{\mathrm{cl}}$ [28], which is a suitable estimation for both measurement cases. Close to the boundaries, in $|Y/D| > 0.3$ (see Fig. 5), it is possible to observe higher values in the experimentally measured velocities, reflecting the flattening of the velocity profile at higher *Re* numbers. The flow velocity near the duct wall should approach a no-slip condition, but could not be measured due to the geometrical restrictions of the Pitot tube.

4. Measurements of acoustical properties

To evaluate the measurement system and test rig, the stationary measurement case ($M=0$) at room temperature ($C=1$) was used. In Fig. 6, experimental results for the acoustical reflection coefficient, plotted as a function of Helmholtz number ($ka=2\pi fa/c$), in terms of magnitude and end-correction for the open duct termination are compared with the theory of Levine and Schwinger [2]. A good correlation between the experimental data and the theory [2] was achieved. In Fig. 6, if the range of $ka \to 0$, the magnitude will approach the unity $|R| \to 1$ and the end-correction $\delta/a \to 0.6133$ as found by Levine and Schwinger [2]. For a higher *ka* range these values will be reduced because of the more efficient acoustic radiation of the duct termination.

In Fig. 7, the magnitude of the reflection coefficient $|R|$ and the end-correction of the reflected wave from the duct opening δ are presented. The measurements are performed at different flow velocities up to $M=0.3$ ($U_{\mathrm{cl}}=130$ m/s) and for a constant jet temperature $T=46$ °C. For all flow cases considered here, the jet is exhausted into a stationary medium with no coflow, i.e., the parameter η in Munt's model is zero.

The measured reflection coefficients are compared with the theoretical ones computed by Munt´s theory [9]. A good correlation between the measured and calculated values is observed (discrepancy less than 2–3%) for all test cases investigated. In our measurements the wave numbers $k_{\pm}$ (see Eq. (4)) were calculated on the basis of the cross-sectional average velocity *U*. In Munt's theory [9] the pipe centreline velocity U_{cl} was used for the flow velocity in the pipe and the jet. As first suggested by Allam and Åbom [15] this choice results in a better agreement between theory and experiments. The need for this approach was explained by Allam and Åbom [15] and later confirmed by da Silva et al. [19], by referring to the

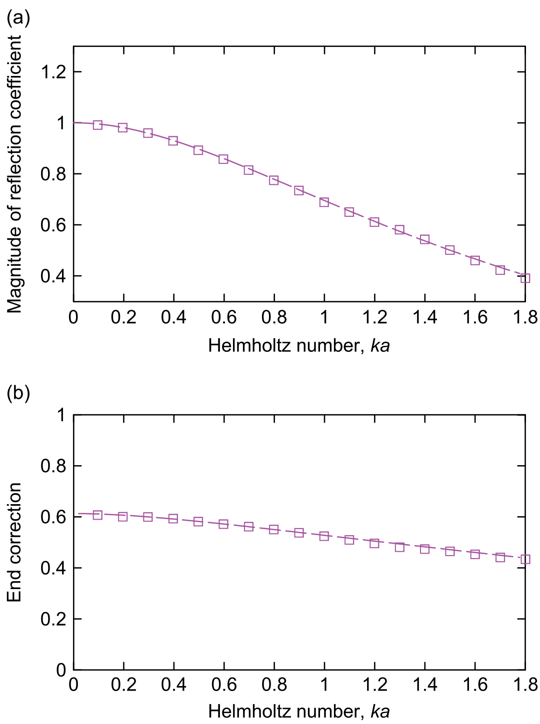

Fig. 6. The magnitude and end-correction of the reflection coefficient for an open duct termination as a function of the Helmholtz number $ka=2\pi fa/c$ for no flow case: □, experiments at $C=1$ and $M=0$; — — —, theory by Levine and Schwinger at $C=1$ and $M=0$.

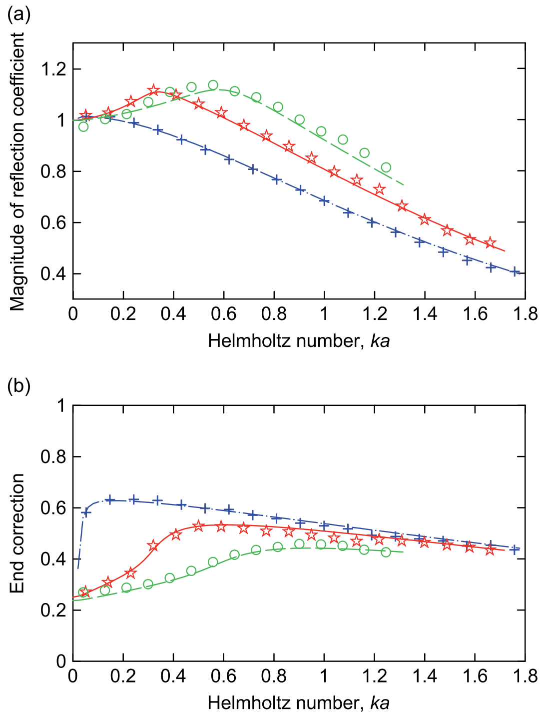

Fig. 7. The magnitude and the end-correction of the reflection coefficient for an open duct termination as a function of the Helmholtz number $ka = 2\pi fa/c$ presented for different Mach numbers. Experiments: +, $C = 1.04$ and $M = 0.005$; ☆, $C = 1.04$ and $M = 0.15$; ○, $C = 1.04$ and $M = 0.3$. Munt's theory: — · — · — ·, $C = 1.04$ and M $= 0.005$; ———, $C = 1.04$ and $M = 0.15$; — — —, $C = 1.04$ and $M = 0.3$.

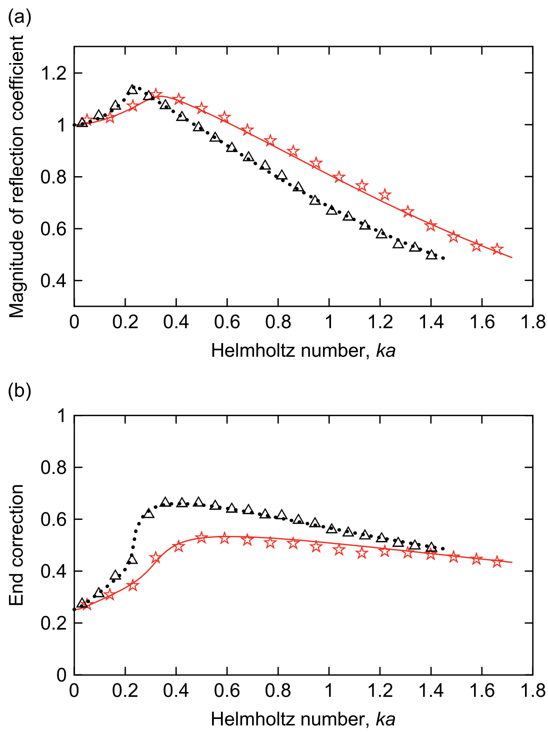

Fig. 8. The magnitude and end-correction of the reflection coefficient for an open duct termination as a function of the Helmholtz number $ka = 2\pi fa/c$ for different jet temperatures. Experiments: ☆, $C = 1.04$ and M $= 0.15$; Δ, $C = 1.27$ and $M = 0.12$. Munt's theory: ———, $C = 1.04$ and $M = 0.15$; …, $C = 1.27$ and $M = 0.12$.

growth of disturbances at the outlet of a circular jet, investigated by Freymuth [29]. Although the discrepancy between the measurements and the model is reduced by using the centreline velocity, the data in Fig. 7 indicate a tendency to underestimate the values for high flow velocity cases.

For all flow cases presented in Fig. 7, the magnitude of the reflection coefficient becomes unity ($|R|=1$) when the Helmholtz number approaches zero ($ka \to 0$), as found by Munt [9]. In addition, for intermediate Helmholtz numbers, reflection coefficient values above unity ($|R|=1$) are observed. In [9] this phenomenon was explained by the transfer of kinetic energy of the flow to the acoustic field via the interaction of the unstable vortex sheet at the lip of the duct, resulting in increased transmitted sound through the open end. The physical meaning of the peak region occurring at approximately $St=ka/M \approx \pi/2$ was also interpreted in [19] by showing that the maximum value of the reflection coefficient occurs when the oscillation period of the acoustic source T equals the time necessary for the vortical instabilities, propagating with $U_v \approx U/2$, to propagate a distance equal to the duct diameter $2a$. For high Helmholz numbers ($He \to 1.82$) the magnitude of the measured reflection coefficient decreases for all the test cases due to the more efficient radiation from the duct opening to the far-field.

For a small Helmholtz number, the value of the end-correction in Fig. 7 is strongly dependent on the flow rate by approaching the value of $\delta/a = 0.2554\sqrt{1-M^2}$ when $ka \to 0$, as predicted by Rienstra [10]. Close to the cut-on ($ka \to 1.82$) the values of the end-correction move toward the no-flow result predicted by Levine and Schwinger [2].

In Fig. 8 the magnitude and end-correction of the reflection coefficients up to the jet temperatures 200 °C and for constant flow velocity ($U_{cl}=65$ m/s) are presented. By increasing the jet temperature, the maximum of the magnitude of the reflection coefficient is increased and slightly shifted to a lower ka value. Otherwise the same trends as in Fig. 7 are observed except for the end-correction, where values above the no-flow case can be observed.

In Fig. 9, the experimental and the theoretical [9] results are divided by the reflection coefficient R_{LS} and the end-correction predicted by Levine and Schwinger [2]. For the low flow velocity case ($U_{cl}=2$ m/s) a minor difference from the prediction of Levine and Schwinger [2] can be observed, indicated by the value of unity over the Helmholtz scale. By increasing the flow velocity, the magnitude of the reflection coefficient will form a slope in the low ka range. When $C \to 1$ the magnitude is constant in the high ka range, whereas the value is decreasing for an increasing jet temperature. For the end-correction, the value will approach 1 close to the cut-on frequency. Also, values above 1 can be observed for high jet temperatures.

Fig. 10 represents the results of the reflection coefficient in a Strouhal scale ($St=ka/M$). For the magnitude of the reflection coefficient the peak value appears at $St \approx \pi/2$, which agrees with the theory presented by Munt [9]. For the end-correction, the results tend to collapse into a single curve for a low Strouhal number.

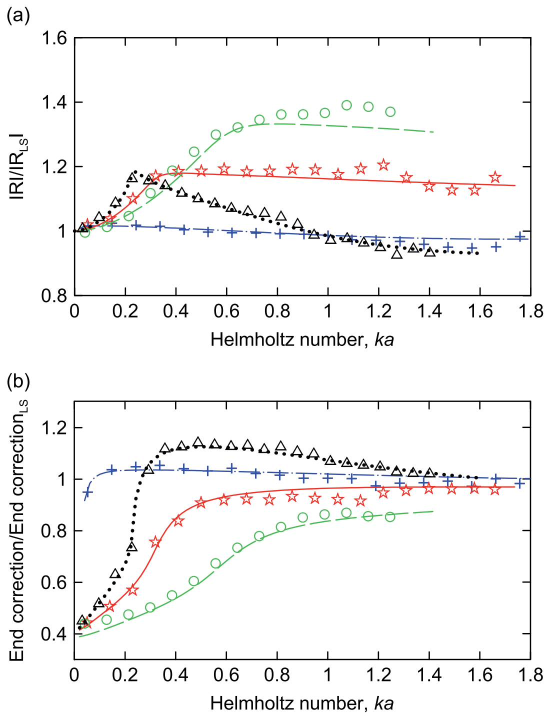

Fig. 9. The ratios of the magnitude and end-correction of the reflection coefficient as a function of the Helmholtz number $ka=2\pi fa/c$. Experiments: +, $C=1.04$ and $M=0.005$; ☆, $C=1.04$ and $M=0.15$; ○, $C=1.04$ and $M=0.3$; △, $C=1.27$ and $M=0.12$. Munt's theory: — · — · — · ·, $C=1.04$ and $M=0.005$; ——, $C=1.04$ and M=0.15; — — —, $C=1.04$ and M=0.3; …, $C=1.27$ and $M=0.12$.

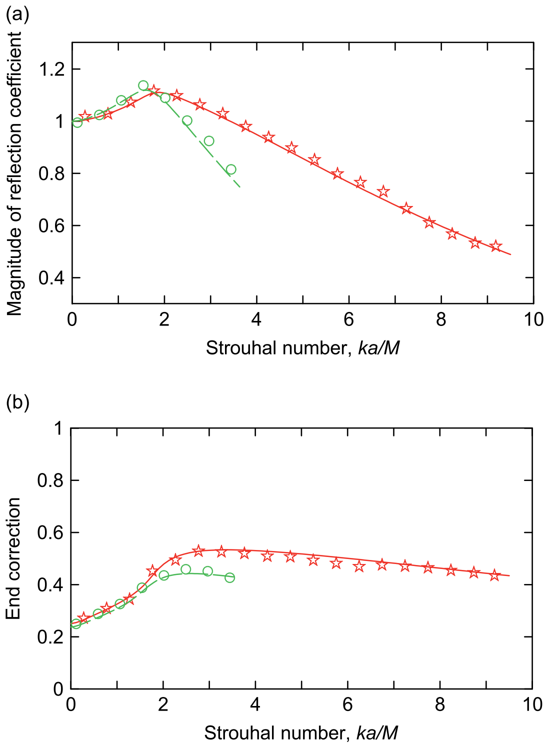

Fig. 10. The magnitude and end-correction of the reflection coefficient for an open duct termination as a function of the Strouhal number St $=ka/M$. Experiments: ☆, $C=1.04$ and $M=0.15$; □, $C=1.04$ and $M=0.3$. Munt's theory: ———, $C=1.04$ and $M=0.15$; — — —, $C=1.04$ and $M=0.3$.

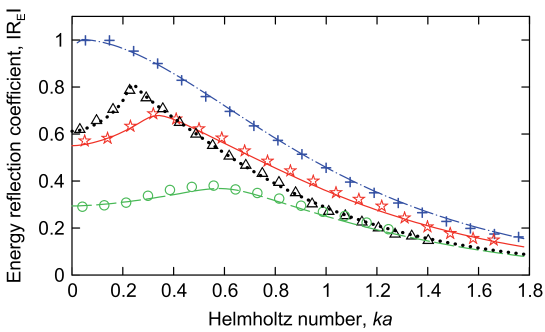

Fig. 11. The magnitude of the energy reflection coefficient for an open duct termination as a function of the Helmholtz number $ka=2\pi fa/c$. Experiments: +, $C=1.04$ and $M=0.005$; ☆, $C=1.04$ and $M=0.15$; ○, $C=1.04$ and $M=0.3$; △, $C=1.27$ and $M=0.12$. Munt's theory: — · — · — ·, $C=1.04$ and $M=0.005$; ———, $C=1.04$ and $M=0.15$; — — —, $C=1.04$ and $M=0.3$; …, $C=1.27$ and $M=0.12$.

In Fig. 11, the magnitude of the acoustic reflection coefficient is presented as an energy reflection coefficient R_E (see Eq. (13)) [23]. For a quiescent fluid ($M\to 0$), almost all the sound energy is found to reflect for low Helmholz numbers, as expected from the theory of Levine and Schwinger [2] where the theory predicts complete reflection at the duct end without any acoustic radiation from the duct opening to the surrounding. For the magnitude of the reflection coefficient in case of flow (see Fig. 7), values above 1 can be observed [9]. Anyhow, this does not conflict with the principle of conservation of energy. The reflection of acoustic energy is strongly dependent on the presence of mean flow. For low Helmholtz numbers the value for the energy reflection coefficient is decreased by increasing the flow velocity. By increasing the Helmholtz number, the value of the reflection coefficient increases up to a certain maximum value. This is a clear indication of sound absorption by vorticity shedding described by Bechert [30] and Howe [16] and which is modeled by Munt [9]. After the reflection coefficient maximum value, the duct termination starts radiating acoustic energy more efficiently to the far-field, which can be confirmed by the lower reflection coefficient values for a high Helmholtz number. It can also be noticed that for the maximum Helmholtz number ($He\to 1.82$) the value for the reflection coefficient becomes close to 0 ($R_E\to 0$) for all the

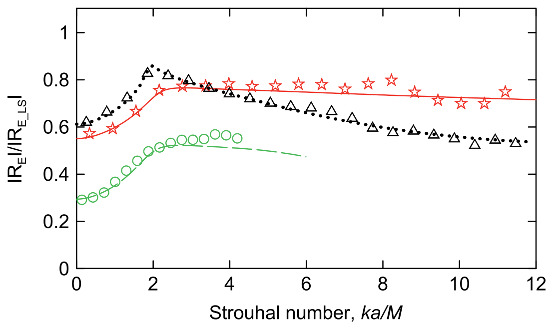

Fig. 12. The ratios of the magnitude of the energy reflection coefficient as a function of the Strouhal number. Experiments: ☆, $C=1.04$ and $M=0.15$; ○, $C=1.04$ and $M=0.3$; Δ, $C=1.27$ and $M=0.12$. Munt's theory: ———, $C=1.04$ and $M=0.15$; — — —, $C=1.04$ and $M=0.3$; …, $C=1.27$ and $M=0.12$.

cases measured. For the high temperature case a higher energy reflection value at low Helmholtz numbers can be observed, indicating a weaker interaction between the acoustic field and the vorticity. This is most easily explained using the model proposed by Bechert [30] from which the vortex interaction (acoustic dissipation) is found to be proportional to the Mach number.

In Fig. 12 the magnitude of the energy reflection coefficient, divided by the energy reflection coefficient calculated by theory of Levine and Schwinger R_{E_LS}, is presented as a function of the Strouhal number. The magnitude in Fig.12 will form a slope in a low St range and the peak value at the same Strouhal number ($St \to \pi/2$) for all the curves can be observed. Similar to the result presented in Fig. 9, the value of magnitude for high St range will be constant for $C \to 1$ and is decreased by increasing the jet temperature.

5. Conclusions

A number of experiments were performed in various subsonic heated jet conditions to study the plane-wave sound reflection from a circular duct opening. It was shown that the overdetermined two-microphone method, together with MSS excitation technique and transducer calibration with flow, gives reliable results for experimental determination of the acoustic properties. The measurements were carried out for flow velocities up to Mach 0.3, increasing the speed range compared to earlier studies and covering the full plane-wave range, i.e., up to Helmholtz numbers 1.8. Furthermore, tests with moderately heated jets (up to 200 °C) were performed to include temperature effects on the reflection properties. It was demonstrated that the experimentally obtained reflection coefficient values agree well with the theoretical model developed by Munt [9]. It should also be noted that the critical ka and St regions where $|R|>1$ were well captured by the experiments. Similar to the earlier works in the field [15,19] the best agreement with the theory was achieved by using the maximum flow velocity value for the theory of Munt rather than the cross-section average. An interesting continuation of the study would be to experimentally determine the acoustic plane-wave reflection coefficient for high subsonic jet speeds or to use different gases with different acoustic properties for jet and the ambient room.

Acknowledgments

The authors would like to acknowledge Estonian Science Foundation (SF2013/SF0140035s12, AR12139 and ETF9441) for the support. Also cooperation and support from the CCGEx centre at KTH in Stockholm is acknowledged.

References

[1] Lord Rayleigh, *Theory of Sound (two volumes)*, Dover Publications, New York, 1877 (re-issued 1945).
[2] H. Levine, J. Schwinger, On the radiation of sound from an unflanged circular duct, *Physical Review* 73 (1948) 383–406.
[3] H.S. Tsien, The transfer functions of rocket nozzle, *Journal of the American Rocket Society* 22 (1952) 139–143.
[4] J.W. Miles, On the reflection of sound at an interface of relative motion, *Journal of Acoustical Society of America* 29 (1957) 226–228.
[5] H.S. Ribner, Reflection, transmission and amplification of sound by a moving medium, *Journal of Acoustical Society of America* 29 (1957) 435–441.
[6] S.M. Candel, Acoustic transmission and reflection by a shear discontinuity separating hot and cold regions, *Journal of Sound and Vibration* 24 (1972) 87–91.
[7] G.F. Carrier, Sound transmission from a tube with flow, *Quarterly of Applied Mathematics* 13 (1956) 457–461.
[8] R.M. Munt, The interaction of sound with a subsonic jet issuing from a semi-infinite cylindrical pipe, *Journal of Fluid Mechanics* 83 (1977) 609–640.
[9] R.M. Munt, Acoustic transmission properties of a jet pipe with subsonic jet flow: 1. The cold jet reflection coefficient, *Journal of Sound and Vibration* 142 (1990) 413–436.
[10] S.W. Rienstra, A small Strouhal number analysis for acoustic wave-jet flow-pipe interaction, *Journal of Sound and Vibration* 86 (1983) 539–556.
[11] A.M. Cargill, Low frequency acoustic radiation from a jet pipe—a second order theory, *Journal of Sound Vibration* 83 (1982) 339–354.
[12] F. Mechel, W. Schlitz, J Dietz, Akustische Impedanz einer luftdurchströmten Öffnung, *Acustica* 15 (1965) 199–206.

[13] D. Ronneberger, Experimentelle Untersuchungen zum akustischen Reflexionsfaktor von unstetigen Querschnittsänderungen in einem luftdurchströmten Rohr, *Acustica* 19 (1967) 222–235.
[14] M.C.A.M. Peters, A. Hirschberg, A.J. Reijnen, A.P.J. Wijnands, Damping and reflection coefficient measurements at low mach and low Helmholtz numbers, *Journal of Fluid Mechanics* 265 (1993) 499–534.
[15] S. Allam, M. Åbom, Investigation of damping and radiation using full plane wave decomposition in ducts, *Journal of Sound and Vibration* 292 (2006) 519–534.
[16] M.S. Howe, The damping of sound by wall turbulent sheer layers, *Journal of Acoustical Society of America* 98 (3) (1995) 1723–1730.
[17] H. Rämmal, J. Lavrentjev, Sound reflection at an open end of a circular duct exhausting hot gas, *Noise Control Engineering Journal* 56 (2) (2008) 107–114.
[18] H. Rämmal, J. Lavrentjev, Determination of acoustic properties for open duct termination in hot jet conditions using FEM simulation, *Proceedings of the 14th International Congress on Sound and Vibration*, Cairns, Australia, 2007.
[19] A.R. da Silva, G.P. Scavone, A. Lefebvre, Sound reflection at the open end of axisymmetric ducts issuing a subsonic mean flow: a numerical study, *Journal of Sound and Vibration* 327 (2009) 507–528.
[20] J.Y. Chung, D.A. Blaser, Transfer function method for measuring in-duct acoustic properties. I. Theory, II Experiments, *Journal of Acoustical Society of America* 68 (3) (1980) 907–921.
[21] S.-H. Jang, J.-G. Ih, On the multiple microphone method for measuring in-duct acoustic properties in the presence of mean flow, *Journal of Acoustical Society of America* 103 (3) (1998) 1520–1526.
[22] E. Dokumaci, A note on transmission of sound in a wide pipe with mean flow and viscothermal attenuation, *Journal of Sound and Vibration* 208 (4) (1997) 653–655.
[23] U. Ingard, V.K. Singhal, Upstream and downstream sound radiation into a moving fluid, *Journal of the Acoustical Society of America* 54 (1973) 1343–1346.
[24] J.H.M. Disselhorst, L. Van Wijngaarden, Flow in the exit of open pipes during acoustic resonance, *Journal of Fluid Mechanics* 99 (2) (1980) 293–319.
[25] M. Åbom, H. Bodén, Error analysis of two-microphone measurements in ducts with flow, *Journal of the Acoustical Society of America* 83 (6) (1988) 2429–2438.
[26] J. Laufer, The structure of turbulence in fully developed pipe flow. NACA Report 1174, 1952.
[27] P. In 't Panhuis, Calculations of the acoustic end correction of a semi-infinite circular pipe issuing a subsonic cold or hot jet with co-flow. Report, Marcus Wallenberg Laboratory, KTH Royal Institute of Technology, November 2003.
[28] H. Schlichting, *Boundary Layer Theory*, McGraw Hill Inc., New York, 1968.
[29] P. Freymuth, On transition in a separated laminar boundary layer, *Journal of Fluid Mechanics* 25 (1965) 683–704.
[30] W. Bechert, Sound absorption caused by vorticity shedding, demonstrated with a jet flow, *Journal of Sound and Vibrations* 70 (1980) 389–405.

CURRICULUM VITAE

1. Personal data

Name	Heiki Tiikoja
Date and place of birth	25.09.1981 Tallinn
Citizenship	Estonian
Marital status	Married
Address	Paldiski mnt. 26A-16, Keila, Estonia
Phone	+352 5153464
E-mail	tiikoja@gmail.com

2. Education

Educational institution	Year	Education
Royal Institute of Technology (KTH), Stockholm	2012	Vehicle and maritime engineering, Licentiate degree
Tallinn University of Technology	2007	Transport engineering, MSc
Tallinn University of Technology	2005	Mechanical engineering, BSc, Cum Laude
Saue Gymnasium	2000	Secondary education

3. Language competence

Language	Level
Estonian	native language
English	fluent C1
Finnish	average B2
Russian	basic skills A2

4. Special courses

Period	Educational or other organisation
14.09.11 – 15.09.11	SIDLAB – Acoustic Design of Mufflers Course, KTH, Sweden
03.07.10 – 05.07.10	Summer School in Aeroacoustics in Low Mach Number Confined Flows, KTH, Sweden
20.04.09 – 24.04.09	The CANTOR Advanced Course, Torino, Italy
13.11.08 – 14.11.08 29.09.08 – 30.09.08	The Graduate School for Combustion Engineering (VINNPRO), KTH/ CCGEx, Sweden

5. Professional employment

Period	Organisation	Position
09.2012 – 07.2013	Tallinn University of Technology	Assistant
10.2009 – 12.2010	Tallinn University of Technology	Researcher
11.2007 – 10.2009	Tallinn University of Technology	Extraordinary researcher

6. Honors/awards

Erik Petersohns Minne stipendium, KTH, 2010
A scholarship for outstanding PhD student, TUT Development Foundation, 2009
A scholarship for outstanding BSc student, TUT Development Foundation, 2004

7. Thesis supervised

Treimuth Tambet, MSc, „Control system design for an electro-magnetic brake in LabVIEW ", Tallinn, 2009
Agnar Birk, MSc, „ Throttle flap drive projection to the motor", Tallinn, 2008

8. Main area of scientific work

Technical acoustics.

9. Other research projects

Subject	Nr of Project	Duration
Analysis and Development of Additive Manufacturing Processes	ETF9441	01.01.12 – 31.12.15
Optimal design of composite and functional material structures, products and manufacturing processes	SF0140035s12	01.01.12 – 31.12.14
Smart composites: design and manufacturing	AR12139	01.07.12 – 31.12.14
Experimental methods for acoustic studies of hot gas flows	ETF7913	01.01.09 – 31.12.11
Rapid Product and Process Realization - theory and methodology	SF0142684s05	01.01.05 – 31.12.10
Development of measurement methods for nonstationary flow noise	ETF6557	01.01.06 – 31.12.08

10. Publications

Lavrentjev, J., Tiikoja, H., Investigation of Wave Propagation and Radiation in Ducts with Arbitrary Environment by Using the Three-microphone Method. Proceedings of the *37th International Congress and Exposition on Noise Control Engineering (INTER-NOISE 2008)*, Shanghai, China, 2008.

Rämmal, H., Tiikoja, H., Åbom, M., Bodén, H., Experimental Facility for the Complete Determination of Sound Transmission in Turbochargers. *Society of Automotive Engineers*, SAE Technical Paper 2010-01-1424, Graz, Austria, 2010, doi:10.4271/2010-01-1424.

Tiikoja, H., Rämmal, H., Åbom, M., Bodén, H., Testrig for Complete Acoustic Characterization of Turbochargers. Proceedings of the *31th International AIAA Aeroacoustics Conference*, Stockholm, Sweden, 2010.

Rämmal, H., Lavrentjev, J., Tiikoja, H., On the Acoustic Reflection at Pipe Opening. Proceedings of the *17th International Congress on Sound and Vibration* (ICSV 17), Cairo, Egypt, 2010.

Tiikoja, H., Rämmal, H., Åbom, M., Bodén, H., Sound Transmission in Automotive Turbochargers. *Society of Automotive Engineers*, SAE Technical Paper 2011-01-1525, Grand Rapids, USA, 2011, doi:10.4271/2011-01-1525.

Tiikoja, H., Rämmal, H., Åbom, M., Bodén, H., Investigations of Automotive Turbocharger Acoustics. *SAE International Journal of Engines* 4:2531-2542, Print ISSN 1946-3936, Naples, Italy, 2011, doi:10.4271/2011-24-0221.

Lavrentjev, J., Rämmal, H., Tiikoja, H., The Passive Acoustic Effect of Automotive Catalytic Converter. *Society of Automotive Engineers*, SAE Technical Paper 2011-24-0219, Naples, Italy, 2011, doi:10.4271/2011-24-0219.

Kabral, R., Rämmal, H., Auriemma, F., Luppin, J., Kõiv, R., Tiikoja, H., Lavrentjev, J., A Novel Design for Cruiser Type Motorcycle Silencer Based on Micro-Perforated Elements. *Society of Automotive Engineers*, SAE Technical Paper 2012-32-0109, Madison, USA, 2012, doi:10.4271/2012-32-0109.

Tiikoja, H., Lavrentjev, J., Rämmal, H., Åbom, M., Experimental Investigations of Sound Reflection from Hot and Subsonic Flow Duct Termination. *Journal of Sound and Vibration*, Volume 333, Issue 3, ISSN 0022-460X, pp. 788-800, 2014, doi: 10.1016/j.jsv.2013.09.030.

ELULOOKIRJELDUS

1. Isikuandmed

Ees- ja perekonnanimi	Heiki Tiikoja
Sünniaeg ja -koht	25.09.1981, Tallinn
Kodakondsus	Eesti
Perekonnaseis	Abielus
Aadress	Paldiski mnt. 26A-16, Keila
Telefon	+372 5153464
E-posti	tiikoja@gmail.com

2. Hariduskäik

Õppeasutus	Lõpetamise aasta	Haridus
Kuninglik Tehnoloogiainstituut (KTH), Stockholm	2012	Litsentsiaat
Tallinna Tehnikaülikool	2007	Transporditehnika, tehnikateaduste magister
Tallinna Tehnikaülikool	2005	Transporditehnika, bakalaureusekraad *Cum Laude*
Saue Gümnaasium	2000	Keskharidus

3. Keelteoskus

Keel	Tase
Eesti keel	emakeel
Inglise keel	kõrgtase C1
Soome keel	kesktase B2
Vene keel	algtase A2

4. Täiendusõpe

Õppimise aeg	Täiendusõppe korraldaja nimetus
14.09.11 – 15.09.11	SIDLAB kursus – summutite akustiline disain, KTH, Sweden
03.07.10 – 05.07.10	Aeroakustika suvekool, KTH, Rootsi
20.04.09 – 24.04.09	CANTOR Kursus, Torino, Itaalia
13.11.08 – 14.11.08 29.09.08 – 30.09.08	Sisepõlemismootorite kursus (VINNPRO), KTH/ CCGEx, Rootsi

5. Teenistuskäik

Töötamise aeg	Tööandja nimetus	Ametikoht
09.2012 – 07.2013	Tallinn Tehnikaülikool	Assistent
10.2009 – 12.2010	Tallinn Tehnikaülikool	Teadur
11.2007 – 10.2009	Tallinn Tehnikaülikool	Erakorraline teadur

6. Tunnustused

Erik Petersohns Minne stipendium, KTH, 2010
Doktorandi stipendium, TTÜ arengufond, 2009
Bakalaureuseõppe stipendium, TTÜ arengufond, 2004

7. Juhendatud lõputööd

Tambet Treimuth, MSc, „Mootoristendi elektrilise piduri juhtsüsteemi programmeerimine LabVIEW keskkonnas", Tallinn, 2009
Agnar Birk, MSc, „Drosselklapi ajami projekteerimine mootorstendile", Tallinn, 2008

8. Teadustöö põhisuunad

Tehniline akustika

9. Teadusprojektid

Teema	Projekti number	Kestus
Digitaalsete otsetootmisprotsesside analüüs ja arendus	ETF9441	01.01.12 – 31.12.15
Komposiit- ja funktsionaalsetest mater-jalidest konstruktsioonide, toodete ja tootmisprotsesside optimaalne projekteerimine	SF0140035s12	01.01.12 – 31.12.14
Targad komposiitmaterjalid: projekteerimine ja valmistamine	AR12139	01.07.12 – 31.12.14
Kõrgtemperatuursete gaaside voolu akustika eksperimentaalsed uurimismeetodid	ETF7913	01.01.09 – 31.12.11
Toodete ja tootmisprotsesside kiire teostamine - teooria ja metodoloogia.	SF0142684s05	01.01.05 – 31.12.10
Mittestatsionaarse voolu müra eksperimen-taalsete uurimismeetodite arendamine	ETF6557	01.01.06 – 31.12.08

10. Publikatsioonid

Lavrentjev, J., Tiikoja, H., Investigation of Wave Propagation and Radiation in Ducts with Arbitrary Environment by Using the Three-microphone Method. Proceedings of the *37th International Congress and Exposition on Noise Control Engineering (INTER-NOISE 2008)*, Shanghai, China, 2008.

Rämmal, H., Tiikoja, H., Åbom, M., Bodén, H., Experimental Facility for the Complete Determination of Sound Transmission in Turbochargers. *Society of Automotive Engineers*, SAE Technical Paper 2010-01-1424, Graz, Austria, 2010, doi:10.4271/2010-01-1424.

Tiikoja, H., Rämmal, H., Åbom, M., Bodén, H., Testrig for Complete Acoustic Characterization of Turbochargers. Proceedings of the *31th International AIAA Aeroacoustics Conference*, Stockholm, Sweden, 2010.

Rämmal, H., Lavrentjev, J., Tiikoja, H., On the Acoustic Reflection at Pipe Opening. Proceedings of the *17th International Congress on Sound and Vibration* (ICSV 17), Cairo, Egypt, 2010.

Tiikoja, H., Rämmal, H., Åbom, M., Bodén, H., Sound Transmission in Automotive Turbochargers. *Society of Automotive Engineers*, SAE Technical Paper 2011-01-1525, Grand Rapids, USA, 2011, doi:10.4271/2011-01-1525.

Tiikoja, H., Rämmal, H., Åbom, M., Bodén, H., Investigations of Automotive Turbocharger Acoustics. *SAE International Journal of Engines* 4:2531-2542, Print ISSN 1946-3936, Naples, Italy, 2011, doi:10.4271/2011-24-0221.

Lavrentjev, J., Rämmal, H., Tiikoja, H., The Passive Acoustic Effect of Automotive Catalytic Converter. *Society of Automotive Engineers*, SAE Technical Paper 2011-24-0219, Naples, Italy, 2011, doi:10.4271/2011-24-0219.

Kabral, R., Rämmal, H., Auriemma, F., Luppin, J., Kõiv, R., Tiikoja, H., Lavrentjev, J., A Novel Design for Cruiser Type Motorcycle Silencer Based on Micro-Perforated Elements. *Society of Automotive Engineers*, SAE Technical Paper 2012-32-0109, Madison, USA, 2012, doi:10.4271/2012-32-0109.

Tiikoja, H., Lavrentjev, J., Rämmal, H., Åbom, M., Experimental Investigations of Sound Reflection from Hot and Subsonic Flow Duct Termination. *Journal of Sound and Vibration*, Volume 333, Issue 3, ISSN 0022-460X, pp. 788-800, 2014, doi: 10.1016/j.jsv.2013.09.030.

DISSERTATIONS DEFENDED AT TALLINN UNIVERSITY OF TECHNOLOGY ON *MECHANICAL ENGINEERING*

1. **Jakob Kübarsepp**. Steel-Bonded Hardmetals. 1992.

2. **Jakub Kõo**. Determination of Residual Stresses in Coatings &Coated Parts. 1994.

3. **Mart Tamre**. Tribocharacteristics of Journal Bearings Unlocated Axis. 1995.

4. **Paul Kallas**. Abrasive Erosion of Powder Materials. 1996.

5. **Jüri Pirso**. Titanium and Chromium Carbide Based Cermets. 1996.

6. **Heinrich Reshetnyak**. Hard Metals Serviceability in Sheet Metal Forming Operations. 1996.

7. **Arvi Kruusing**. Magnetic Microdevices and Their Fabrication methods. 1997.

8. **Roberto Carmona Davila**. Some Contributions to the Quality Control in Motor Car Industry. 1999.

9. **Harri Annuka**. Characterization and Application of TiC-Based Iron Alloys Bonded Cermets. 1999.

10. **Irina Hussainova**. Investigation of Particle-Wall Collision and Erosion Prediction. 1999.

11. **Edi Kulderknup**. Reliability and Uncertainty of Quality Measurement. 2000.

12. **Vitali Podgurski**. Laser Ablation and Thermal Evaporation of Thin Films and Structures. 2001.

13. **Igor Penkov**. Strength Investigation of Threaded Joints Under Static and Dynamic Loading. 2001.

14. **Martin Eerme**. Structural Modelling of Engineering Products and Realisation of Computer-Based Environment for Product Development. 2001.

15. **Toivo Tähemaa**. Assurance of Synergy and Competitive Dependability at Non-Safety-Critical Mechatronics Systems design. 2002.

16. **Jüri Resev**. Virtual Differential as Torque Distribution Control Unit in Automotive Propulsion Systems. 2002.

17. **Toomas Pihl**. Powder Coatings for Abrasive Wear. 2002.

18. **Sergei Letunovitš**. Tribology of Fine-Grained Cermets. 2003.

19. **Tatyana Karaulova**. Development of the Modelling Tool for the Analysis of the Production Process and its Entities for the SME. 2004.

20. **Grigori Nekrassov**. Development of an Intelligent Integrated Environment for Computer. 2004.

21. **Sergei Zimakov**. Novel Wear Resistant WC-Based Thermal Sprayed Coatings. 2004.

22. **Irina Preis**. Fatigue Performance and Mechanical Reliability of Cemented Carbides. 2004.

23. **Medhat Hussainov**. Effect of Solid Particles on Turbulence of Gas in Two-Phase Flows. 2005.

24. **Frid Kaljas**. Synergy-Based Approach to Design of the Interdisciplinary Systems. 2005.

25. **Dmitri Neshumayev**. Experimental and Numerical Investigation of Combined Heat Transfer Enhancement Technique in Gas-Heated Channels. 2005.

26. **Renno Veinthal**. Characterization and Modelling of Erosion Wear of Powder Composite Materials and Coatings. 2005.

27. **Sergei Tisler**. Deposition of Solid Particles from Aerosol Flow in Laminar Flat-Plate Boundary Layer. 2006.

28. **Tauno Otto**. Models for Monitoring of Technological Processes and Production Systems. 2006.

29. **Maksim Antonov**. Assessment of Cermets Performance in Aggressive Media. 2006.

30. **Tatjana Barashkova**. Research of the Effect of Correlation at the Measurement of Alternating Voltage. 2006.

31. **Jaan Kers**. Recycling of Composite Plastics. 2006.

32. **Raivo Sell**. Model Based Mechatronic Systems Modeling Methodology in Conceptual Design Stage. 2007.

33. **Hans Rämmal**. Experimental Methods for Sound Propagation Studies in Automotive Duct Systems. 2007.

34. **Meelis Pohlak**. Rapid Prototyping of Sheet Metal Components with Incremental Sheet Forming Technology. 2007.

35. **Priidu Peetsalu**. Microstructural Aspects of Thermal Sprayed WC-Co Coatings and Ni-Cr Coated Steels. 2007.

36. **Lauri Kollo**. Sinter/HIP Technology of TiC-Based Cermets. 2007.

37. **Andrei Dedov**. Assessment of Metal Condition and Remaining Life of In-service Power Plant Components Operating at High Temperature. 2007.

38. **Fjodor Sergejev**. Investigation of the Fatigue Mechanics Aspects of PM Hardmetals and Cermets. 2007.

39. **Eduard Ševtšenko**. Intelligent Decision Support System for the Network of Collaborative SME-s. 2007.

40. **Rünno Lumiste**. Networks and Innovation in Machinery and Electronics Industry and Enterprises (Estonian Case Studies). 2008.

41. **Kristo Karjust**. Integrated Product Development and Production Technology of Large Composite Plastic Products. 2008.

42. **Mart Saarna**. Fatigue Characteristics of PM Steels. 2008.

43. **Eduard Kimmari**. Exothermically Synthesized B_4C-Al Composites for Dry Sliding. 2008.

44. **Indrek Abiline**. Calibration Methods of Coating Thickness Gauges. 2008.

45. **Tiit Hindreus**. Synergy-Based Approach to Quality Assurance. 2009.

46. **Karl Raba**. Uncertainty Focused Product Improvement Models. 2009.

47. **Riho Tarbe**. Abrasive Impact Wear: Tester, Wear and Grindability Studies. 2009.

48. **Kristjan Juhani**. Reactive Sintered Chromium and Titanium Carbide-Based Cermets. 2009.

49. **Nadežda Dementjeva**. Energy Planning Model Analysis and Their Adaptability for Estonian Energy Sector. 2009.

50. **Igor Krupenski**. Numerical Simulation of Two-Phase Turbulent Flows in Ash Circulating Fluidized Bed. 2010.

51. **Aleksandr Hlebnikov**. The Analysis of Efficiency and Optimization of District Heating Networks in Estonia. 2010.

52. **Andres Petritšenko**. Vibration of Ladder Frames. 2010.

53. **Renee Joost**. Novel Methods for Hardmetal Production and Recycling. 2010.

54. **Andre Gregor**. Hard PVD Coatings for Tooling. 2010.

55. **Tõnu Roosaar**. Wear Performance of WC- and TiC-Based Ceramic-Metallic Composites. 2010.

56. **Alina Sivitski**. Sliding Wear of PVD Hard Coatings: Fatigue and Measurement Aspects. 2010.

57. **Sergei Kramanenko**. Fractal Approach for Multiple Project Management in Manufacturing Enterprises. 2010.

58. **Eduard Latõsov**. Model for the Analysis of Combined Heat and Power Production. 2011.

59. **Jürgen Riim**. Calibration Methods of Coating Thickness Standards. 2011.

60. **Andrei Surzhenkov**. Duplex Treatment of Steel Surface. 2011.

61. **Steffen Dahms**. Diffusion Welding of Different Materials. 2011.

62. **Birthe Matsi**. Research of Innovation Capasity Monitoring Methodology for Engineering Industry. 2011.

63. **Peeter Ross**. Data Sharing and Shared Workflow in Medical Imaging. 2011.

64. **Siim Link**. Reactivity of Woody and Herbaceous Biomass Chars. 2011.

65. **Kristjan Plamus**. The Impact of Oil Shale Calorific Value on CFB Boiler Thermal Efficiency and Environment. 2012.

66. **Aleksei Tšinjan**. Performance of Tool Materials in Blanking. 2012.

67. **Martinš Sarkans**. Synergy Deployment at Early Evaluation of Modularity of the Multi-Agent Production Systems. 2012.

68. **Sven Seiler**. Laboratory as a Service – A Holistic Framework for Remote and Virtual Labs. 2012.

69. **Tarmo Velsker**. Design Optimization of Steel and Glass Structures. 2012.

70. **Madis Tiik**. Access Rights and Organizational Management in Implementation of Estonian Electronic Health Record System. 2012.

71. **Marina Kostina**. Reliability Management of Manufacturing Processes in Machinery Enterprises. 2012.

72. **Robert Hudjakov**. Long-Range Navigation for Unmanned Off-Road Ground Vehicle. 2012.

73. **Arkadi Zikin**. Advanced Multiphase Tribo-Functional PTA Hardfacings. 2013.

74. **Alar Konist**. Environmental Aspects of Oil Shale Power Production. 2013.

75. **Inge Roos**. Methodology for Calculating CO_2 Emissions from Estonian Shale Oil Industry. 2013.

76. **Dmitri Shvarts**. Global 3D Map Merging Methods for Robot Navigation. 2013.

77. **Kaia Lõun**. Company's Strategy Based Formation of e-Workplace Performance in the Engineering Industry. 2013.

78. **Maido Hiiemaa**. Motion Planner for Skid-Steer Unmanned Ground Vehicle. 2013.

79. **Dmitri Goljandin**. Disintegrator Milling System Development and Milling Technologies of Different Materials. 2013.

80. **Dmitri Aleksandrov**. Light-Weight Multicopter Structural Design for Energy Saving. 2013.

81. **Viktoria Baškite**. Green Framework Development for Used Industrial Equipment Life Cycle Assessment and Extension. 2014.